

https://dspace.org/

Inhibition of Schistosoma japonicum glutathione transferase by Cibacron Blue: insights from structural, functional and molecular modelling studies

Hlabano, Babongiwe

2018

https://hdl.handle.net/10539/27108

Hlabano, Babongiwe (2018) Inhibition of Schistosoma japonicum glutathione transferase by Cibacron Blue : insights from structural, functional and molecular modelling studies, University of the Witwatersrand, Johannesburg, <http://hdl.handle.net/10539/27108>

Downloaded from a DSpace repository. https://dspace.org/

Inhibition of *Schistosoma japonicum* glutathione transferase by Cibacron Blue: Insights from structural, functional and molecular modelling studies

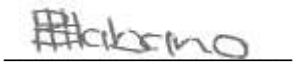
Babongiwe Hlabano

A dissertation submitted to the Faculty of Science, University of the Witwatersrand Johannesburg, in fulfilment of the requirements for the degree of Master of Science.

July, 2018

DECLARATION

I declare that this dissertation is my own, unaided work. It is being submitted for the degree of Master of Science in the University of the Witwatersrand, Johannesburg. It has not been submitted for any other degree or examination at any other University.



Babongiwe Hlabano

25th day of July, 2018

ABSTRACT

Schistosomiasis is a leading neglected tropical disease, caused by blood flukes of the genus *Schistosoma*. Around 200 million people worldwide are affected, with the majority in Sub-Sahara Africa. Currently, only praziquantel is used for the treatment of schistosomiasis and its exclusive use has led to concerns of rise of praziquantel resistant *Schistosomes*. There is therefore a need for the development of new anti-schistosomal drugs. Schistosoma species lack the cytochrome P-450 detoxification mechanism, an important mechanism in human detoxification cycle, thus making *Schistosoma* glutathione S-transferase (GST) one of the main enzyme for detoxification of electrophilic and hydrophobic compounds. *Schistosoma japonicum* GST (SjGST) is an attractive drug/vaccine target against schistosomiasis. In this study, the mechanism of inhibition of SjGST by Cibacron Blue 3G-A (CB3GA) was investigated. Soluble SjGST was recombinantly expressed and purified successfully to homogeneity. SjGST maintained dimeric structure in the presence of CB3GA. IC_{50} value of CB3GA was determined to be 100 nM. Michaelis-Manten kinetic studies where performed in the presence and absence of CB3GA and showed that SjGST has high affinity for glutathione compared with CDNB. Lineweaver–Burk plots indicated that CB3GA is an uncompetitive and mixed inhibitor to the G-site and H-site respectively. Induced fit docking predicted that CB3GA binds to the L-site consistent with kinetic inhibition studies. MM-GBSA predicted free binding energy of SjGST and CB3GA was ΔG_{Pred} = -310 kJ/mol compared with experimental free energy of binding of ΔG_{Exp} = -49 kJ/mol. CB3GA is an efficient inhibitor of SjGST that binds to the dimer interface of SjGST altering catalytic activity of both the G-site and H-site. The unique characteristic of the L-site provides an opportunity for highly specific rational drug design.

DEDICATION

To my mom and dad "I'm getting closer"

Gogo maNyathi lo Baba Muhle "lakusasa lingadinwa eGabula"

My family and loved ones who have stood by my side.

ACKNOWLEDGEMENTS

To my supervisor, Dr. Ikechukwu A. Achilonu, I am most grateful for your guidance, patience and extending your valuable knowledge through the course of my research. Your love for science is contagious. I am a better scientist today, “daalu nke ukwuu”.

Prof H.W. Dirr for his support. “I have realised my potential”

Tshireletso “Fam” Mentor for his assistance in computational work. “It’s done”.

Members of the Protein Structure-Function Research Unit for providing a good working environment.

The University of the Witwatersrand and the Council for Scientific and Industrial Research (CSIR) for financial assistance.

TABLE OF CONTENTS

DECLARATION i

ABSTRACT ii

ACKNOWLEDGEMENT iv

TABLE OF CONTENTS v

LIST OF FIGURES viii

LIST OF TABLES ix

ABBREVIATIONS x

CHAPTER I: INTRODUCTION 1

1.1 Schistosomiasis overview 2

1.2 Problem statement 2

1.3 Rationale 3

1.4 Novelty 4

1.5 Aim 4

1.6 Objectives 4

1.7 Overview 5

CHAPTER II: LITERATURE REVIEW 6

2.1 Schistosomiasis 7

2.1.1 Background 7

2.1.2 Schistosoma life cycle 9

2.1.3 Pathogenesis of schistosomiasis 9

2.1.4 Treatment of schistosomiasis 11

2.2 Oxidative stress in Schistosoma 12

2.3 Helminth glutathione S-transferases 13

2.4 Schistosoma glutathione S-transferase 14

2.5 Enzyme inhibition 15

2.6 Enzyme inhibition kinetics 17

2.7 Molecular docking 20
2.8 Scoring molecular docking 22
2.9 Theoretical binding affinity 23

CHAPTER III: MATERIALS AND METHODS 25
3.1 Materials 26
3.2 Methods 26
3.2.1 Plasmid construct 26
3.2.2 Overexpression 26
3.2.3 Soluble fraction harvesting 28
3.2.4 Purification: Glutathione-Agarose affinity chromatography 28
3.2.5 Analysis of protein purity using SDS-PAGE 29
3.2.6 Protein concentration determination 30
3.2.7 Spectroscopic studies 31
3.2.7.1 Far-UV circular dichroism 31
3.2.7.2 Intrinsic tryptophan fluorescence spectroscopy 33
3.2.7.3 Extrinsic ANS fluorescence spectroscopy 34
3.2.8 Size exclusion high performance liquid chromatography 36
3.2.9 Enzyme activity assay 37
3.2.10 Enzyme activity inhibition 39
3.2.11 Molecular docking studies 40
3.1.11.1 Force field calculation 40
3.1.11.2 Protein preparation 40
3.1.11.3 Ligand preparation 41
3.1.11.4 Induced fit docking 41
3.1.11.5 Binding affinity prediction 43

CHAPTER IV: RESULTS 44
4.1 Protein expression and purification 45
4.2 Structural Characterisation 45
4.2.1 Far-UV circular dichroism 48

4.2.2 Intrinsic tryptophan fluorescence spectroscopy 48
4.2.3 Extrinsic ANS fluorescence spectroscopy 48
4.3 Size exclusion high performance liquid chromatography 52
4.4 Enzyme activity assay 52
4.5 Enzyme activity inhibition 55
4.6 Molecular docking studies 60
4.7 Binding affinity calculation 60

CHAPTER V: DISCUSSION 61

CHAPTER VI: REFERENCES 76

APPENDIX 86

LIST OF FIGURES

Figure 2.1: Worldwide distribution of schistosomiasis 8

Figure 2.2: Schistosomiasis life-cycle. 10

Figure 2.3: Structure of *S.japonicum* GST.....16

Figure 2.4: Enzyme kinetics graphs. 19

Figure 2.5: Enzyme inhibition kinetics graphs. 21

Figure 3.1: Map of pGEX-4T-1 vector. 27

Figure 3.2: Structure of CB3GA. 32

Figure 3.3: Structure of ANS. 35

Figure 3.4: GSH/CDNB conjugation reaction 38

Figure 3.5: Molecular docking flowchart. 42

Figure 4.1: Expression and purification analysis. 46

Figure 4.2: Protein quantification and absorbance spectra of SjGST 47

Figure 4.3: Far-UV CD spectra of SjGST 49

Figure 4.4: Intrinsic tryptophan fluorescence spectra of SjGST.....50

Figure 4.5: Extrinsic ANS fluorescence spectra of SjGST. 51

Figure 4.6: SE-HPLC profiles of SjGST. 53

Figure 4.7: Inhibition of SjGST by CB3GA. 54

Figure 4.8: Michaelis-Menten plots for SjGST. 56

Figure 4.9: SjGST G-site inhibition kinetics 58

Figure 4.10: SjGST H-site inhibition kinetics 59

Figure 4.11: Induced fit molecular docking of CB3GA into SjGST. 61

Figure 4.12: Induced fit molecular docking of CB3GA into human Pi-GST.....62

Figure 4.13: MM-GBSA docking of CB3GA into SjGST 63

Figure 4.13: Docking protocol validation.....65

Figure A1: Linear progress curve for SjGST activity.....88

LIST OF TABLES

Table 1: Reagent components of Tricine-SDS-PAGE gel.....30

Table 2: DICHROWEB analysis for secondary structural composition of SjGST 49

Table 3: Kinetic properties of SjGST in the presence of CB3GA.....57

Table 4: Binding free energy estimation for SjGST-CB3GA complex.....64

Table A1: Volumes used for SjGST specific activity determination 87

Table A2: Liner progress curve properties of SjGST activity.....89

ABBREVIATIONS

°C	degrees Celsius
A_{280}	Absorbance at 280 nm
ANS	8-Anilino-1-naphthalene-sulfonic acid
CB3GA	Cibacron Blue 3G-A
CDNB	1-chloro-2,4-dinitrobenzene
DTT	Dithiothreitol
E. coli	*Escherichia coli*
ETDA	Ethylenediaminetetra-acetic acid
Far- UV CD	Far Ultraviolet circular dichroism
GSH	Reduced glutathione
G-site	Glutathione binding site in GSTs
GST	Glutathione S-transfarase
H-site	Hydrophobic, electrophilic substrate binding site in GSTs
IFD	Induced fit docking
IPTG	Isopropyl β-D-1-thiogalactopyranoside
K_m	Michelis-Manten constant
L-site	Non-substrate ligand binding site in GSTs
mg/ml	miligrams/millilitre
MM-GBSA	Molecular Mechanics Generalized Born Surface Area
OD_{600}	optical density at 600 nm
PDB	Protein Data Bank
SDS-PAGE	sodium dodecyl sulfate polyacrylamide gel electrophoresis
SE-HPLC	Size exclusion high performance liquid chromatography
SjGST	Schistosoma japonicum glutathione S-transferase
V_{max}	Maximal velocity
ΔG	Change in Gibbs free energy
ΔG_{Exp}	Experimental free energy of binding
ΔG_{Pred}	Predicted free energy of binding

The IUPAC-IUBMB three and one letter codes for amino acids are used

CHAPTER I
INTRODUCTION

1.1 Overview of Schistosomiasis

Schistosomiasis (Bilharzia) is a leading parasitic disease in terms of public health impact, accounting for 40% of tropical disease burden, if malaria is excluded (Adenowo *et al*., 2015). Schistosomiasis is caused by a parasitic blood flukes of genus *Schistosoma*, infections pose serious burden to socio-economic state of countries affected. The main species affect humans are *S. japonicum, S. haematobium,* and *S. mansoni*, all three have different clinical manifestations. The parasitic disease is prevalent in Sub-Saharan Africa, which has the most impoverished populations in the world (Muhumuza *et al*., 2009). The disease has remained a neglected tropical disease, despite the disease having detrimental socio-economic impact (WHO, 2017). However, recently some attention has been drawn to schistosomiasis due to a possibility of being associated with human immunodeficiency virus (HIV). In a study by Secor (2012), genital schistosomiasis infection was an apparent co-factor in the transmission of HIV. In another study by Kallestrup *et al*., (2006), HIV infected patients responded poorly to schistosomiasis chemotherapy.

The preventive and first line of treatment of all types of schistosomiasis rely heavily on the extensive use of praziquantel. Treatment with praziquantel has high cure rates with reduced transmission and morbidity (Cioli et al., 2014). Even though praziquantel is effective after a single dose, it does not protect individuals from re-infection (Rollinson, 2009). This is a huge problem, especially in young children, where repeated parasitic infections lead to chronic diseases such as impaired learning (cognitive) and growth (physiological), splenomegaly, anaemia, fibrosis and granulomatous reactions for some tissues due to repeated inflammation (Jordan *et al*., 1993).

1.2 Problem statement

Praziquantel is currently the only drug against schistosomiasis and is the basis of schistosomiasis mass control worldwide (WHO, 2017). The mechanism of action of praziquantel against schistosomiasis remains unknown. Praziquantel was introduced to schistosomiasis endemic areas for morbidity control and has been in use for more than four decades. Prolonged use of the praziquantel can act as a selection pressure for the emergence of minor pre-existing resistant sub-populations of *Schistosoma* (Wang *et al*., 2012). Drug resistance remains a concern for schistosomiasis control because of the largescale and repeated use of the drug in the treatment of disease. There are many factors that lead to emergence of drug resistant strains in general. In

helminths, extensive use of praziquantel, in low sub-curative dose led to the development of resistance to the recommended therapeutic dose (Ismail *et al*., 1994). In mice infected with *S. mansoni*, treatment with a sub-curative dose, led to the rise of praziquantel resistant strains (Fallon and Doenhoff, 1994). Schistosomiasis endemic areas usually have limited resources and health authorities are compelled to equally share drugs. In most cases a sub-curative dosage is used to cover a wider population (Baan *et al*., 2016; De Sousa *et al*., 2014; Doenhoff *et al*., 2009). This is one example where current practices act as selective pressure for the emergence of praziquantel resistant strains. The use of praziquantel will increase in the foreseeable future, whether given alone or co-administered with other anthelminthic in integrated control programs (De Sousa *et al*., 2014). Praziquantel resistance remains a threat and requires adequate monitoring of current mass drug administration programs. The effect of drugs selective pressures and long-term drug use for treatment of schistosomiasis is poorly understood. There is no alternative drug for schistosomiasis treatment if resistance emerges. Therefore, a need to develop novel anti-schistosomal drugs.

1.3 Rationale

Oxamniquine and metrifonate are the other two drugs used to treat schistosomiasis. However, oxamniquine can only treat intestinal *S. mansoni* schistosomiasis (Ferrari *et al*., 2003). Metrifonate is only effective against urinary *S. haematobium* schistosomiasis (Feldmeier and Chitsulo, 1999). The challenge with these two drugs is the limited specificity against different types of schistosomiasis; hence, they are inadequate in mass control of schistosomiasis. Other disadvantages of both drugs are that they have a high operational cost per dose and unpleasant side effects (Reich *et al*., 1998). These factors carry a heavy financial burden in the eradication of schistosomiasis in endemic countries most of which have a low gross domestic product (Adenowo *et al*., 2015). Therefore, the new drug to be developed requires to be highly effective against all forms of schistosomiasis, cheap and easily distributed with no special conditions needed such as refrigerated logistics.

Upon the entry to the human host schistosomes rapidly transform from free-swimming infective cercariae to endoparasitic schistosomules. These migrate and access the circulatory system to site of infection (bladder or intestines) (Jordan *et al*., 1993). During these stages schistosomes undergo various morphological, physiological and biochemical changes into adult phase, in order to adapt

and ensure survival (Ressurreição *et al*., 2016). The series of changes is accompanied by high oxidative stress from internally (physiological changes) and externally (host immune response) (Alger and Williams, 2002). Hence, to abate oxidative stress schistosomes must possess adequate mechanisms of detoxification systems. These rely on reducing equivalents from the disulfide oxidoreductases, glutathione (GSH) and thioredoxin (Alger and Williams, 2002). *Schistosoma* species have limited detoxification enzymes such as superoxide dismutase, glutathione peroxidase, glutathione *S*-transfarase and catalase. Glutathione *S*-transferase (GST) is one of the major enzyme involved in detoxification in *Schistosoma*. GSTs catalyse conjugation of GSH with endogenous xenobiotic compounds for elimination from the cell (Brophy and Barrett, 1990). GST serves as a suitable drug target because *Schistosoma* GST (SGST) serves as a primary defence against oxidative damage and toxic electrophilic xenobiotics (Brophy and Barrett, 1990). Hence, inhibition of SGST may be adverse to *Schistosoma*. In this study, focus will be on the inhibition of *S. japonicum* GST (SjGST) which will serve as a model for all *Schistosoma* species because all *Schistosoma* GSTs have similar structural fold and function.

1.4 Novelty

Cibacron Blue 3G-A (CB3GA) is a GST inhibitor. The mode of inhibition of CB3GA on SjGST has not been established. The kinetics of SjGST inhibition by CB3GA will help to understand the functional properties of SjGST. The findings can then be applied to aid rational drug design against *Schistosoma* GSTs.

1.5 Aim

The aim of the study is to biophysically characterise *S. japonicum* glutathione S-transferase (SjGST) inhibition by CB3GA.

1.6 Objectives

In order to accomplish the aim of the study, the objectives of this study are to:

- recombinantly express and purify SjGST.
- characterise the secondary structure of SjGST using Far-ultraviolet circular dichroism (Far-UV CD).

- characterise the tertiary structure of SjGST using intrinsic tryptophan fluorescence and extrinsic 8-Anilino-1-naphthalenesulfonic acid (ANS) fluorescence.
- characterise quaternary structure of SjGST in the presence and absence of CB3GA using size exclusion high performance liquid chromatography SE-HPLC.
- determine specific activity SjGST in the presence and absence of CB3GA
- use molecular docking and MM-GBSA in order to describe the interaction between SjGST and CB3GA.

1.7 Overview of the dissertation

The report begins in Chapter 2 (Literature review) were background information relating information on schistosomiasis and glutathione S-transferases is provided. Chapter 3 (Materials and Methods) provides details on the techniques and methodologies used in this study to monitor the effect of CB3GA on SjGST. Chapter 4 (Results) here observations of this study are presented. This chapter explains results obtained in this study. Chapter 5 (Discussion) explains and analyses the findings of the study. The chapter provides a link of this study with pre-existing knowledge on CB3GA and SjGST. The conclusions and future work are presented.

CHAPTER II
LITERATURE REVEIW

2.1 Schistosomiasis

2.1.1 Background

Schistosomiasis "Bilharzia" is a neglected tropical disease (NTD) caused by parasitic helminths (blood flukes) of the genus *Schistosoma* (Jordan *et al*., 1993). The disease affects mostly poverty-stricken populations in Asia, Sub-Saharan Africa and South America (Figure 2.1). The term NTDs, "neglected" is due to low funding and acknowledgement of the disease by the pharmaceutical industries, even though it represents a grave threat to health in these under-developed regions (da Paixão Siqueira *et al*., 2017). These communities have inadequate supply of clean water and in most cases no access to sanitary facilities, which promotes the spread of the disease (WHO, 2013). There are three main species that affect humans, *S. mansoni and S. japonicum* and *S. haematobium.* Urinary schistosomiasis is caused by *S. haematobium* and *S. mansoni* while intestinal schistosomiasis is caused *S. japonicum* (Wang *et al*., 2012). *S. mansoni* is endemic to South America and some parts of Egypt and Arabic countries. *S. japonicum* is endemic in China and Philippines. In Africa all species of *Schistosoma* are present, in some cases co-infection of individuals with different species have been observed (Fong, 2012). The disease affects 193-207 million people, and 600-799 million more people are at risk of being infected, pregnant women and children have the highest burden of infection (Chitsulo *et al*., 2000). Mortality has been estimated at 280,000 deaths per annum in Sub-Saharan Africa (van der Werf *et al*., 2003). Disability due to schistosomiasis covers a wide range of effects, which include anaemia, diminished physical and mental fitness and stunted growth due to malnutrition. In severe cases schistosomiasis can lead to disfigurement of limbs, which include lymphatic filariasis or blindness, due to trachoma and onchocerciasis (da Paixão Siqueira *et al*., 2017). 1.7 million disability-adjusted life years (DALYs) are estimated to be lost due to schistosome infections (WHO, 2013). Epidemiology of schistosomiasis is an interplay of ecological, biological, social and economic factors with interaction of various hosts and life-cycle stages (Huang and Manderson, 1992). Freshwater bodies seem to play an important role by defining host range schistosomiasis (Brown, 2002). This has been key in the recent extension of schistosomiasis affected areas in Africa (Adenowo *et al*., 2015). Attempts to measure the economic impact of schistosomiasis from loss of working capacity, disability and public health funding have been futile due to underestimation of many parameters made due to lack of accurate statistics (Sady *et al*., 2013).

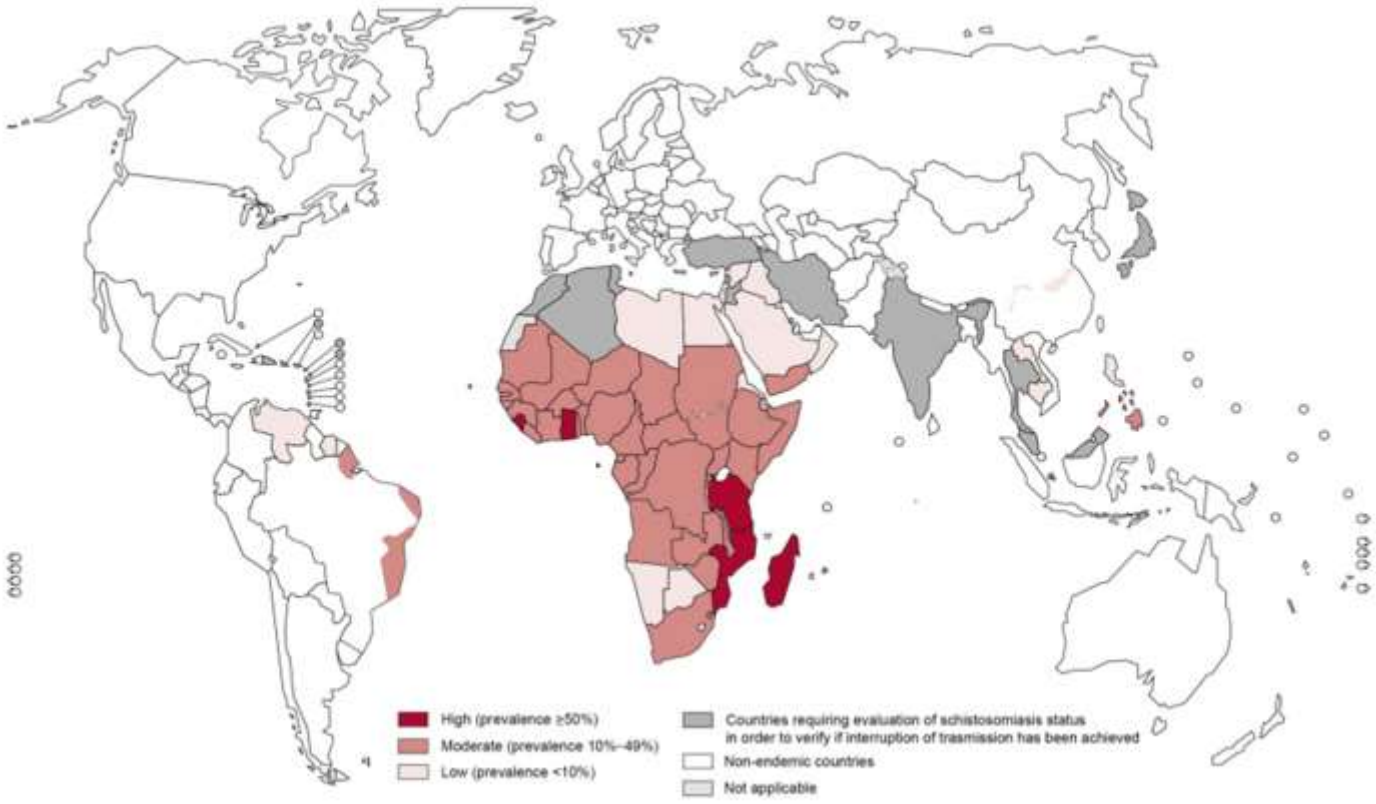


Figure 2.1: Worldwide distribution of schistosomiasis. Adapted World Health Organization online resource: http://gamapserver.who.int/mapLibrary/ [Accessed 19/03/2018]

In most cases individuals in schistosomiasis endemic areas are also co-infected with other parasitic diseases such as hook worm and malaria.

2.1.2 Schistosoma life cycle

Schistosoma species have a complex life cycle (Figure 2.2) that has multiple hosts, with a series morphological and biochemical conversions between: the intermediate snail host, two free-swimming aquatic larval forms, and a warm-blooded mammalian host (Figure 2.2) (Jolly *et al*., 2007). Humans are the only common host, in the inter-host pathway of *Schistosoma* species; thus, posing a challenge for the control of the disease. Humans acquire schistosomiasis by getting into contact with *Schistosoma* skin-penetrating larvae-contaminated waters during occupational activities. Most populations were schistosomiasis is prevalent rely on agriculture and fishing for their livelihood. The general life cycle of *Schistosoma* species (Figure 2.2) starts with egg-containing urine/stool being deposited into water. The egg hatches and releases miracidium. The miracidium then infects freshwater snail, which divides inside the snail and transforms into numerous sporocysts which further divide into hundreds of cercariae. The cercariae escape the snail and swim to find and penetrate the skin of a mammalian host. Each *Schistosoma* species has a limited snail host range; hence, the transmission is dependent on host snail habitat (Colley and Secor, 2014). In humans the larva accesses the circulatory system and ends up as a young adult in the portal vessels in the liver. The male and female worms pair up for the rest of the life cycle in humans. They migrate downstream to the bladder or small intestines. The female lays eggs, which are secreted via urine or stool (Abdalla *et al*., 2002).

2.1.3 Pathogenesis of Schistosomiasis

Morbidity due to schistosomiasis infection is characterised by three stages; migratory (cercarial dermatitis and swimmer's itch), acute (katayama syndrome) and chronic (organ specific) schistosomiasis. Clinical manifestations of schistosomiasis are due to eggs trapped in the host tissue. The eggs secrete antigens, which initiate granulomatous host immune response characterised by lymphocytes which produce T-helper-2 cytokines, eosinophils and activated macrophages (Pearce and MacDonald, 2002). The process of granuloma formation induces chronic inflammation leading to tissue damage (Peterson and von Lichtenberg, 1965). Pathology associated with chronic schistosomiasis has a wide range of clinical manifestations which are

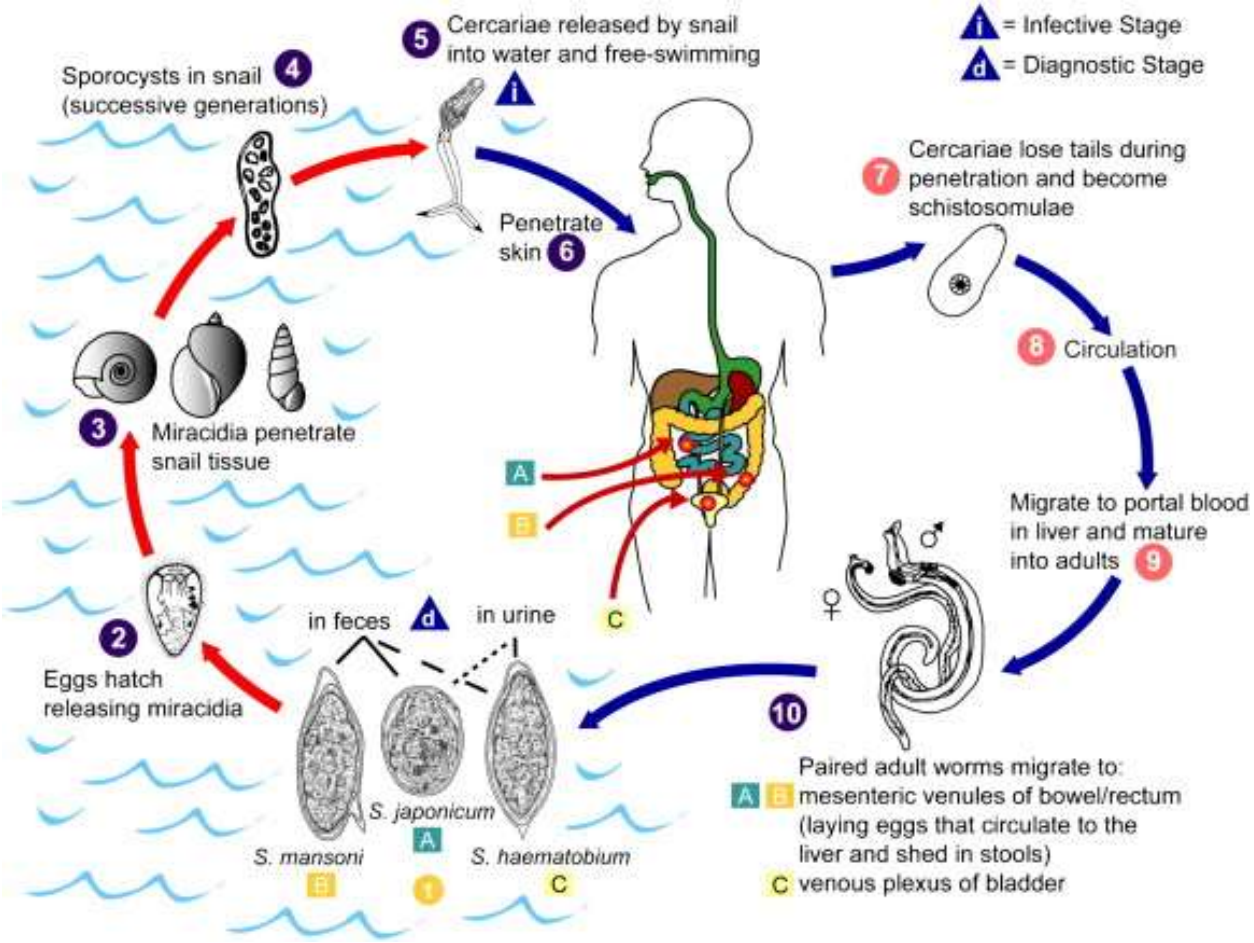


Figure 2.2: Schistosomiasis life-cycle. The stages are denoted by numbers (1) elimination from the host as egg (diagnostic stage) (2) miracidia hatching, (3) infection intermediate hosts freshwater snail, (4) Sporocysts multiply within snails, (5) release of cercariae into water (infective stage), (6) skin penetration infecting human host, (7) schistosomulae development, (8) circulation in human host, (9) maturation within portal vasculature, and (10) paired adult worms migrate to target organs. Adapted from the Centre for Disease Control and Prevention online resources: http://www.dpd.cdc.gov/dpdx [Accessed 19/03/2018].

species-dependent such as genital lesions, bladder, calcification of tissues, bloody diarrhoea and urinary tract infections (Wami, 2015) . Childhood development is severely affected by repeated schistosome infection, which compromises the immune system (Jordan et al., 1993). In female's genital schistosomiasis causes infertility, menstrual disorders and dyspareunia. This is due to *Schistosoma* eggs that find their way to the genital region causing granulomas in the uterus. During pregnancy, *Schistosoma* infection alters the uterine environment leading to severe anaemia, low birth weight infants and increased maternal and infant mortality rates. Tissue damage can lead to susceptibility of infection and co-infection by bacterial and viral infections such as HIV in genital manifestations of schistosomiasis (Mazigo *et al*., 2014). The nature of the host immune response, is the determinant of pathological changes associated with schistosome infections; hence, determining severity of the infection (Ressurreição *et al*., 2016).

2.1.4 Treatment of schistosomiasis

Praziquantel, a pyrazinoisoquinoline derivative, is the first line of defence against all forms of schistosomiasis. However, the mode of action of the drug is not understood. It is the primary basis for schistosomiasis control worldwide (Doenhoff *et al*., 2009). Praziquantel is highly effective with cure rate of 75-82% after 6-8 week upon initial treatment with tolerable side effects (Reich *et al*., 1998). Praziquantel is effective against adult worms. But has poor activity against immature schistosome larvae. Therefore, there is high risk of re-infection, which calls for rounds of treatment for control of schistosomiasis (WHO, 2013). The drug affects the physiology and morphology of the schistosomes, by altering intracellular voltage-gated calcium ion (Ca^{2+}) levels in the adult worm. The exposure of schistosomes to praziquantel disrupts the calcium transport, thereby triggering rapid and sustained contraction of the worm's tegument. This exposes schistosomes surface antigens of the worm to attack by the host immune system (Doenhoff *et al*., 2008). Efficacy of praziquantel is reliant on the presence of mature antibodies to act against the parasite (Harnett and Kusel, 1986). Praziquantel has managed to reduce the prevalence of schistosomiasis in humans in the endemic areas such as China, Japan and Tunisia. However, it fails in reducing new infections and transmission (Zhou *et al*., 2005). Humans are the most common host for schistosomes, therefore persisting snail populations cause cycles of re-infection.

Metrifonate and oxamniquine are two other drugs that have been used to treat schistosomiasis. However, due to lack of efficacy against all *Schistosoma* species, high cost, low efficacy and low operational convenience. Praziquantel remains a drug of choice for the treatment of schistosomiasis. Currently Bilhvax and Sm14 are schistosomiasis vaccines that have made it to the clinical trials (Ricciardi and Ndao, 2015). Extensive use of praziquantel with a poorly understood mode of action has called for the search for alternative drugs. Resistance against praziquantel is a legitimate concern since the drug has been used since the 1970's. In a study in Senegal by Southgate (1997) , praziquantel showed a reduced cure rate against *S. mansoni* (36%) compared with the expected 90% cure rate. In a mass schistosomiasis treatment in Egypt 1.6% of the treated population sample showed no sign of treatment by passing viable eggs thus high doses were required for effective treatment (Ismail *et al*., 1996). In Senegal and Egypt, *S.mansoni* has been observed to have reduced sensitivity to praziquantel. However, resistance has not been established at significant rates. Resistance against praziquantel has been induced and established in laboratory conditions (Fallon and Doenhoff, 1994; Ismail *et al*., 1994).

2.2 Oxidative stress in Schistosoma

Schistosoma species undergo extensive physiological and morphological changes, which are accompanied by production of reactive oxidative species. Upon entry into the human host, *Schistosoma* elicits host immune response. The host defence is mediated by reactive oxidative species against *Schistosoma*. Hence, they need to possess efficient detoxification systems for survival. Three anti-oxidant enzymes are expressed by *Schistosoma* species namely; glutathione peroxidase, superoxide dismutase and GST (Zelck and Von Janowsky, 2004). Anti-oxidant systems in *Schistosoma* are limited. Thus, these three enzymes are critical for survival of schistosomes with limited salvage pathways for detoxification (Zelck and Von Janowsky, 2004). Glutathione peroxidase is involved in hydrogen peroxide detoxification via glutathione oxidation (Arthur, 2001). Superoxide dismutase is responsible for the dismutation of toxic superoxide radicals into oxygen and hydrogen peroxide via oxidative metal potentials (Mkoji *et al*., 1988). GSTs are involved in the conjugation of electrophilic xenobitic compounds with GSH. GSTs also neutralise reactive oxidative species from lipid peroxidation, which act on cell membranes (Zelck and Von Janowsky, 2004). This links GST with the membrane, suggesting that it might be involved in parasite defence against host immune response (Braschi *et al*., 2006). Mechanisms in

Schistosoma detoxification remain unclear, despite relevance to drug development and drug resistance. These may be exploited for rational drug design to sensitise the parasite for the host immune defence mechanism leading to elimination of schistosomiasis.

2.3 Helminth glutathione S-transferases

GSTs are a major class of multifunctional enzymes found across aerobic organisms' kingdoms. GST are involved detoxification by conjugating GSH with a wide range of electrophilic xenobiotic compounds (Mannervik *et al*., 1988; Oakley *et al*., 1999). GSTs also have non-catalytic functions, such as intracellular transport of hydrophobic ligands (Bhargava *et al*., 1978). Helminths have a limited number of detoxification enzymes and lack the cytochrome P-450 detoxification mechanism present in humans (Brophy and Barrett, 1990). GSTs have been found in all helminth species suggesting critical role in homeostasis and survival. Helminths express more cytosolic GSTs than microsomal GSTs and few secretory GSTs (Brophy and Pritchard, 1994). Level of expression and activity of GST is species-dependent. However, helminths with a naked tegument seem to have higher GST activity (Brophy, 1988). Twelve different classes of cytosolic GST have been identified and classified namely; Alpha, Beta, Delta, Mu, Phi, Pi, Theta, Kappa, Sigma, Tau, Omega and Zeta. Classification is based on primary and tertiary structure similarities, immunological identity, kinetic and substrate/inhibitor specificity (Sheehan, 2001). GSTs are dimeric proteins with a molecular weight of around 50 000 Da. A representative structure for each class has been solved using crystallography, which shows all classes have a similar structural fold despite varying primary structures (Mannervik *et al*., 1988). Non-mammalian GSTs exhibit unique biological activity when compared with mammalian GSTs such as regeneration of *S*-thiolated proteins, conjugation of GSH with endogenous ligands, involvement in metabolic pathways other than detoxification and removal of reactive oxygen species (superoxide radical and hydrogen peroxide). This functional diversity is due to the properties of the thiol group that participates in redox transitions, thiol exchange reactions, thioether formation, and radical scavenging (Graminski et al.,1989)

2.4 Schistosoma japonicum glutathione S-transferase

Schistosoma japonicum GST (SjGST) has two isoenzymes of molecular weight 26 000 Da and 28 000 Da, which are primary detoxification enzymes in the parasite (McTigue *et al*., 1995a). The SjGST 26-kDa isoenzyme has been extensively studied. All information will be based on this isoenzyme. Each subunit of SjGST contains 218 amino acids which fold to form two distinct domains: N-terminal domain (residue 1-78) which contains three alpha helixes and four anti-parallel beta sheets, this domain is referred to as the thioredoxin fold (Figure 2.3) (McTigue *et al*., 1995b). The thioredoxin fold forms the hydrophobic core of SjGST based on the helix packing. This fold has been shown to facilitate hydrophobic collapse of GST hence, detecting the folding mechanism (Martin, 1995). The N-terminal domain contains the catalytic glutathione binding site "G-site" (Lim *et al*., 1994). The larger C terminal domain (residue 85-218) contains five alpha helixes and an extended coil (residue 195-218). The C terminal domain contains the "H-site", which binds to hydrophobic substrates. The H-site is highly diverse which renders the binding site with an extensive range of possible substrates. The binding affinity and catalytic efficiency for the different compounds vary in GST classes (Torres and Landa, 2008). SjGST contains sequence synonymous with SNAIL/TRAIL in mammals, which is another determinant in GST classification. The two domains are linked by a short sequence (residue 77-84) (McTigue *et al*., 1995b). The SjGST fold is similar to known GST structures; however, it contains a distinct loop (residue 33-41) (McTigue *et al*., 1995b). The G-site is highly specific than the H-site, however the two sites work together to promote GSH conjugation of electrophilic substrates. A functional SjGST contains two subunits, this dimeric form is critical for stabilising the tertiary structure of the enzyme (Figure 2.3). The dimer interface is leads to the formation of a unique long and narrow non-substrate binding site (L-site) (McTigue *et al*., 1995b). The ligandin binding site "L-site" is poorly understood among GST families because of limited information on the structural, thermodynamic and ligandin function. The structural differences specifically the L-site and G-site, suggest that SjGST belongs to a new class of GSTs. Even though SjGST is classified under Mu-GST, SjGST does not contain the loop between β2 strand and α2 helix, which is a property of Mu-GST isoenzymes (McTigue *et al*., 1995a). Kinetic properties of SjGST and parasites GST are generally understudied. Available sources have multiple variations; hence, not comparable. Studies on SjGST have been done using GSH for G-site and 1-chloro-2,4-dinitrobenzene (CDNB) for the H-site. SjGST has a higher affinity for GSH compared to CDNB (Torres and Landa, 2008).

GSTs are bi-substrate enzyme, the order and mode of substrate interaction is dependent on the GST isoform. Unlike other cytosolic GSTs that exhibit random order of substrate binding, rat liver alpha-GST and SjGST preferentially bind to GSH. SjGST displays random sequential single-displacement mechanism (Stefanidis et al., 2018). SjGST is a structurally unique GST expressed in all stages of the *Schistosoma* life cycle. Therefore, it is a suitable chemotherapeutic target for the treatment of schistosomiasis.

2.5 Enzyme inhibition

Enzymes are biological catalyst with high substrate specificity and tight regulation (control). Therefore, enzymes are good therapeutic targets because they modulate cellular activities (Kraut *et al*., 2003). On the other hand, inhibitors have a direct effect on the enzyme target. Therefore, can act as catalytic controls which can be used to study the mode of enzyme action. Development and characterisation of inhibitors to regulate the enzyme activity are very important for disease treatment. Inhibitors have been used in the classification of different GSTs (Mannervik *et al*., 1988; Sheehan *et al*., 2001). Therefore, an inhibitor can be used to give insight on the catalytic mechanism, binding topology, contributions and requirements of substrates for catalysis by SjGST. Enzyme assays are used to study enzyme activities, they are used to determine the rates of enzyme-catalysed reactions and play crucial importance in understanding enzyme kinetics and enzyme inhibition studies. GSTs catalyse a wide range of reactions in the cell. GST is usually studied using the GSH/CDNB (1-chloro-2,4-dinitrobenzene) conjugation reaction is commonly used for assaying GST enzymatic activity. In this study SjGST activity relates to the activity of SjGST based on the GSH/CDNB conjugation assay.

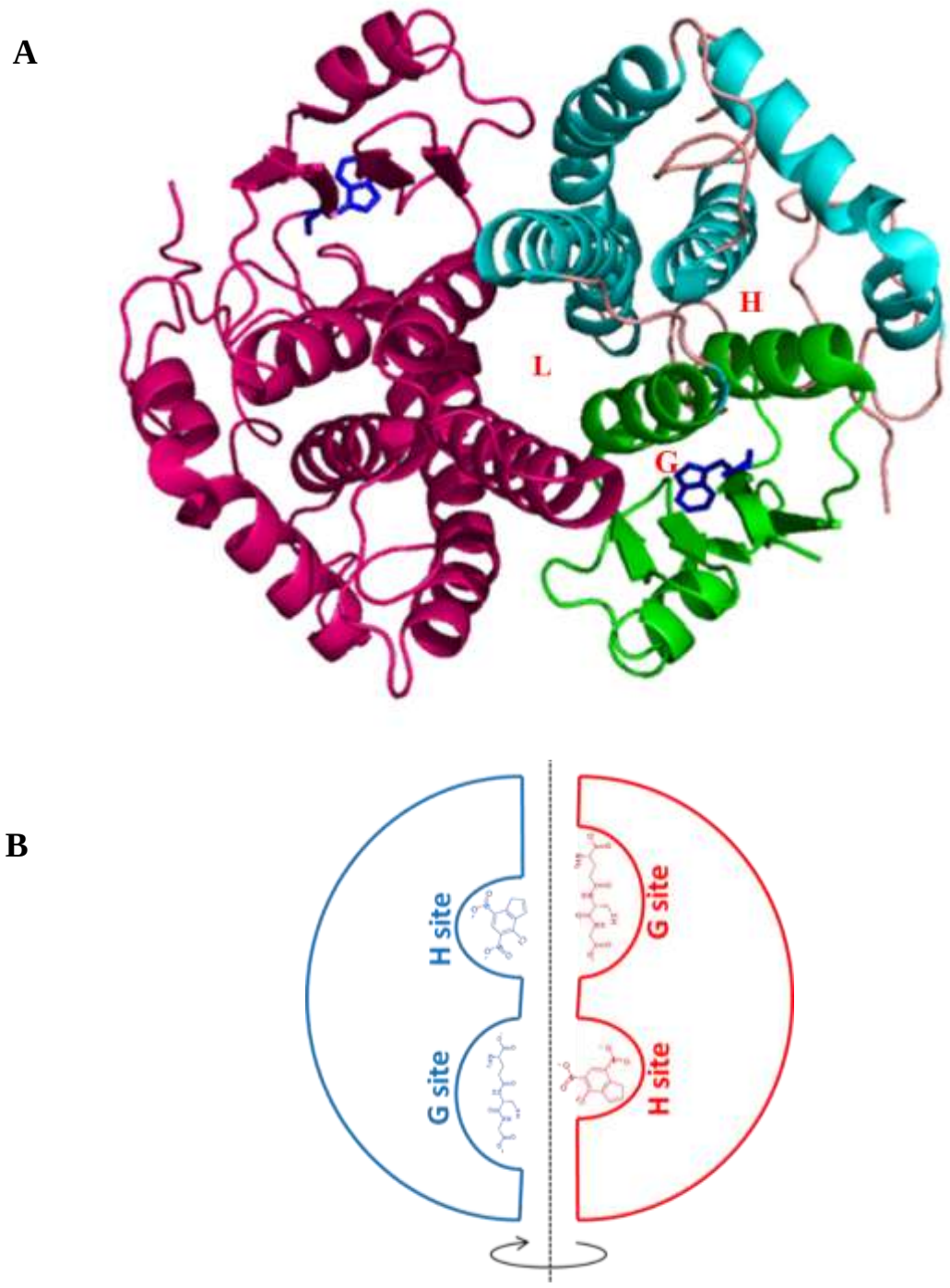


Figure 2.3: Structure of *S. japonicum* GST. (A) Ribbon diagram of the crystal structure of dimeric structure of SjGST viewed down the crystallographic 2-fold axis of the dimer. One subunit is in magenta and the other is showing the two domains: Domain I (green) and Domain II (blue). Trp 7 is shown in blue. The letters represent: G-site (G), H-site (H) and L-site (L). The figure was generated using PyMol and PDB file 1DUG (Ware *et al*., 1999). **(B)** Schematic representation of SjGST showing the G-site and H-site.

2.6 Enzyme inhibition kinetics

Enzyme kinetics is mathematical description of factors affecting enzyme catalysed reactions. Enzyme assays are used to study enzyme activities, in which kinetic parameters are derived to study enzyme behaviour. Leonor Michaelis and Maud Menten were the first to interpret enzyme kinetics with their classic Michaelis-Menten kinetics (Michaelis and Menten, 1913). Michaelis-Menten equation is the commonly used mathematical model for enzyme kinetics. It is based on a reaction of an enzyme (E) with one active site acting on one substrate (S). In this reaction, the enzyme and substrate are in equilibrium with the ES complex, which can proceed to form the product (P) or revert back to free enzyme and substrate. With the assumption that the product formed does not affect the equilibrium when the initial rate is measured (steady-state conditions), the reaction follows the pathway in Equation (1):

$$E + S \underset{k_{-1}}{\overset{k_1}{\rightleftarrows}} ES \xrightarrow{k_2} E + P \qquad (1)$$

were k_1, k_{-1} and k_2 are rate constant for each step, these are used define the Michaelis-Menten constant K_M Equation (2):

$$K_M = \frac{k_{-1} + k_2}{k_1} \qquad (2)$$

where K_M is the Michaelis-Menten constant. The prerequisite of the model is that, the enzyme is not allosteric and [E] << [S]. The K_M value is unique for each enzyme and varies with a given substrate. This parameter it is obtained using Equation (3):

$$V_0 = \frac{V_{max}[S]}{K_M + [S]} \qquad (3)$$

where V_0 is initial velocity which relates to substrate concentration [S] and V_{max} is maximum reaction velocity. The hyperbolic plot of the Michaelis-Menten equation (Figure 2.4A), K_M is the substrate concentration when the reaction velocity is half of V_{max}.

There are challenges in obtaining kinetic parameters K_M and V_{max} directly from the hyperbolic Michaelis-Menten plot because reaction velocity tends to increase with [S] while approaching V_{max}

asymptotically. Lineweaver-Burk equation is one of the strategies used to linearize Michaelis-Menten equation (Figure 2.4B) for easier determination of K_M and V_{max} (Equation 4):

$$\frac{1}{V_0} = \left(\frac{K_M}{V_{max}}\right)\frac{1}{[S]} + \frac{1}{V_{max}} \quad (4)$$

Inhibitors are molecules that bind to enzymes and prevent efficient enzyme catalysis. There are two types of inhibitors: irreversible and reversible inhibitors (Saboury, 2009). Irreversible inhibitors bind to enzymes in a permanent manner through the formation of covalent bonds altering the enzyme (active site) chemical structure. The binding site of the irreversible inhibitor is usually away from the active site altering the position of the enzyme catalytic residues; hence, reducing or halting enzyme efficiency (Saboury, 2009). A reversible inhibitor is categorised in to four classes namely: competitive, uncompetitive, non-competitive and mixed. Inhibitors bind to enzyme via noncovalent interactions such as hydrogen bonds, electrostatic and hydrophobic interactions. Competitive inhibitors are usually analogues of the substrate and they bind in the active site of the enzyme. The binding affinities of the competitive inhibitors vary; hence, the extent of inhibition varies with different competitive inhibitors. Since the competitive inhibitor competes for the same site as the substrate, increasing substrate concentration reduces inhibition (Segel, 1975). This increases the chance of enzyme-substrate interaction rather than enzyme-inhibitor interaction. In competitive inhibition, the enzyme takes longer to reach V_{max}, and K_M increases to a higher substrate concentration (Figure 2.5A). In uncompetitive inhibition, the inhibitor binds to the enzyme-substrate complex. Inhibitor binding site is made available by the conformational change of the enzyme upon binding to the substrate, forming an inactive enzyme-substrate-inhibitor complex (Segel, 1975). Increasing substrate concentration alleviates degree of inhibition. However, in this case K_M and V_{max} are reduced depending on the characteristics of the inhibitor (Figure 2.5B).

K_M is unchanged because the enzyme affinity for the substrate is conserved, while V_{max} is decreased. Increasing substrate concentration does not relieve inhibition (Figure 2.5C). Mixed inhibition is a special type of inhibition, where the inhibitor binds to a different site that is not the

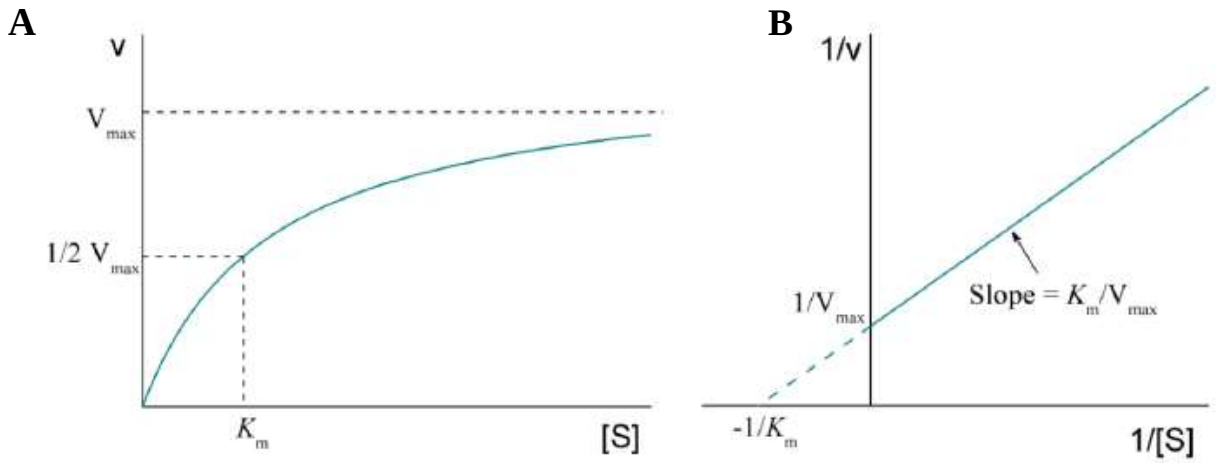


Figure 2.4: Enzyme kinetics graphs. (A) Michaelis-Menten equation graphical plot of reaction velocity (v) against substrate concentration [S]. **(B)** Lineweaver-Burk graphical plot of 1/v against 1/[S]. K_m and V_{max} can be determined directly by the intersection on the *x*-axis and *y*-axis respectively. In both cases enzyme concentration is kept constant. Adapted from Jiang (2013).

active site. However, binding of both the substrate and the inhibitor influences the binding of the other. This type of inhibition is not a mixture of the types of inhibition; rather the substrate and K_M is unchanged because the enzyme affinity for the substrate is conserved, while V_{max} is decreased. Increasing substrate concentration does not relieve inhibition (Saboury, 2009) (Figure 2.5C).K_M and V_{max} are both altered depending of the inhibitor/substrate interaction (Figure 2.5D). Mixed inhibition is particularly important for GST since they have an additional binding site, which allows for binding of other molecules besides GST substrates (van Bladeren and van Ommen, 1991). Lineweaver-Burk plots in the presence of different inhibitor concentrations helps to determine the mode of enzyme inhibition. The understanding of enzyme kinetic parameters is derived from graphical profiles rather than the actual numerical derivations from the kinetics graphs. Thermodynamics and binding kinetics parameters and binding kinetics parameters and binding kinetics parameters are a better strategy in the qualitative analysis of enzyme inhibition.

2.7 Molecular docking

Molecular docking is a theoretical tool used to study the structure of molecular recognition events *in-silico*. Docking is of importance for rational drug design because it enables prediction of molecular organisation of protein-ligand complexes (Sousa *et al*., 2006). It is a useful tool since there is a limited number of protein crystal structures bound to desired ligand. Docking acts as a measure to identify leading molecules (virtual screening) for drug design; thus, saving time and money. Docking has become a standard prerequisite for drug discovery (Chaudhary and Mishra, 2016). Docking programs typically have three key components: depiction of the binding site, algorithm for conformational search which generates binding poses and an affinity prediction using scoring functions. There are a number of docking software available in the market such as AUTODOCK, GLIDE, FLexX, ICM, DOCK and CHARMM to mention a few. The aim of molecular docking is to firstly determine the lowest energy conformation of: (1) ligand

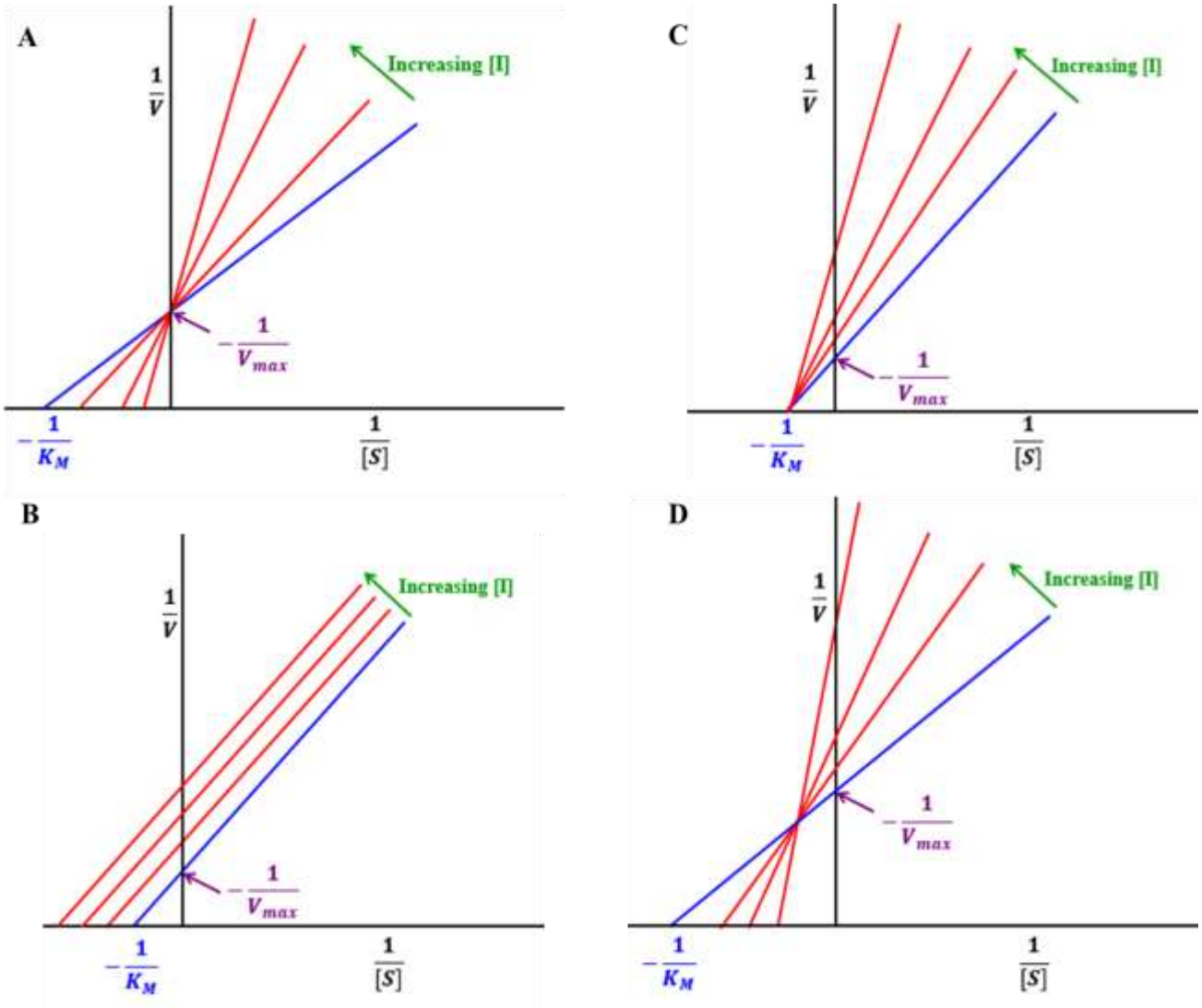


Figure 2.5. Enzyme inhibition kinetics graphs. Lineweaver-Burk plots representing different types of inhibition. Plots of 1/v against 1/[S] in the absence and in the presence of different inhibitor concentrations: **(A)** Competitive inhibition, **(B)** Uncompetitive **(C)** Non-competitive **(D)** Mixed.

.

conformation in the active site and (2) protein-ligand complex. Secondly, assess (score) the ligand orientation in the protein binding site. Advancement of this technique has allowed to be a reliable method to study protein-ligand complexes, one being the ability to dock a fully flexible ligand to a protein (which was not possible previously) (Carlson, 2002a). Protein crystal structures used for docking are rigid, however proteins are realistically non-static. To achieve protein flexibility in molecular docking is computationally expensive, in most cases it cannot be resources to achieve this are not available. Therefore, it is a better strategy to allow for flexibility of the ligand at least to explore possible binding conformations in the static protein binding site during docking (Teague, 2003). There are challenges that are associated with protein and/or ligand flexibility, including providing binding site for a non-binding ligand, increased protein affinity for ligand and determination of multiple minimised protein energy states (Carlson, 2002a). Current docking tools have incorporated induced fit and lock-and-key mechanism to counter for protein flexibility (Sherman *et al*., 2006). There are a number of limitations with docking such as the absence/inaccurate cellular solvent, rigid binding site and inherent software errors (Sousa *et al*., 2006).

2.8 Scoring of molecular docking

Scoring functions are used to predict binding affinity of the protein and ligand (Sousa *et al*., 2006). There are three classes of scoring functions force field based, knowledge based and empirical based (Liu and Wang, 2015). Scoring is a critical step in docking, which enable to distinguish the true binding site from the alternative binding sites and/or between random and active compounds. Scoring functions examine protein-ligand interactions, which are driven by a number of non-covalent interactions such as hydrogen bonding, ionic interactions, van der Waals forces and hydrophobic packing. In most docking studies, solvents are excluded from docking due high number of degrees of freedom for solvent molecules. These are accounted for in some scoring functions after docking (Wong and Lightstone, 2011). Rigorous analysis binding conformations. Exhaustive analysis of the scoring functions comes with the demand of high computational power, in most cases this may not be feasible with available computational power. Therefore, scoring functions are oversimplified and many assumptions are made for less tedious and cheaper work hence compromising accuracy and speed of ligand docking (Tame, 2005). Different scoring functions can be used to satisfy the need for the research question at hand. Scoring functions rank

the protein-ligand complexes giving an indication of which protein-ligand conformation is favourable. Depending on the research question one can make use of the ranking suitable for their study. The highest ranked conformation should be the closest to the crystallographic structure with lower root-mean-square deviation of atomic positions (RMSD). However, in some cases the crystallographic structures are not available for comparison purposes (Alfarano, 2010).

2.9 Theoretical binding affinity

Molecular docking and scoring provide the most energy minimised protein-ligand complex however, lack in binding affinity prediction. This is because molecular docking only provides affinities based on single protein-ligand complex and does not account for protein flexibility (Srivani *et al*., 2007). Trade off of speed and physical accuracy in docking makes it rarely accurate to predict binding affinity. Therefore, molecular docking fitness requires to be replaced by thermodynamic parameters which account for appropriate binding contributors. Binding energy calculations are done using alternative scoring functions. Molecular docking is a pre-requisite for all binding affinity predictions by providing starting structures to determine free energy of binding. There are various post-processing methods used to estimate free energy of binding such as linear interaction energy analysis, free-energy perturbation, thermodynamic integration molecular mechanics Poisson−Boltzmann surface area (MM-PBSA) and the molecular mechanics generalized Born surface area (MM-GBSA) (Srivastava and Sastry, 2012). MM-PBSA and MM-GBSA are the commonly used functions due to lower demand in computational power. They estimate free energy of binding from changes in configurational entropy, solvation free energy and gas-phase energy upon protein-ligand complex formation. MM-PBSA and MM-GBSA also have a robust sampling of physical and conformations of the ligand and protein. Hence, they take longer to process and need more computational power compared to normal docking. MM-PBSA and MM-GBSA protocols generates characteristic bound and unbound structures in explicit solvent using molecular mechanics simulations or by energy minimisation of a protein-ligand complex. The aim is to compare average enthalpy of bound and unbound states, thereby estimating the change in binding enthalpy. Water is removed during the process and the binding free energies and enthalpies are assessed using known (Poisson-Boltzmann or Generalized Born) representation of water. Binding free energy estimate accounts for the change in solvation free energy and the enthalpy change using the explicit solvent (Mobley and Dill, 2009). MM-GBSA is the preferred

method for estimating binding affinity than MM-PBSA in most cases, since it has been shown to produce better affinity determination results (Hou *et al*., 2010).

CHAPTER III

MATERIALS AND METHODS

3.1 Materials

Glycerol stock of *Escherichia coli* T7 cells transformed pGEX-4T-1 (Figure 3.1) encoding SjGST was a gift from Blessing Oyiogu. Yeast extract, tryptone, isopropyl thioglucopyranoside (IPTG), ampicillin, imidazole, Tris, glycerol, β-mercaptoethanol, Tris, Tricine, Coomassie Brillant Blue R-250, Urea, 8-Anilinonaphthalene-1-sulfonic acid (ANS), CB3GA, Na_2HPO_4, (Ethylenedinitrilo)tetraacetic acid (ETDA), Dithiothreitol (DTT) and Sodium chloride (NaCl) were supplied by Sigma Aldrich. Electrophoresis casting apparatus purchased from Bio-Rad. *Escherichia coli* T7 competent cells were from (New England Biolabs)

3.2 Methods

3.2.1 Plasmid construct

Expression vector pGEX-4T-1 was not modified since it contains *S.japonicum* GST as a fusion tag for protein expression. Crystal structure of native SjGST matches that of recombinant SjGST from pGEX vectors (McTigue *et al*., 1995a). Recombinant SjGST from the vector contains a nine residue peptide at its C-terminus. Expression of SjGST is under the control of an IPTG inducible tac promoter. No background expression has been observed under the tac promoter which is a hybrid of the lac and trp promoter (De Boer *et al*., 1983) and confers ampicillin resistance to cells transformed with pGEX-4T-1.Vector plasmid map is shown in Figure 2.1.

3.2.2 Overexpression

Overnight culture was prepared by inoculating 10 µl of SjGST glycerol stock to 100 ml of 2×YT media [1.6% (w/v) tryptone, 1% (w/v) yeast extracts and 0.5% (w/v) NaCl] supplemented with 100 µg/ml of ampicillin and 30 µg/ml chloramphenicol. The solution was incubated overnight at 37°C 230 rpm in Excella® E24 benchtop incubator shaker. Overnight cultures were diluted 1:50 with fresh 2×YT supplemented with ampicillin and chloramphenicol to a final concentration 30 µg/ml and 100 µg/ml respectively. The flasks were incubated at 37°C at 230 rpm in a shaker. Growth of the cells was monitored by measuring optical density at 600 nm (OD_{600}) using Jasco V630 spectrophotometer. At OD_{600} of 0.5, the culture was incubated on ice for 15 min. Overexpression of SjGST was induced by addition IPTG to a final concentration of 0.25 mM.

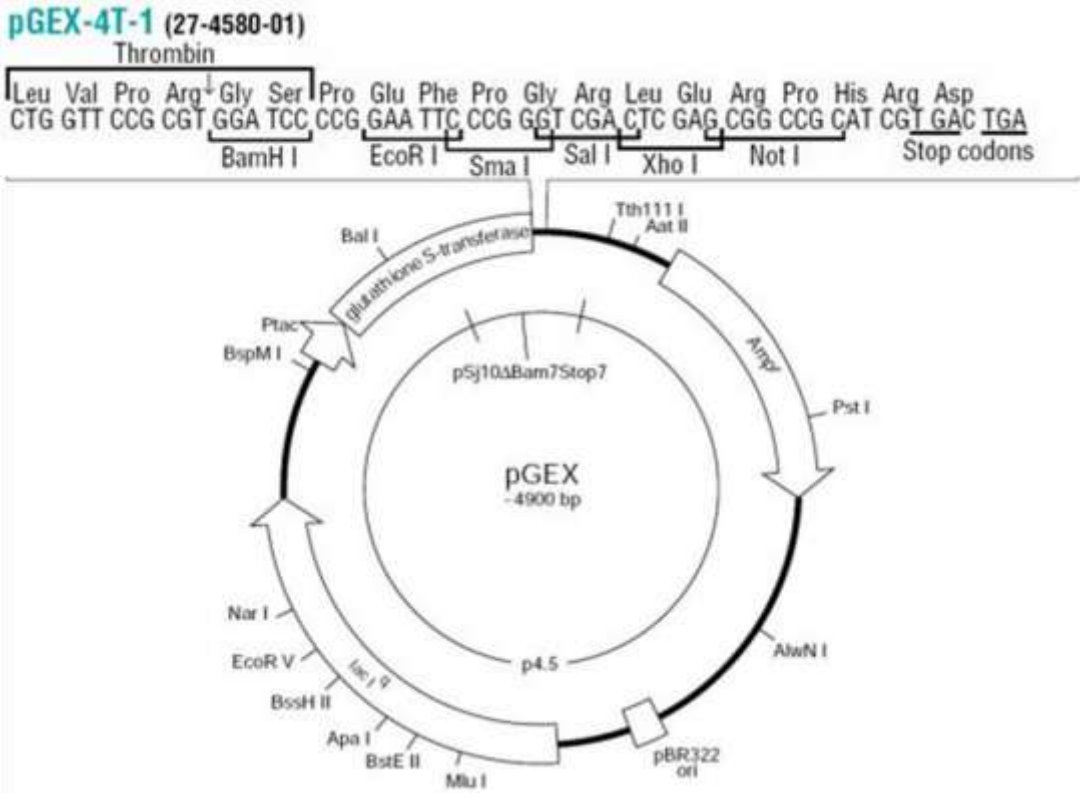


Figure 3.1: **Map of pGEX-4T-1 vector.**

The flasks were then incubated at 30°C at 230 rpm in a shaker for 6 h. These conditions were advised by pGEX 4T-1 supplier (G.E. Healthcare, U.S.A.)

Bacterial cells were harvested by centrifugation at 5000×*g* for 30 min at 4°C. Supernatant was discarded and the cells were re-suspended in resuspension buffer [50 mM Tris-HCl, 150 mM NaCl, 0.1µM phenylmethane sulfonyl fluoride, 0.4 mg/ml lysozyme, pH 7.4]. Pellet obtained from 500 ml of media was re-suspended in 10 ml of resuspension buffer and incubated at -80°C overnight to facilitate cell lysis.

3.2.3 Soluble fraction harvesting

Cells where thawed at 37°C and thereafter cells were then incubated in ice for 1 hour to cool. Sonication was used to lyse the cells at two-minute intervals on ice to avoid overheating. The procedure was done until the cells attained water-like consistency. Based on the findings by Blessing Oyiogu SjGST is soluble after overexpression. The soluble fraction was obtained by centrifugation of lysate at 23000×*g* for 30 min at 4°C. The supernatant and pellet were separated and reserved.

3.2.4 Purification: Glutathione-Agarose affinity chromatography

Affinity chromatography is a method used to separate biological mixtures on the basis of reversible specific biological interactions. The technique uses covalently bound glutathione on solid chromatographic support (agarose) to entrap proteins that can bind to glutathione. GSTs have high affinity for glutathione hence bind to the matrix isolating GSTs from other proteins. GSTs have higher affinity for free reduced GSH compared to immobilised GSH leading to the elution of GST-GSH complex. Glycine at very low pH (2-3) or high pH (9-11) can be used to elute GSTs from GSH-agarose column by disrupting hydrogen bonding, ionic and hydrophobic interactions between immobilised GSH and GSTs. Conditions such as pH, temperature, buffer system and type of GST can also affect the efficacy purification. Advantage of using affinity chromatography is the reversibility of the binding of the binding partners hence this serves as an ideal method to separate the protein of interest.

In this experiment a 20 ml GSH-agarose column was connected to the automated ÄKTAprime chromatographic system combined to a computer with PrimeView 1.0 software (GE Healthcare, Sweden) for purification. The column was equilibrated with 100 ml of equilibration buffer [50

mM Tris-HCl, 150 mM NaCl, 10% (v/v) glycerol, 0.02% (w/v) NaN_3, pH 7.4]. The supernatant collected from lysing cells was loaded in to the column (40 ml) and was allowed to flow through the column at 2 ml/min. The flow through was collected and kept for analysis in case SjGST did not bind to the column. The column was washed to remove any unbound proteins and weakly bound proteins to avoid contamination of SjGST using 100 ml wash buffer [50 mM Tris-HCl,150 NaCl, 10% (v/v) glycerol, 0.02% (w/v) NaN_3, pH 7.4]. A single step elution was done to elute SjGST using 10 mM glycine-NaOH, pH 10. The elution was monitored at A_{280} and fractions with $A_{280} > 0.5$ were pooled together. The pooled together fractions were immediately dialysed to storage buffer dialysing the protein in storage buffer [20 mM Na_2HPO_4, 1 mM EDTA, 0.02% sodium azide, pH 6.5] at 4°C. SDS-PAGE was used to assess purity and homogeneity of purified SjGST.

3.2.5 Analysis of protein purity using SDS-PAGE

Sodium dodecyl sulfate polyacrylamide gel electrophoresis (SDS-PAGE) is an analytic procedure that enables the separation of bio-molecules based on their molecular weight and their movement in an electric field (Laemmli, 1970). The proteins move through the matrix proportional to molecular weight because presence of SDS gives the molecules an overall negative charge. SDS is an anionic detergent, when heated with protein sample it denatures the protein to elongated conformation. The binding of SDS to protein is proportional to molecular weight with 1.4 g of SDS binding to 1 g of protein. Further denaturation of protein samples is enhanced by the addition of β-Mercaptoethanol, which breaks down disulfide bonds in the protein, hence attaining a more elongated structure. In this experiment a tricine-SDS-PAGE developed by (Schägger, 2006), which has a high resolving capacity compared to the glycine-SDS-PAGE (Laemmli, 1970) was used to analyse the purity of the protein sample and estimate the molecular weight based upon the molecular standards resolved alongside the protein samples.

The gel components were made as follows: Monomer solution [48 g of acrylamide and 1.5 g of bisacrylamide in 100 ml of deionised water], Gel buffer (×3) [3 M Tris, 1 M Tricine, 0.3% SDS (w/v)), anode buffer (×10) 1 M Tris, 0.225 M HCl, pH 8.9], cathode buffer (×10) [1 M Tris, 1 M Tricine, 1% SDS (w/v)) and initiator reagent (10% (w/v) ammonium persulfate]. The reagents were mixed as shown in Table 1:

Table 1: Reagent components of Tricine- SDS-PAGE gel**.**

Reagent	4% staking gel	10% separating gel
Monomer solution (ml)	1	6
Glycerol (g)	-	3
Gel buffer (ml)	3	10
Add Water to final volume (ml)	12	30
Initiator reagent (µl)	90	150
TEMED* (µl)	15	30

*To be added last before casting

The mixture was cast in a 72.5×107.5×1.5 mm^3 and allowed to polymerise. The samples were prepared by mixing reducing sample buffer [12% SDS (w/v), 6% mercaptoethanol (v/v), 30% glycerol (w/v), 0.05% Coomassie blue R-250, 150 mM Tris-HCl, pH 7.0] in a ratio 1:2 with each sample to be analysed, 10 µl of sample loaded to each well. Molecular weight marker (Bio-Rad Precision Plus Protein Standards, All Blue Standards) was loaded on the first lane to estimate the size if the purified protein. Electrophoresis was carried out at 60 V for the first 30 min to allow for effective staking of proteins, thereafter the voltage was increased to 160 V until the tracking dye reached 0.5 mm from the gel edge. The gels were stained with Coomassie stain solution [0.1 % (w/v) Coomassie dye in 1:5:4 (v/v/v) acetic acid-methanol-water solution] for 2 hours. The gels were de-stained using 1:5:4 (v/v/v) acetic acid-methanol-water solution until the unbound stain was removed. The images of the gel where visualised using Bio-Rad Gel Doc™ XR+ System. A pure protein sample will contain no extra bands other than the protein of interest in the gel. A standard curve of Log Molecular weight against R_f will be plotted to estimate the molecular weight of the purified protein.

3.2.6 Protein concentration determination

The concentration of SjGST was determined by using an equation which is an adaptation Beer-Lambert law. Double dilution technique was used to produce concertation factors of 0.1, 0.05, 0.025, 0.0125, 0.00625, 0.003125 and 0.001563. Absorbance of the samples were determined by a JascoV- 630 spectrophotometer at A_{280} and A_{340}. A_{340} was used to check aggregation of the protein. All absorbance readings were corrected using a blank. A linear regression was fitted to the

seven points for $A_{280.}$ The slope of the line was factored into the Equation (5) to determine protein concentration below:

$$Concetration = \frac{Molecular\ weight\ \times slope}{\varepsilon\ \times path\ lenght\ (cm)} \quad (5)$$

were molar extinction coefficient (Ɛ) of 85720 M^{-1} cm^{-1}determined using Protparam algorithm, implemented in Expasy.org (Gasteiger *et al*., 2005) and path length used was 1 cm. All measurements were done at 20°C.

3.2.7 Spectroscopic studies

CB3GAa triazine dye (Figure 3.2) an inhibitor of GSTs. All spectroscopic studies were done in the absence of CB3GA. This is due to the fact that CB3GA interferes with resultant spectra in a concentration dependent manner. The spectra alterations were observed at 10 nM CB3GA concentration.

3.2.7.1 Far-UV circular dichroism

Secondary structure characterisation was done using Far-UV circular dichroism which measures the difference in absorption of left and right circularly polarised light of chiral chromophores, which are optically active or placed in solvents that are optically active. To obtain a CD spectrum, dichroism is measured as a function of wavelength (Kelly and Price, 2000). Far-UV CD is measured at a range 190 to 250 nm at this range, the peptide back bone is the principal chromophore hence giving global secondary structure of the protein. There is a weak but broad n→π* transition at 220 nm and a more intense π→π* transition around 190 nm. These give characteristic far-UV CD spectra which is indicative of secondary structure composition of the protein based on amide bond transitions (Kelly *et al*., 2005). A far-UV CD spectrum gives a trace of the global secondary structure of a protein however it does not quantify α-helical, β-sheet and random coil composition of the protein. Algorithms can be used to quantify secondary

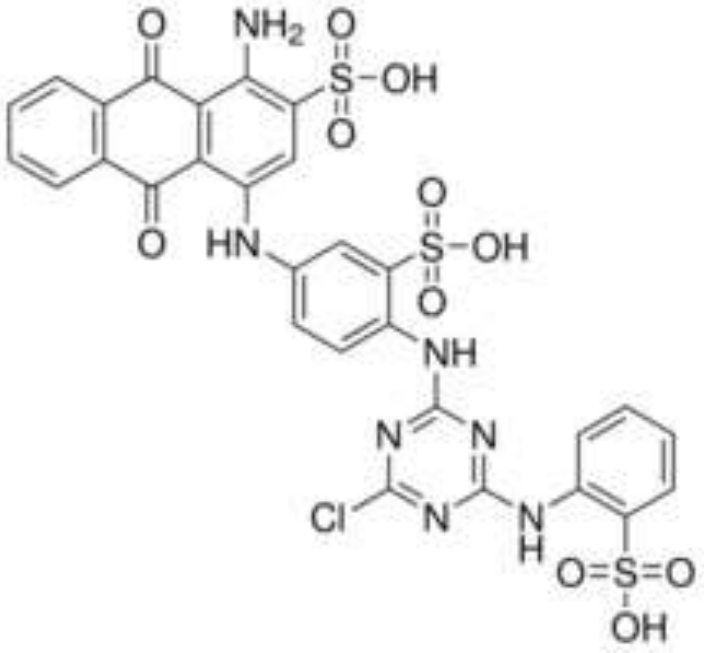


Figure 3.2: Structure of CB3GA.

structural composition of a protein by using data obtained from Far-UV CD such as DICHROWEB (Whitmore and Wallace, 2004). In this study Far-UV CD was used to determine secondary structure profile of SjGST and the actual values of secondary structure composition were determined using DICHROWEB algorithm.

Far-UV CD was done using Jasco J-1500 spectropolarimeter. Protein (native and denatured) concentration used was 3 μM of in 20 mM Na_2HPO_4, 1 mM EDTA, 0.02 % (w/v) sodium azide, 2 mM DTT pH 7.4 and 8 M urea for the denatured protein sample at a range of 190 nm to 250 nm in 0.2 mm quartz cuvette with 1 nm band width, 200 nm/min scan speed and the readings were an average 5 accumulations. The temperature was kept constant at 20 °C using a Peltier temperature control system. The percentage of α-helixes and β-sheets was determined using DICHROWEB algorithm. The values to be used for the plot were corrected by subtracting Far-UV CD of the buffer from the protein. Molar ellipticity per mean residue deg.cm^2.dmol^{-1} was calculated by the Equation (6):

$$[\theta] = \frac{100 \times \theta}{Cnl} \tag{6}$$

where θ is the measured ellipticity in millidegree, C is the protein concentration in mM, n is the number of residues, and l is the path length (cm).

The spectra obtained using Equation (2) is to be submitted to DICHROWEB (Whitmore and Wallace, 2004) server, CONTINLL algorithm implemented to estimate α-helices, β-strands, and β-turns as a fraction of amino acid involved in the formation of each secondary structural component with respect to the amino acids involved in the formation of unordered forms.

3.2.7.1 Intrinsic tryptophan fluorescence spectroscopy

Molecules absorb light this induces the passage of electrons from the single ground electronic level S_0 to an excited state S_n (n > 1). The molecule becomes unstable and should return to a ground state, fluorescence is the emission which results from the lower orbital of paired electrons from an excited singlet state (Lakowicz, 1999). Intrinsic fluorescence spectroscopy arises from the aromatic amino acids tryptophan, tyrosine and phenylalanine. Tryptophan residues are commonly used for most protein fluorescence studies. This is because tryptophan has a higher quantum yield

compared to tyrosine and phenylalanine. Most proteins have a limited number of tryptophan residues therefore act as a better probe. The indoles ring of tryptophan is highly sensitive changes in its micro-environment. This enables the detection of minute changes in the tertiary structure of the protein (Lakowicz, 1999).

Analysis of intrinsic fluorescence was done by preparing 3 μM of protein (native and denatured) in 20 mM Na_2HPO_4, 1 mM EDTA, 0.02% (w/v) sodium azide, 2 mM DTT pH 7.4 and 8 M urea for the denatured protein sample using Jasco FP-6300 fluorescence spectrometer. Tryptophan was selectively excited at 295 nm and emission was monitored at a range of 300-450 nm with scan speed of 200 nm/min using a 1 mm quartz cuvette. Excitation and emission band width filters were set at 5 nm and 2.5 nm respectively. All final readings were an average of three accumulations for each sample. The values used for the plot were corrected by subtracting the fluorescence values of the buffer.

3.2.7.2 Extrinsic ANS fluorescence spectroscopy

8-Anilino-1-naphthalene sulfonate (ANS) (Fig 3.3) is an amphiphilic dye that is used to monitor surface hydrophobicity by binding to hydrophobic surfaces of protein. Upon binding a blue shift in the emission maximum wavelength and an increase of quantum yield is observed when compared to free ANS (Matulis and Lovrien, 1998). Mechanisms of ANS binding to protein is via non-covalent interactions, such as ion pairing between positively charged amino acids (arginine, lysine, histidine) and negatively charged sulfonate group of ANS (Hawe et al., 2008). ANS samples were prepared by dissolving 1g of ANS in 2 ml of 20 mM Na_2HPO_4, 1 mM EDTA, 0.02% (w/v) sodium azide, 2 mM DTT pH 7.4, due to the hydrophobic nature of ANS it was allowed to dissolve in the buffer for 2 hours in a rotator covered with foil, to avoid reaction with light. The concentration of ANS was determined by Beer-Lambert law at 350 nm wavelength using molar extinction coefficient of 5000 $M^{-1}.cm^{-1}$ (Hawe *et al*., 2008). The samples for ANS fluorescence studies were prepared by incubating 3 μM of protein with 100 μM of ANS in 20 mM Na_2HPO_4, 1 mM EDTA, 0.02 % (w/v) sodium azide, 2 mM DTT pH 7.4 for 30 min in the dark. Readings of free ANS were obtained using Jasco FP-6300 fluorescence spectrophotometer.

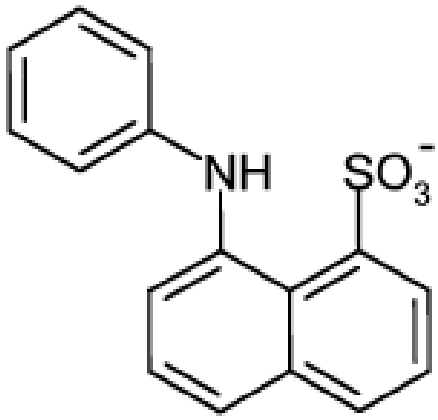


Figure 3.3: **Structure of ANS**

ANS was excited at 390 nm and emission was monitored at a range of 380-600 nm with scan speed of 200 nm/min using a quartz cuvette with 1 cm path length. Excitation and emission band width filters were set at 5 nm. All final readings were an average of three accumulations for each sample. The values used for the plot were corrected by subtracting the values of the buffer.

3.2.8 *Size exclusion high performance liquid chromatography*

Size exclusion high performance liquid chromatography (SE-HPLC) is a technique that separates proteins based on hydrodynamic volume (size), diffusion coefficient and surface properties. The separation is hugely reliant on the inert particles packed into the column. The column matrix has an exclusion limit were molecules with size above the limit will be excluded from the matrix and elute first. However smaller molecules will with in the matrix taking longer time to elute. Hence this is the basis of size exclusion chromatography.

Quaternary structure of SjGST was characterised using SE-HPLC using Phenomenex Gel Filtration /Size Exclusion silica column, Yarra 3u SEC-2000 with Phenomenex SecurityGuard ULTRA guard column. The apparatus was connected to a Shimadzu Prominence HPLC system (SPD20A). The column was equilibrated with filtered and degassed 20 mM Na_2HPO_4, 200 mM NaCl, 1 mM EDTA, 0.02% sodium azide, pH 7.4, flow rate of the system was kept constant at 0.25 ml/min for 30 minutes these conditions were kept for all samples for consistency. Calibration of the column was done by loading Bio-Rad Gel Filtration standards which contain Bovine thyroglobulin (670 kDa), γ-globulin (154 kDa), Ovalbumin (44 kDa), Myoglobulin (17 kDa), Vitamin B12 (1.35 kDa) which were used to plot the standard curve to determine size of the unknown sample. Standards were run each time when the buffer system was changed to account for changes in the system. Analysis of SjGST was done by injecting 20 µl sample of 10 µM SjGST in 20 mM Na_2HPO_4, 200 mM NaCl, 1 mM EDTA, 2 mM DTT, 0.02% sodium azide, pH 7.4. Examination of the effect of oxidation on the structure of SjGST was done in the absence of DTT. A 20 µl sample of 10 µM SjGST in 20 mM Na_2HPO_4, 200 mM NaCl, 1 mM EDTA, 0.02% sodium azide, pH 7.4 was loaded into the column pre-equilibrated with the same buffer. The effect of CB3GA was done by pre-incubating 10 µM of SjGST in 1 mM CB3GAfor 1 hour and loaded in

column pre-equlibrated with 20 mM Na2HPO4, 200 mM NaCl, 1 mM EDTA, 2 mM DTT, 0.02% sodium azide, 1 mM CB3GA, pH 7.4.

3.2.9 SjGST activity assay

GSH-CDNB conjugation assay was used to determine the specific activity of SjGST according to Habig *et al*. (1974). GSTs catalyse conjugation of 1-chloro-2,4-dinitrobenzene (CDNB) to GSH forming chromophoric product 1-(*S*-glutathionyl)-2,4- dinitrobenzene. SjGST activity was monitored at 340 nm by measuring the formation of 1-(*S*-glutathionyl)-2,4-dinitrobenzene with extinction co-efficient of 9600 $M^{-1}cm^{-1}$ using Jasco V- 630 spectrophotometer. The reaction pathway is shown in Figure 3.4. The assay was carried out in 20 mM Na_2HPO_4, 1 mM EDTA, 0.02% (w/v) sodium azide, 2 mM DTT pH 7.4 buffer and recorded at 20°C. The assay had a final concentration of 1 mM GSH and 1 mM CDNB in 3% (v/v) ethanol. SjGST concentration was varied between 0 nm to 50 nm. All reactions were followed as linear progress curves for 60 seconds. All reactions were corrected for by subtracting the non-enzymatic control data from final obtained data. Specific activity ($\mu mol.min^{-1}.mg^{-1}$) was determined using a linear regression slope between initial velocity of complex formation(1-(*S*-glutathionyl)-2,4-dinitrobenzene) ($\mu mol.min^{-1}$) versus protein amount (mg).

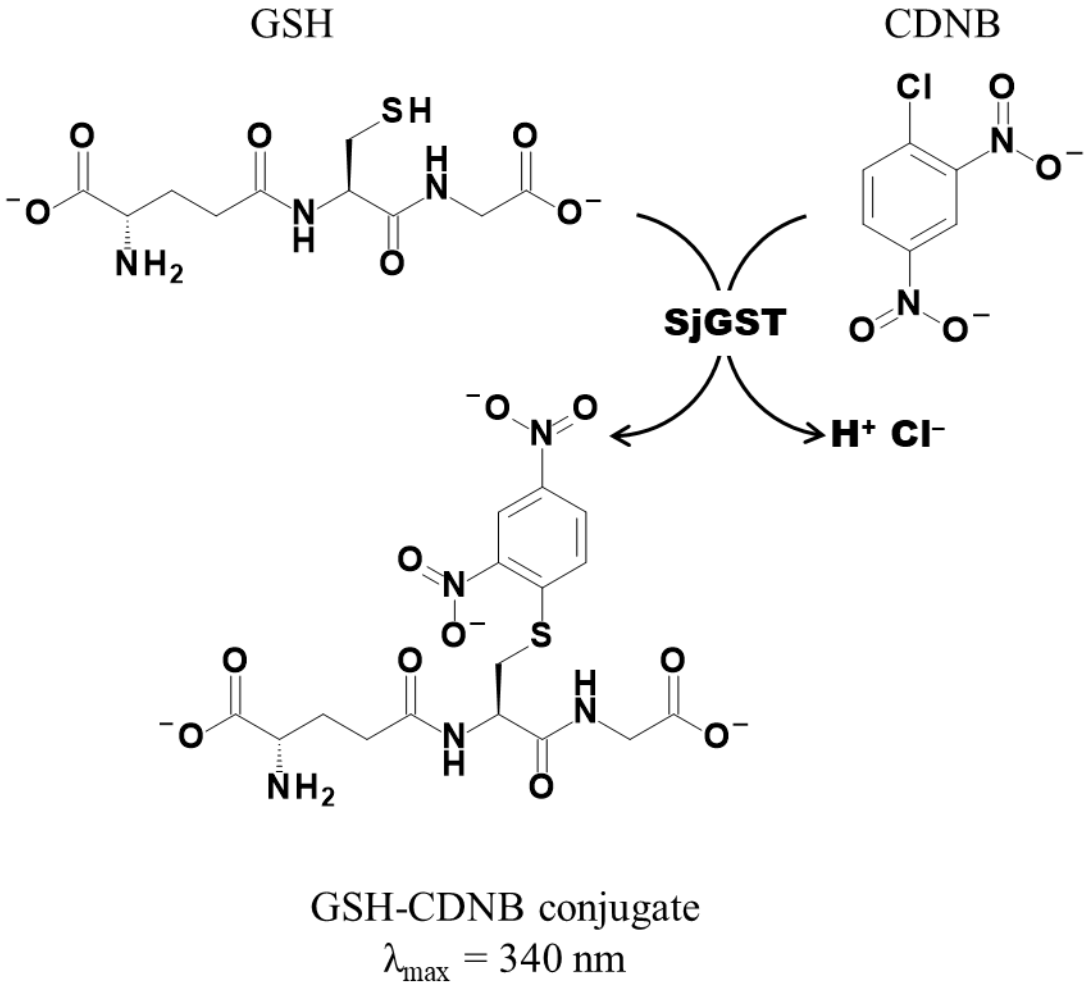


Figure 3.4: GSH/CDNB conjugation reaction. SjGST catalysed conjugation of 1-chloro-2,4-dintrobenzene (CDNB) with glutathione (GSH), forming S-2,4-dinitrophenylglutathione (Glutathione-CDNB conjugate) which absorbs at 340 nm.

3.2.10 Enzyme activity inhibition

Effect of CB3GAon SjGST was to be determined by the use of inhibition assays. The IC_{50} value of CB3GAwas determined according to (Yalçin *et al*., 1983) by measuring SjGST activity in 100 mM Na_2HPO_4, 1 mM EDTA, pH 6.5 presence of 1 mM GSH, 1 mM CDNB and different concentrations CB3GA. The IC_{50} values were calculated by plotting percentage activity values versus log inhibitor concentration. IC_{50} was determined by fitting Standard Curves macro in SigmaPlot 12.0, using the Four Parameter Logistic Equation with the Equation (7):

$$y = min + \frac{max - min}{1 + \left(\frac{x}{EC_{50}}\right)^{-Hillslope}} \quad (7)$$

were min is the bottom of the curve, max is top of the curve, EC_{50} is the half-maximal effective concentration. Equivalent definition of inhibition curves IC_{50} (half-maximal inhibitory concentration). Hillslope is the slope of the curve at its midpoint.

The response of SjGST to the variation of CDNB and GSH concentrations in the presence of different CB3GAconcentrations (0 nM, 50 nM, 100 nM and 200 nM). Apparent K_M and V_{max} values were determined by nonlinear regression analysis by fitting data points were fitted to the Michaelis-Menten model (Equation 4) using Sigma Plot 12.0. Apparent K_M and V_{max} values for GSH were using a GSH range from 0 mM to 10 mM and a fixed CDNB concentration of 1.0 mM. The apparent K_M and V_{max} values for CDNB were determined using a CDNB range from 0.1 to 2 mM with a final GSH concentration of 1 mM. Double reciprocal, Lineweaver–Burk plots were derived from the Michaelis-Menten curve to determine the mode of inhibition of CB3GAon SjGST.

3.2.11 Docking studies

Molecular docking methods are routinely used for theoretical prediction of protein–ligand interactions. Work done by Sastry *et al*. (2013) served as guideline for the docking studies. In this study a single step protocol for the preparation of ligand (CB3GA) and protein (SjGST). Docking was carried out using Induced fit docking protocol, which accounts for both receptor and ligand flexibility.

3.2.11.1 Force field calculations

Computational force field calculations were performed using Schrödinger Maestro 11.2 software. The calculations were carried out based on the force field OPLS (optimised potentials for liquid simulations). The structure of the SjGST was kept rigid while CB3GA was flexible during the calculation. The resulting structures were obtained from the result of 1000 calculation cycles.

3.2.11.2 Protein preparation

The structure of SjGST was obtained from Protein Data Bank (PDB: 1DUG). The role of protein preparation in molecular docking serves as a procedure to correct structures of proteins before initial docking experiments. It is a prerequisite for all computational work to correct crystal structures by adding missing hydrogens, remove ambiguous protonation states and include missing side chains and loops. Schrodinger-Maestro 11.2, Protein Preparation Wizard (PrepWizard) was used for preparation of SjGST (PDB: 1DUG). Protein preparation involved hydrogen bond optimisation using ProtAssign which involved assessment terminal Asn, Gly and His which are sampled to analyse 180° flips. Hydroxyl hydrogens, thiol hydrogens and protonated or neutral states of His, Glu, Asp and two His tautomeric forms contribute to the hydrogen bond network. An exhaustive mode protocol was used for hydrogen bond optimisation. The following step involved protein minimisation using Impref module of Impact and OPLS-2005 force field. All water molecules are removed from the structure. For validation of the docking results human Pi-GST (PDB: 5DCG) was used and was prepared the same way as SjGST.

3.2.11.3 Ligand preparation

Energy minimization CB3GA structure was performed using the OPLS-2005 force field. The Ligprep (LigPrep, 2009) module was used to prepare CB3GA using default parameters in Schrödinger software, Maestro 11.2.

3.2.11.4 Induced fit docking

Induced Fit (IFD) protocol Schrodinger-Maestro 11.2 (Sherman *et al*., 2006) was done for docking CB3GA onto SjGST. The IFD protocol, complex factor in docking studies which predicts accurate ligand-binding modes and associated structural movements in the protein using a flexible ligand. CB3GA was docked into rigid SjGST using soften potential docking which reduces steric clashes. In most protein structures, some side chains assume unfavourable rotameric states which hamper ligand binding. Glide was used to generate a docking grid file of the active centres of the SjGST to get detailed information about possible binding motifs using default parameters using OPLS 2005 force field. Calculations were run on HTVS mode (High-Throughput Virtual Screening) using default settings, flow chat (Figure 3.5). Glide XP (Friesner *et al*., 2004) was used for all the docking calculations. Emodel, a composite energy scoring function of Glide XP Score was used for this study. It combines ligand-receptor molecular mechanics and ligand strain energy to select a correctly docked ligand. Emodel has a more significant weighing force field component such as Van der Waals, Coulombic interactions, strain energy of the ligand and electrostatic energies. It is a better measure of the analysis of different ligand binding conformations, if one ligand is used. RMSD value to was used validate the docking protocol by analysing the conformational similarity of the docked structure and solved crystal structure. The higher the value of RMSD the lower the conformational similarity. This was done by repeating the IFD protocol used, to dock GSH into 1DUG and comparing the GSH conformation with a solved crystal structure of SjGST-GSH complex (PDB: 1UA5) (Kursula et al., 2005).

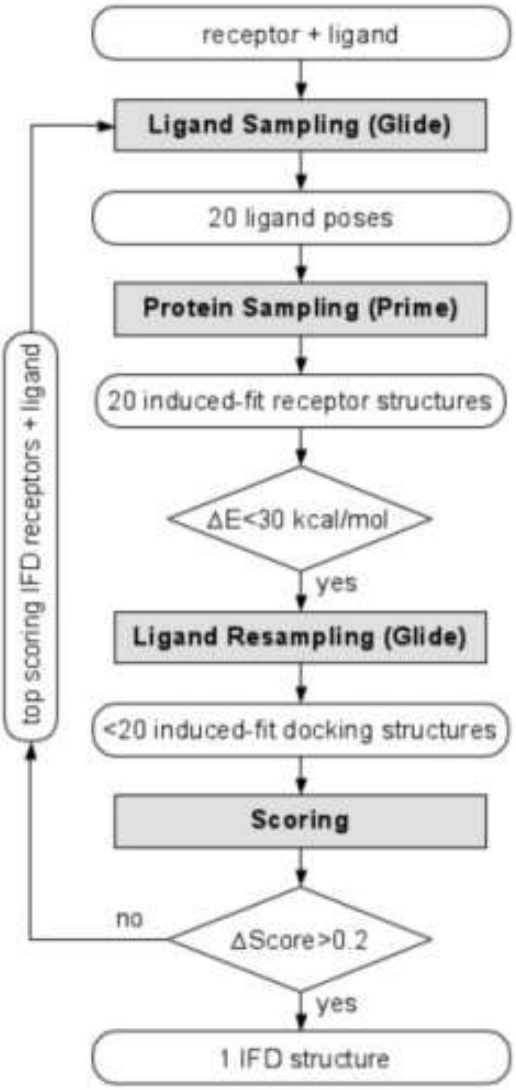


Figure 3.5: Molecular docking flowchart. Induced fit docking flowchart showing steps involved in docking. Δ*E* is the energy difference form the lowest energy structure. Adapted from Friesner *et al*. (2004)

3.2.11.5 Binding affinity prediction

Protein and ligand were prepared the same as IFD studies. The first step was Glide docking using Rigid Receptor Docking (RRD) protocol (Friesner *et al*., 2004). SjGST-CB3GA with highest Emodel score was chosen for the binding energy prediction.

Prime/MM-GBSA was performed to estimate the binding affinity of SjGST to CB3GA, calculation of the binding-free energy (ΔG_{bind}) was done using the Equation (8) (Lyne *et al*., 2006):

$$\Delta G_{bind} = \Delta E_{MM} + \Delta G_{SOL} + \Delta G_{SA} \quad (8)$$

where ΔE_{MM} is the difference in the minimized energies between the SjGST-CB3GA complex and the sum of the energies of the free SjGST and CB3GA. ΔG_{SOLV} is the difference in the GBSA solvation energy of SjGST-CB3GA complex and the sum of the solvation energies for the free SjGST and CB3GA. ΔG_{SA} is the difference in surface area energies for the complex and the sum of the surface area energies for the free SjGST and CB3GA. The simulation was performed based on the SjGST-CB3GA complex conformation obtained from Glide docking. Prime local optimization feature was used to minimise CB3GA pose. Energies of SjGST-complex were calculated with the OPLS-2005 force field and Generalized Born/Surface Area continuum solvent model. CB3GA strain energy was also accounted for during the calculation. Experimental free energy of binding ΔG_{exp} was determined using IC_{50} value adapted from (Gadhe *et al*., 2014) using Equation (9):

$$\Delta G \approx RTInIC_{50} \quad (9)$$

were R is gas constant, T is temperature in Kelvin.

CHAPTER IV

RESULTS

4.1 Protein expression and purification

SjGST was expressed using the protocol recommended by the supplier as described in Section 3.2.2. Purification profile of SjGT is shown in Figure 4.1A. High protein yeild was attained as shown in Figure 4.1B lysate lane. SjGST is soluble as it was found in the supernatant of the lysed cells as shown in Figure 4.1B. Purification of SjGST was successfully achieved using GSH-agarose affinity chromatography. Most of SjGST did bind to the GSH-agarose column as shown by flow-through lane in Figure 4.1B. SjGST was eluted using glycine (pH 10) using single step elution method. Purified protein came out as a single band with ~98% purity with an approximate molecular weight of 27 kDa (Figure 4.1B) which deviates from to momomeric SjGST with a theoretical molecular mass of 26 kDa.

Protein concentration was determined using an adaptation of Beer-Lambert law (Equation 1). Concentration of SjGST was determined using a plot shown in Figure 4.2A. Expasy ProtParam (Gasteiger *et al*., 2005) was used to determine theoretical SjGST extinction coefficient of 42 860 $M^{-1}cm^{-1}$ at 280nm was used to determine a protein concentration. Protein yield was 4.8 - 7.8 mg of purified SjGST per 6 grams of wet *E. coli* T7 cells from 1 L of bacterial culture. Absorbance spectra of purified SjGST (Figure 4.2B) is characteristic of a protein with a trough at 250 nm and a peak at 280 nm. There is no peak at 340 nm indicating no protein aggregation.

4.2 Spectroscopic studies

All spectroscopic studies were done in the absence of CB3GA. This is due to that CB3GA interferes with resultant spectra in a concentration dependent manner. The spectra alterations were observed at low concentration 10^{-5} M of CB3GA. This effect was observed both for Far-UV CD and fluorescence spectroscopy. Hence it was not possible to monitor structural changes of SjGST in the presence of CB3GA. All spectroscopic studies were done in 20 mM Na_2HPO_4, 1 mM EDTA, 0.02% (w/v) sodium azide, 2 mM DTT pH 7.4 buffer at 20°C.

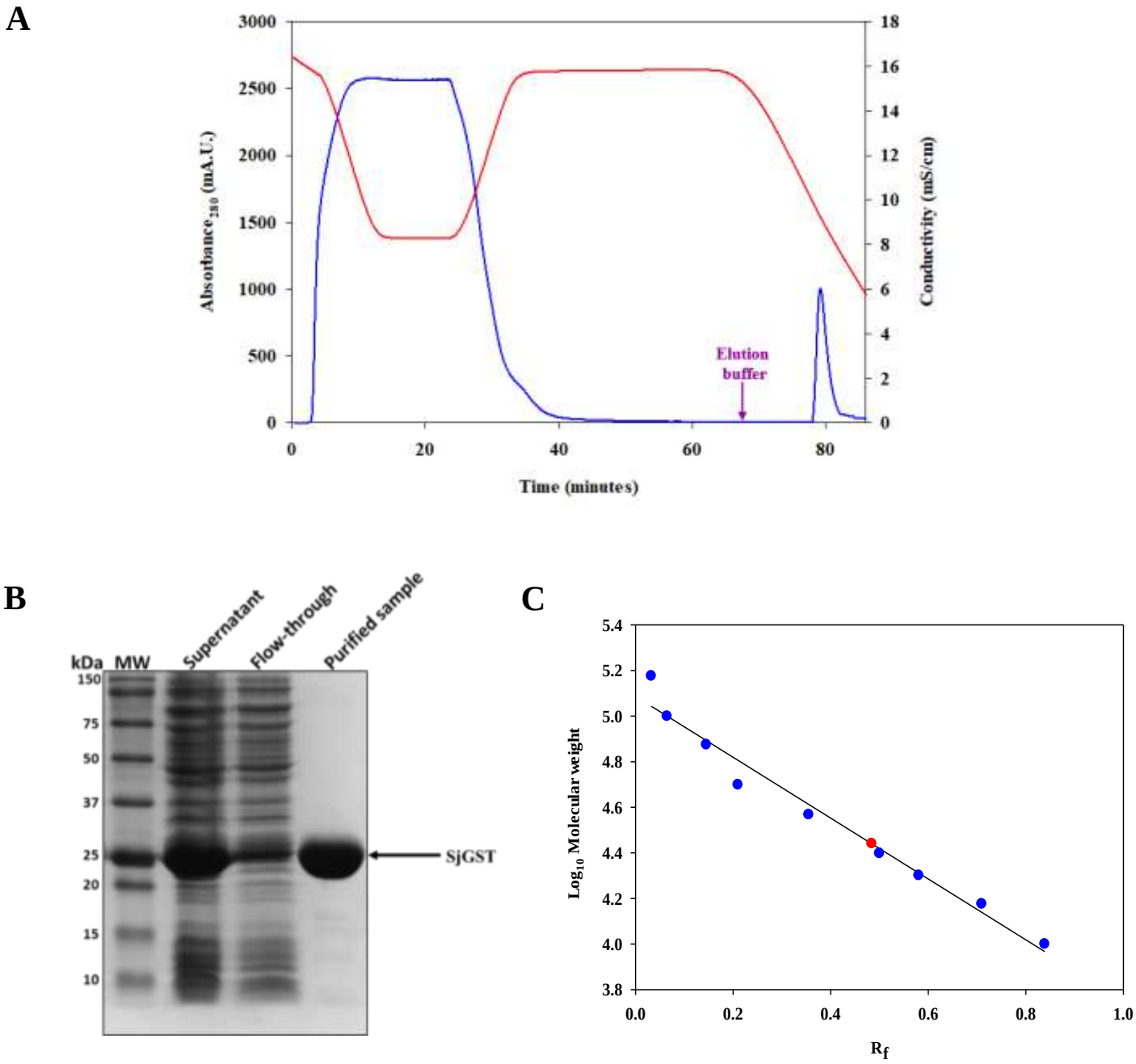
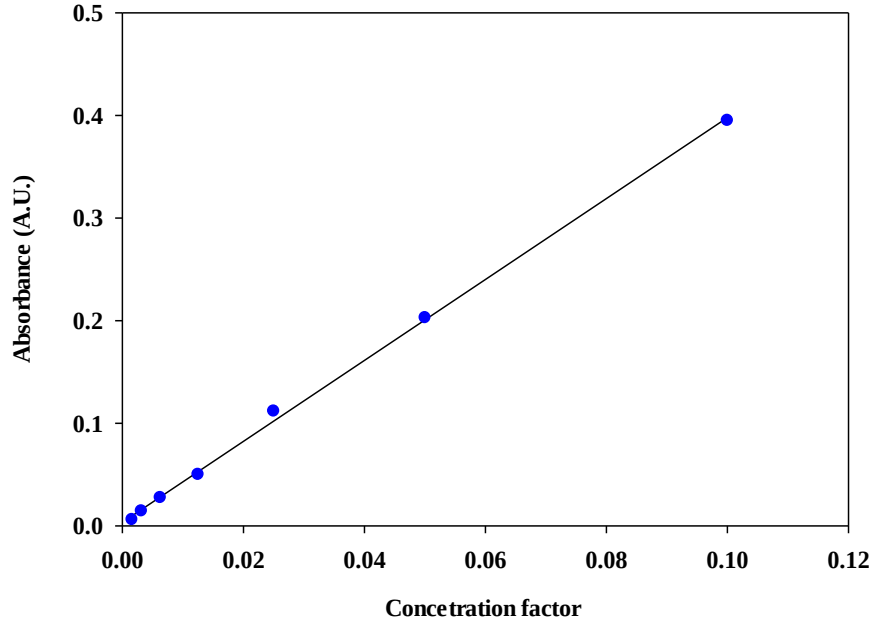


Figure 4.1: Expression and purification analysis of SjGST. Purification of SjGST was achieved using GSH-agarose column. **(A)** The blue line represents absorbance at 280 nm, broad peak represents supernatant injection. The sharp peak represents elution of protein bound to GSH-Agarose resin corresponding to purified sample in Figure 3.1B below. The red line represents conductivity an indicator of protein elution during protein purification. The purple arrow indicates time where elution buffer (glycine, pH 10) was introduced into the system. **(B)** SDS-PAGE analysis of the purification of SjGST. Analysis of the samples was done using 12% (w/v) polyacrylamide gel stained with Coomassie Brilliant Blue R-250. 15 µl of sample was loaded into each well. The gel indicates that eluted protein homogeneous and pure. **(C)** Standard curve Log Molecular weight against R_f using molecular weight standards from gel in Figure 3.1B. Equation of the line is $y = -1.3344x + 5.0864$ with $R^2 = 0.9723$. Molecular weight of SjGST was determined to be 27 kDa

A



B

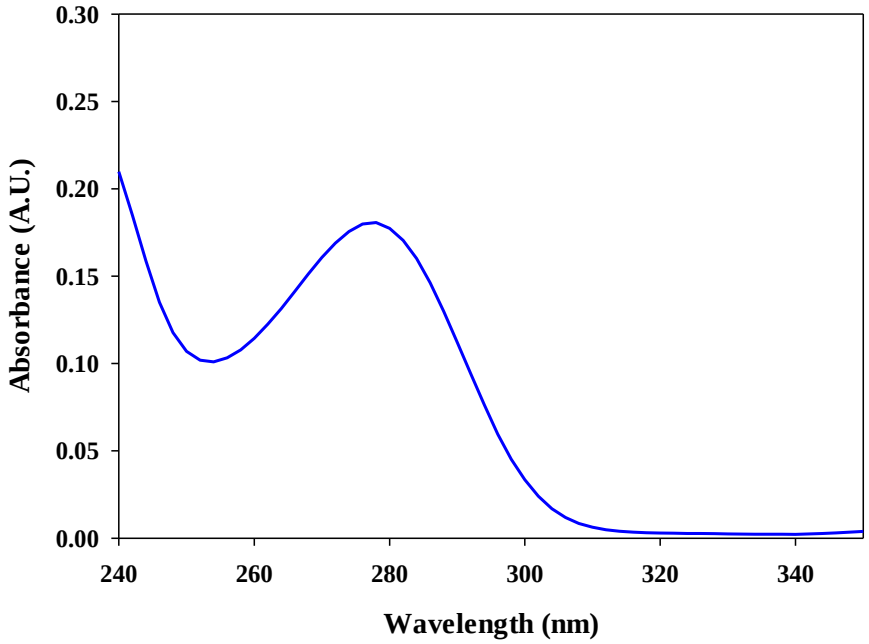


Figure 4.2: Protein quantification and absorbance spectra of SjGST. (A) Protein quantification graph of SjGST with slope of 7.654 and R^2 value of 0.99. Final concentration of purified SjGST was determined to be 4.8 mg of SjGST per 6 grams of wet *E. coli* T7 cells**. (B)** Absorbance spectra of SjGST, absorbance maximum is at 280 nm and no signal dictated at 340 nm indicating absence of aggregated protein. Protein concentration of 3 µM was used.

4.2.1 Far-UV CD

Far-UV CD was used to monitor the secondary structure of SjGST between 250 nm and 190 nm. The spectra were plotted as mean residue ellipticity versus wavelength as shown in Figure 4.3. The spectra exhibited troughs at 208 nm and 222 nm and a peak at 193 nm. This is indicative of proteins with high helical content. SjGST lost all secondary structure arrangement in the presence of 8 M urea as shown in Figure 4.3. This is shown by the loss of indicative signals of secondary structure as in the native state of SjGST. The structural analysis using DICHROWEB indicated that SjGST is predominantly alpha helical (98%) see Table 2.

4.2.2 Tryptophan fluorescence spectroscopy

Tertiary structure of SjGST was investigated using fluorescence spectroscopy. The technique servers as an intrinsic probe on the micro-environment around tryptophan residues. SjGST has four tryptophan residues on each subunit therefore they are adequate to give a high quantum yield upon selective excitation at 295 nm. Fluorescence emission maximum of SjGST is ~ 340 nm, indicating partial exposure to solvent (Figure 4.4). The spectrum displays a shoulder at the peak. In the presence of 8M urea, fluorescent properties of tryptophan were lost with a flat spectrum being observed (Figure 4.4).

4.2.3 Extrinsic ANS fluorescence

ANS is an anionic dye that is generally used an extrinsic probe for detection of ordered hydrophobic regions in protein. Unbound ANS displays reduced quantum yield in an aqueous environment, upon binding to a hydrophobic patch on a protein ANS displays increased quantum yield coupled with a blueshift. In Figure 4.5 in the presence of SjGST an increased quantum yield and a blueshift from 519 nm to 498 nm is observed indicating a solvent accessible hydrophobic patch on the surface of SjGST.

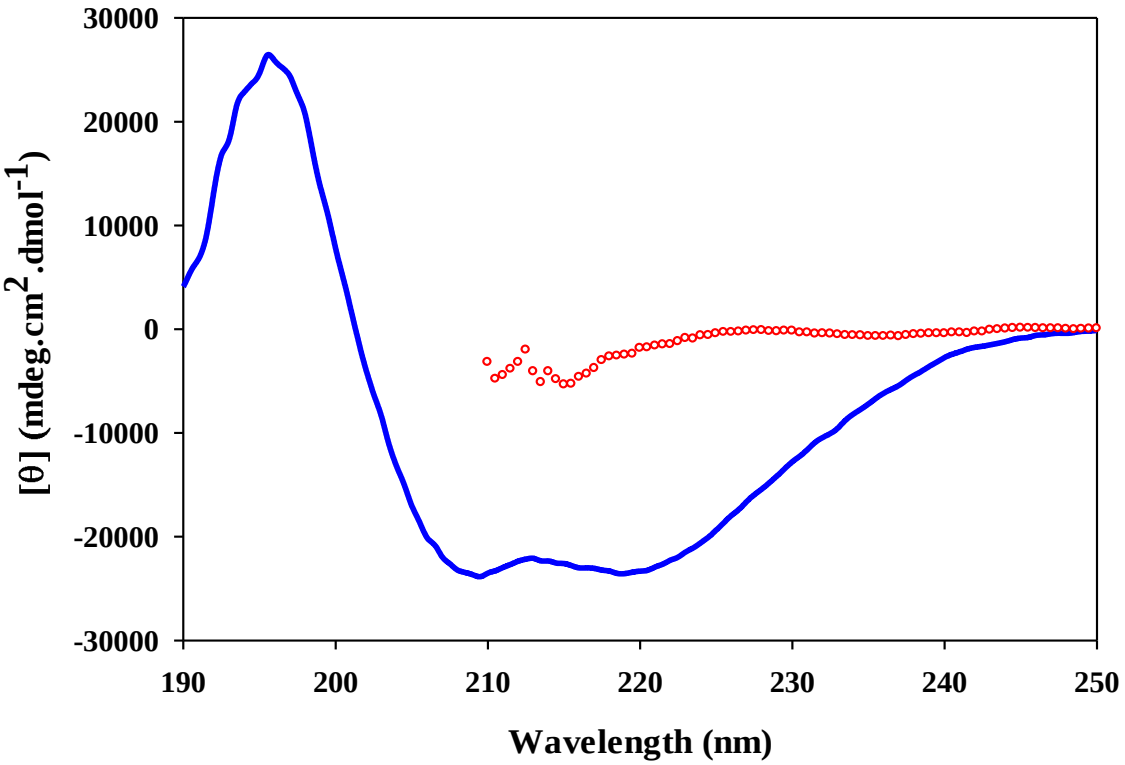


Figure 4.3: Far-UV CD spectra of SjGST. Spectra of native (blue line) and denatured using 8 M urea (red dotted line). Protein concentration for both experiments is 3 μM in 20 mM Na_2HPO_4, 1 mM EDTA, 0.02% (w/v) sodium azide, 2 mM DTT pH 7.4 buffer and recorded at 20°C. The plot is the average of three buffer corrected experiments.

Table 2: DICHROWEB analysis to determine secondary structural composition of SjGST.

	Helix1	Helix2	Strand1	Strand2	Turns	Unordered	Total
SjGST	0.457	0.518	0	0.025	0	0	1

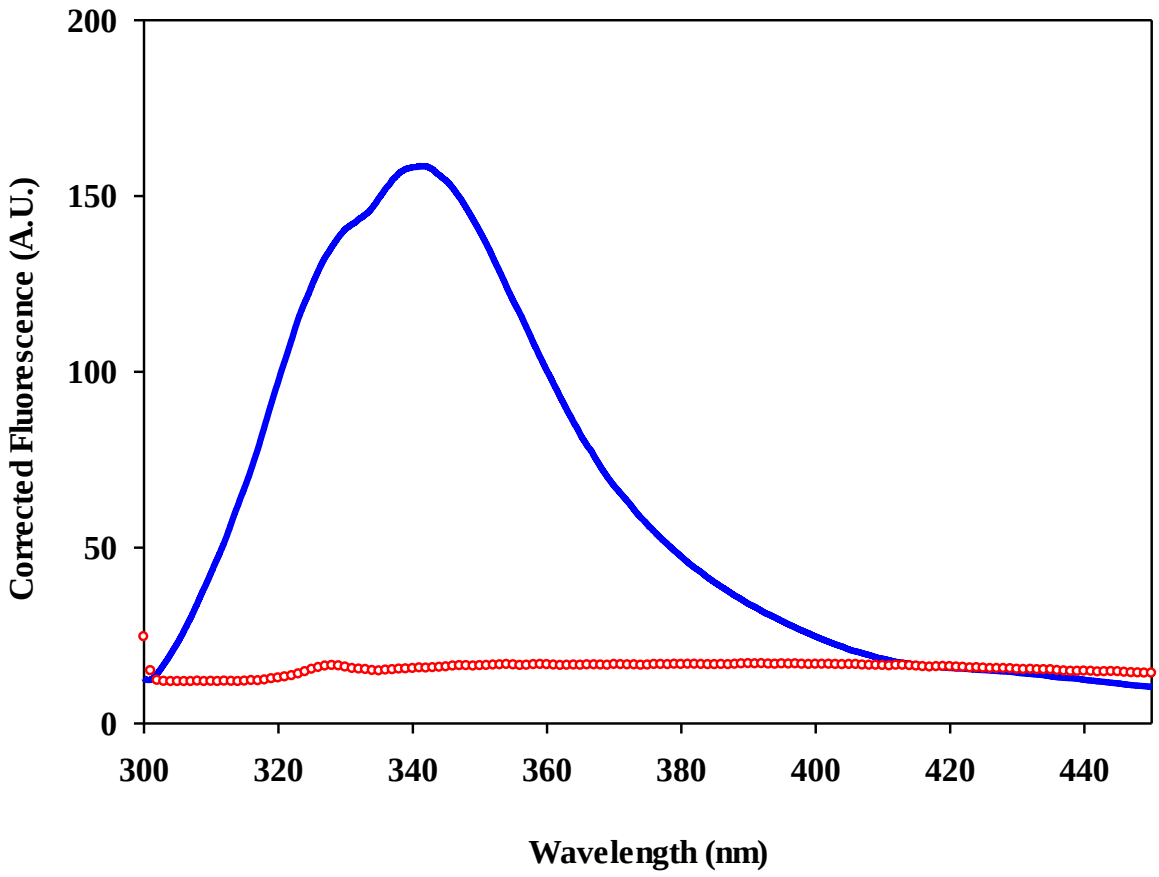


Figure 4.4: Intrinsic tryptophan fluorescence spectra of SjGST. Tertiary structure of SjGST is based on the micro-environment of tryptophan in native protein (blue line) and denatured protein (red dotted line) using 8 M urea. Protein concentration for both experiments is 3 μM in 20 mM Na_2HPO_4, 1 mM EDTA, 0.02% (w/v) sodium azide, 2 mM DTT pH 7.4 buffer and recorded at 20°C. Tryptophan was excited at 295 nm. The plot is the average of three buffer-corrected experiments.

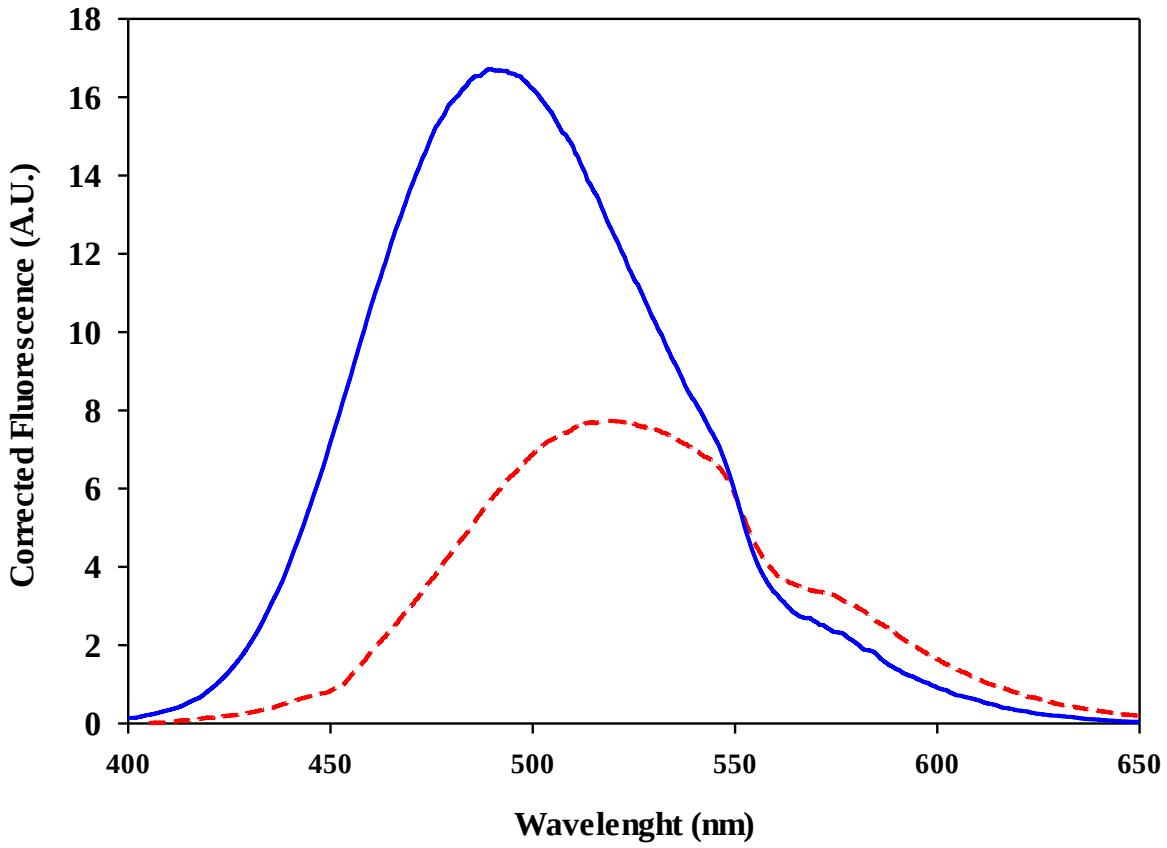


Figure 4.5: Extrinsic ANS fluorescence spectra of SjGST. The emission spectrum of ANS fluorescence (excitation at 390 nm) was measured with pre-incubation of 3 μM SjGST with 100 μM ANS in 20 mM Na_2HPO_4, 1 mM EDTA, 0.02% (w/v) sodium azide, 2 mM DTT pH 7.4 buffer and recorded at 20°C. SjGST bound to ANS (blue line) and control free ANS (red dashed line). ANS was excited at 390 nm. Blueshift emission with increased quantum yield from 519 nm to 498 nm. The plot is the average of three buffer-corrected experiments.

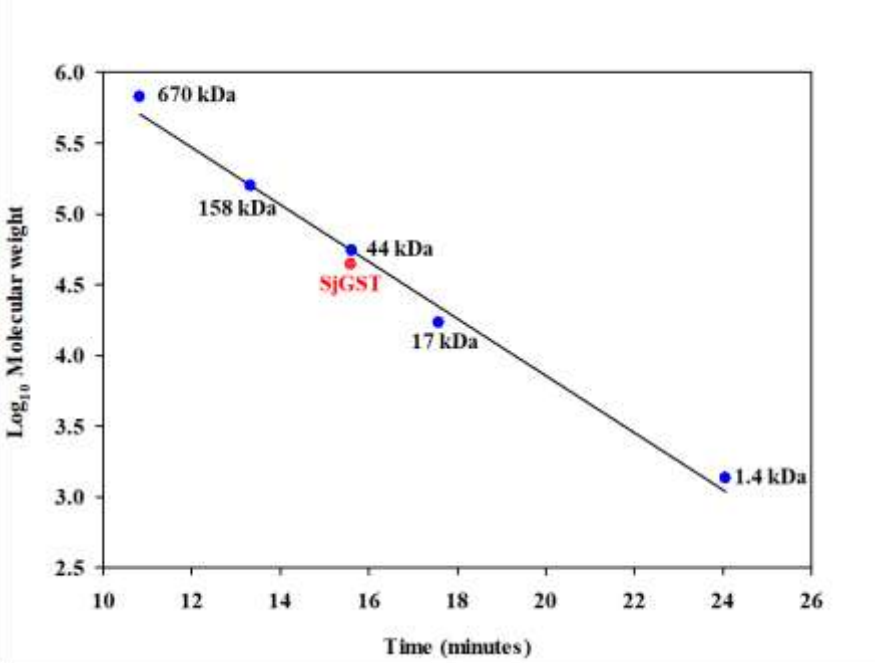
4.3 Size exclusion high performance liquid chromatography SE-HPLC

Size exclusion high performance liquid chromatography (SE-HPLC) was used to assess the oligomeric and hydrodynamic volume of SjGST. The experiment was carried out in 20 mM Na_2HPO_4, 1 mM EDTA, 0.02% (w/v) sodium azide, 2 mM DTT pH 7.4 buffer and recorded at 20°C. Gel filtration standards were used for the calibration of the column. A standard curve of Log of molecular weight against retention time was plotted as shown in Figure 4.6A. The standard curve was then used to determine the molecular weight of SjGST. The elution profile of SjGST indicated that the apparent molecular weight of SjGST is 55 kDa corresponding to the dimeric and functional form of the protein (Figure 4.6B). However, it is larger than the theoretical molecular weight of 52 kDa determined using Expasy ProtParam (Gasteiger *et al*., 2005). In the presence of saturating concentration of 1mM of CB3GA, quaternary structure SjGST was not altered as shown in Figure 4.6B, since it has the same retention time as apo-SjGST. In the absence of a reducing agent DTT, SjGST undergoes oxidative aggregation due to the presence of three exposed cysteine residues per monomer. These form intermolecular disulfide bond to form higher order oligomeric larger than 430 kDa as shown in Figure 4.6B. SE-HPLC elution profile in Figure 4.6B shows that all protein used in this study was homogenous and pure because SjGST eluted as a single peak with no artefacts observed.

4.4 Enzyme activity assay

GSH CDNB-conjugation assay (Habig and Jakoby, 1981) was used to determine the enzyme activity of SjGST. Figure 4.7B shows the specific activity of SjGST in the presence and absence of CB3GA. Activity of the enzyme is monitored spectrophotometrically at 340 nm on the basis of the extinction coefficient for the product 1-(S-dinitrophenyl)-2,4-dinitrobenzene (ε_{340nm} = 9.6 $mM^{-1}cm^{-1}$). SjGST specific activity ($\mu mol.min^{-1}.mg^{-1}$) was obtained using the slope of a linear fit of activity ($\mu mol.min^{-1}$) plotted obtained through experimental data against amount of protein (mg) used. The assay was carried out in 100 mM Na_2HPO_4, 1 mM EDTA, pH 6.5 at 20°C with final concentration of 1 mM CDNB and 1 mM GSH. The details on obtaining specific activity is fully described in the Appendix.

A



B

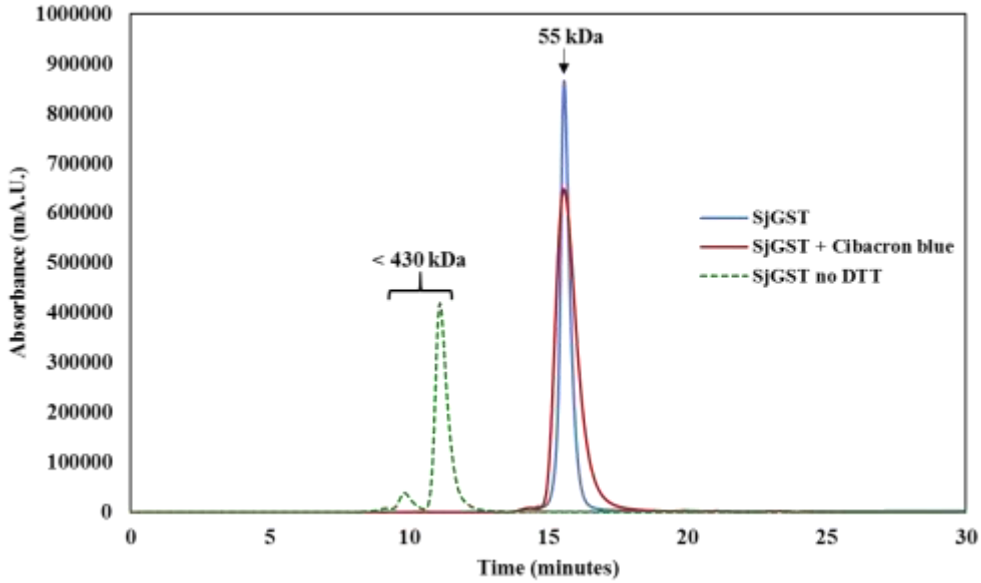
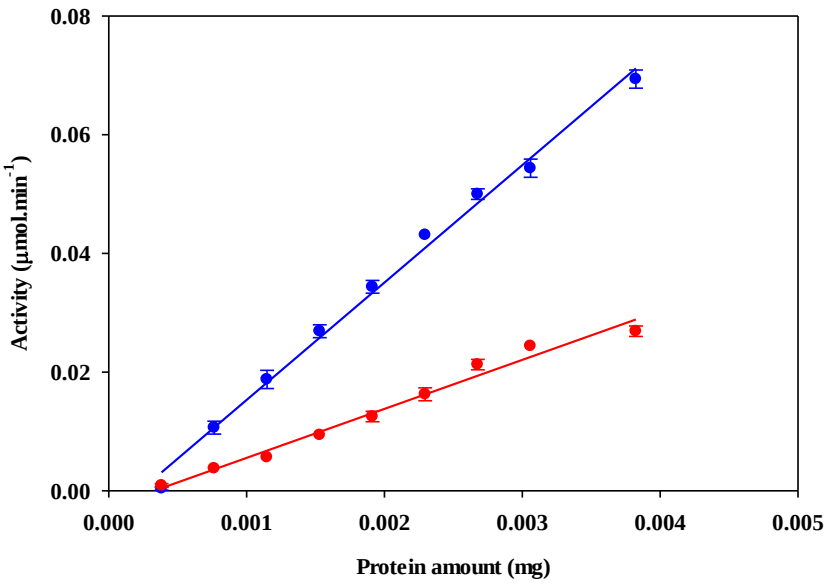


Figure 4.6: SE-HPLC profiles of SjGST. (A) Standard curve of gel filtration standards for SE-HPLC calibration, 670 kDa - bovine Thyroglobulin, 154 kDa - γ-globulin, 44 kDa - Ovalbumin, 17 kDa - Myoglobulin, 1.35 kDa - Vitamin B12. The retention time of SjGST (red dot) correlates to 55 kDa. **(B)** Quaternary structure characterisation of SjGST. Chromatograms showing apo-SjGST (blue line), SjGST with 1 mM CB3GA (red line), Apo-SjGST without DTT (green dashed line). All experiments were done with a flow rate of 0.25 ml.min^{-1} at 20°C. Protein concentration of 10 μM in 20 mM Na_2HPO_4, 200 mM NaCl, 1 mM EDTA, 0.02% (w/v) sodium azide, 2 mM DTT, pH 7.4 with the exception for the sample without DTT.

A



B

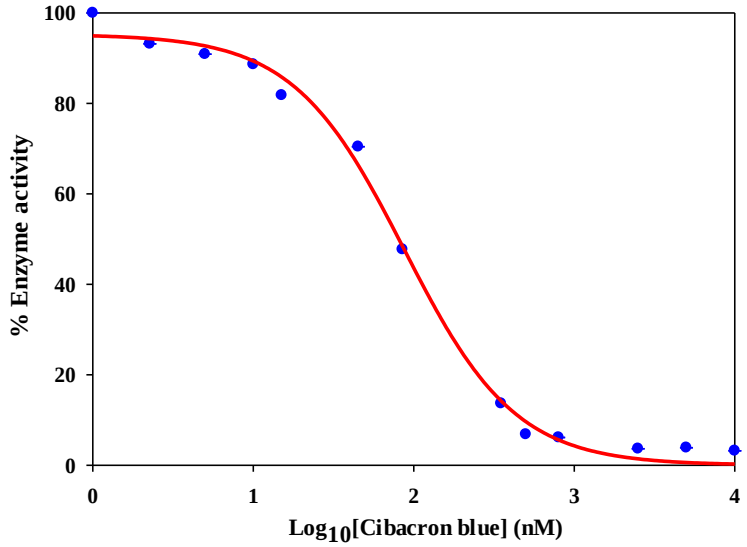


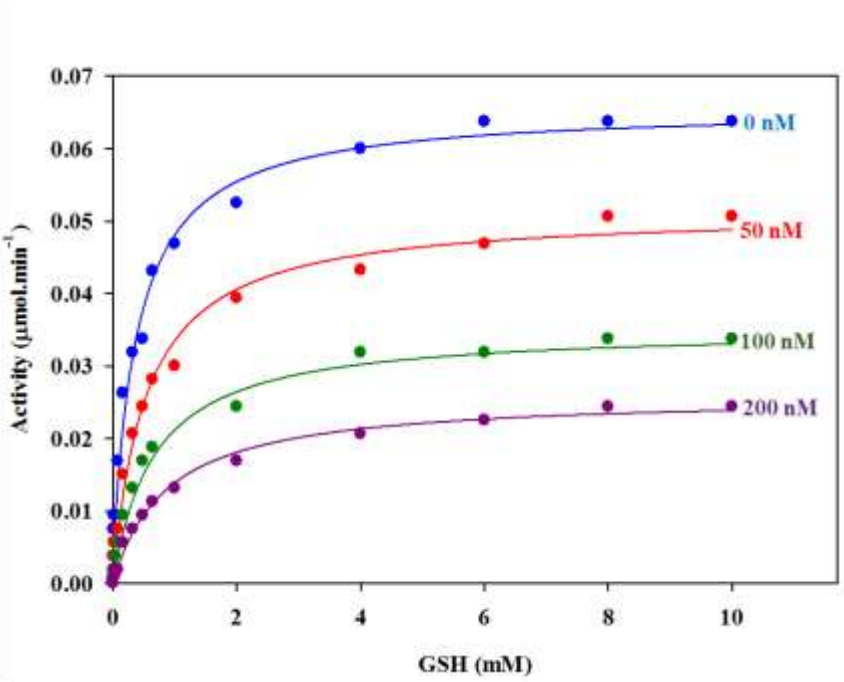
Figure 4.7: Inhibition of SjGST by CB3GA. GSH-CDNB conjugation assay was performed in 100 mM Na_2HPO_4, 1 mM EDTA and 0.02% (w/v) sodium azide, pH 6.5 at 20°C with a final concentration of 1 mM GSH and 1 mM CDNB. **(A)** Enzyme activity obtained for SjGST (blue line) 19.8 µmol.min^{-1}.mg^{-1} and SjGST with CB3GA (red line) is 8.3 µmol.min^{-1}.mg^{-1} with R^2 value of 0.9942 and 0.9816 respectively. Specific enzyme activity was obtained from the slope of the fit curve. Each point on the curve was done in triplicate with error bars representing standard deviation. **(B)** IC_{50} of CB3GA was determined using GSH-CDNB conjugation activity assay. CB3GAinhibited SjGST activity at nanomole range IC_{50} = 100 nM ± 7.2 with R^2 = 0.996. The values were calculated using nonlinear regression using four parameter logistic curves implemented in Sigma Plot 12.0. The values are mean ± standard error of mean with each value done in triplicate.

CB3GA is a known inhibitor of GSTs, however studies with SjGST are not available. The study assumed that that CB3GA does inhibit SjGST. The IC_{50} curve was constructed using GSH-CDNB conjugation to determine the amount of CB3GA needed to inhibit SjGST activity by 50% (Figure 4.7A). IC_{50} of CB3GA value was determined to be 100 nM. IC_{50} value determined (100 nM) from the curve was used to monitor the effect of CB3GA on the specific activity of SjGST as shown in Figure 4.7B. Specific activity values obtained for SjGST (19.8 $\mu mol.min^{-1}.mg^{-1}$) and SjGST with CB3GA (8.3 $\mu mol.min^{-1}.mg^{-1}$). CB3GA showed 50 % inhibition effect on SjGST.

4.5 Enzyme activity inhibition

Effect of CB3GA on the activity of SjGST was further analysed by the use of steady state kinetics to determine the mode of inhibition of CB3GA. GSH-CDNB conjugation assay was used for all kinetic studies in 100 mM Na_2HPO_4, 1 mM EDTA and 0.02% (w/v) sodium azide, pH 6.5 at 20°C. Enzyme activity was measured at different substrate concentration with fixed SjGST concentration for different CB3GAconcentrations. SjGST followed Michaelis-Menten kinetics in both cases when GSH and CDNB were used as substrates as shown in Figure 4.8A and Figure 4.8B respectively, saturation was reached in all cases. Mode of inhibition was determined by the use of Lineweaver-Burk plots (Figure 4.9A and Figure 4.10). Analysis of SjGST with GSH as the substrate, the Lineweaver-Burk plot indicate mixed inhibition (Figure 4.9A) with plots not intersecting on either *x*-axis or *y*-axis. Dixon plots were used as an aid to identify inhibition behaviour (Figure 4.9B). Parallel lines in a Dixon plot were obtained, indicating uncompetitive inhibition of SjGST by CB3GA. Analysis of SjGST with CDNB as the substrate the Lineweaver-Burk plot indicate non-competitive inhibition (Figure 4.10) with plots intersecting on the *x*-axis.

A



B

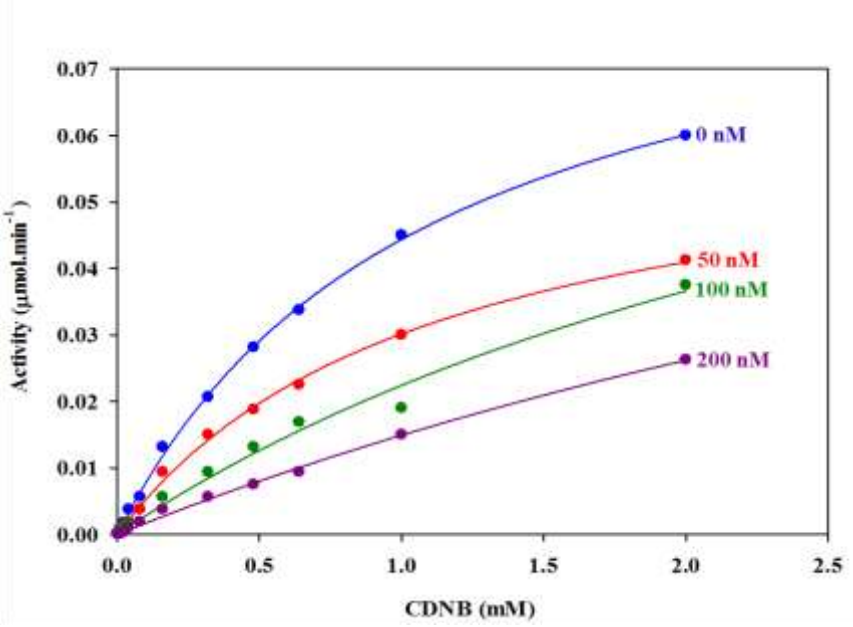
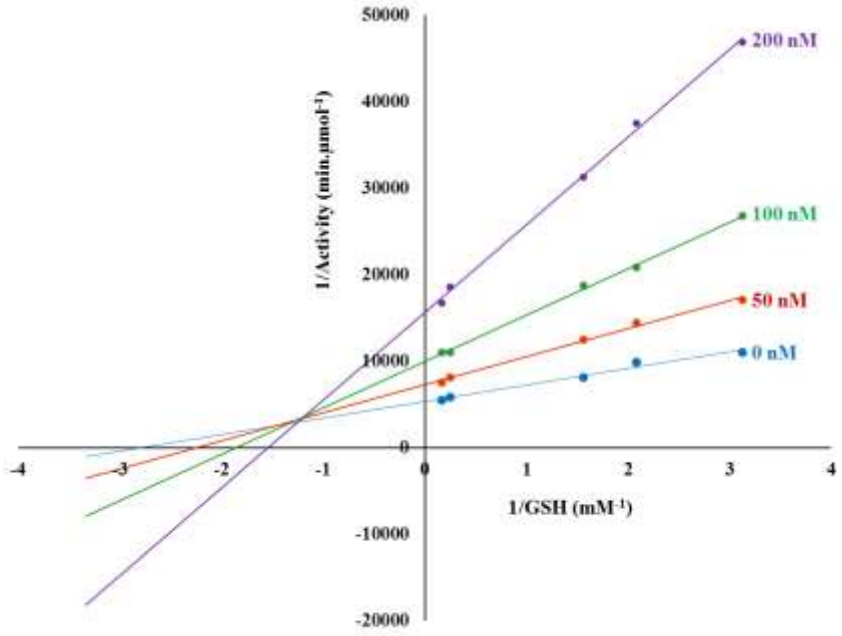


Figure 4.8: Michaelis-Menten plots for SjGST. Nonlinear regression analysis of enzyme activity against substrate concentration. The GSH-CDNB conjugation assay was performed in in 100 mM Na_2HPO_4, 1 mM EDTA and 0.02% (w/v) sodium azide, pH 6.5 at 20°C. Different CB3GAconcentrations were used 0 nM, 50 nM, 100 nM and 200 nM with final enzyme concentration of 30 nM. Sigma Plot 12 was used to fit the data to a hyperbolic curve non-linear regression analysis. Each data point was done in triplicate plotting the average and error bars represent standard deviation of mean. SjGST concentration was fixed at 30 nM. (A) GSH as substrate. (B) CDNB as substrate. Both GSH and CDNB saturated SjGST with R^2 values above 0.94.

Table 3: Kinetic properties of SjGST in the presence of CB3GA.

[CB3GA] (nm)	GSH		CDNB	
	V_{max} (μmol.min^{-1})	K_M (mM)	V_{max} (μmol.min^{-1})	K_M (mM)
0	0.065 ± 0.0002	0.325 ± 0.0005	0.093 ± 0.0002	1.096 ± 0.0045
50	0.051 ± 0.0001	0.533 ± 0.0058	0.064 ± 0.0002	1.115 ± 0.0073
100	0.035 ± 0.0002	0.667 ± 0.0012	0.047 ± 0.0006	1.935 ± 0.0004
200	0.026 ± 0.0005	0.871 ± 0.0067	0.029 ± 0.0018	1.392 ± 0.0012

A



B

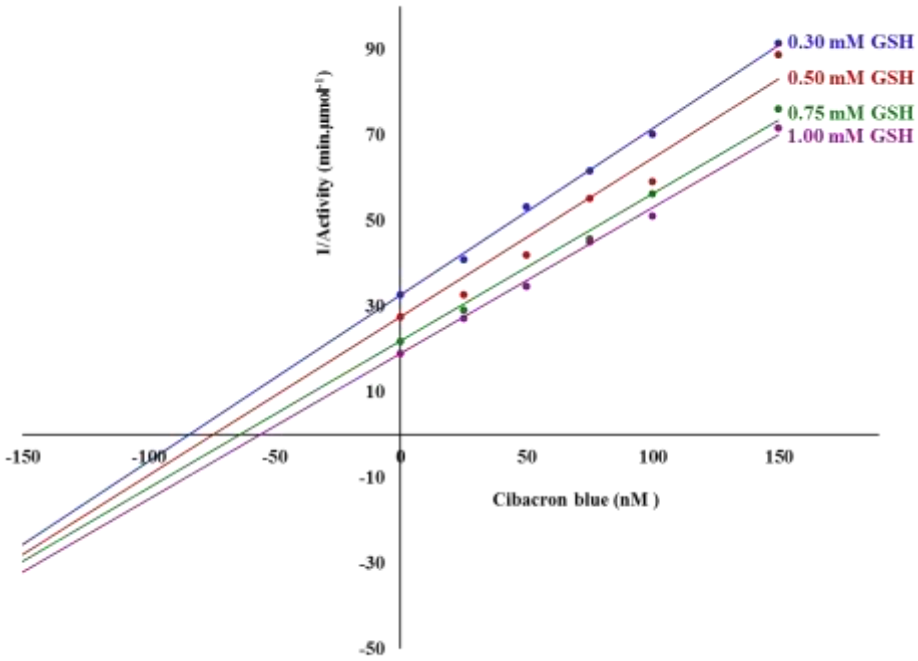


Figure 4.9: SjGST G-site inhibition kinetics. Lineweaver-Burk plots of 1/activity against 1/[GSH] were derived from Michaelis-Menten plot (Figure 3.8A). (A) Mixed inhibition of SjGST by CB3GAas indicated by a Lineweaver-Burk plot. (B) Uncompetitive inhibition of SjGST by CB3GAas shown by parallel lines in a Dixon plot.

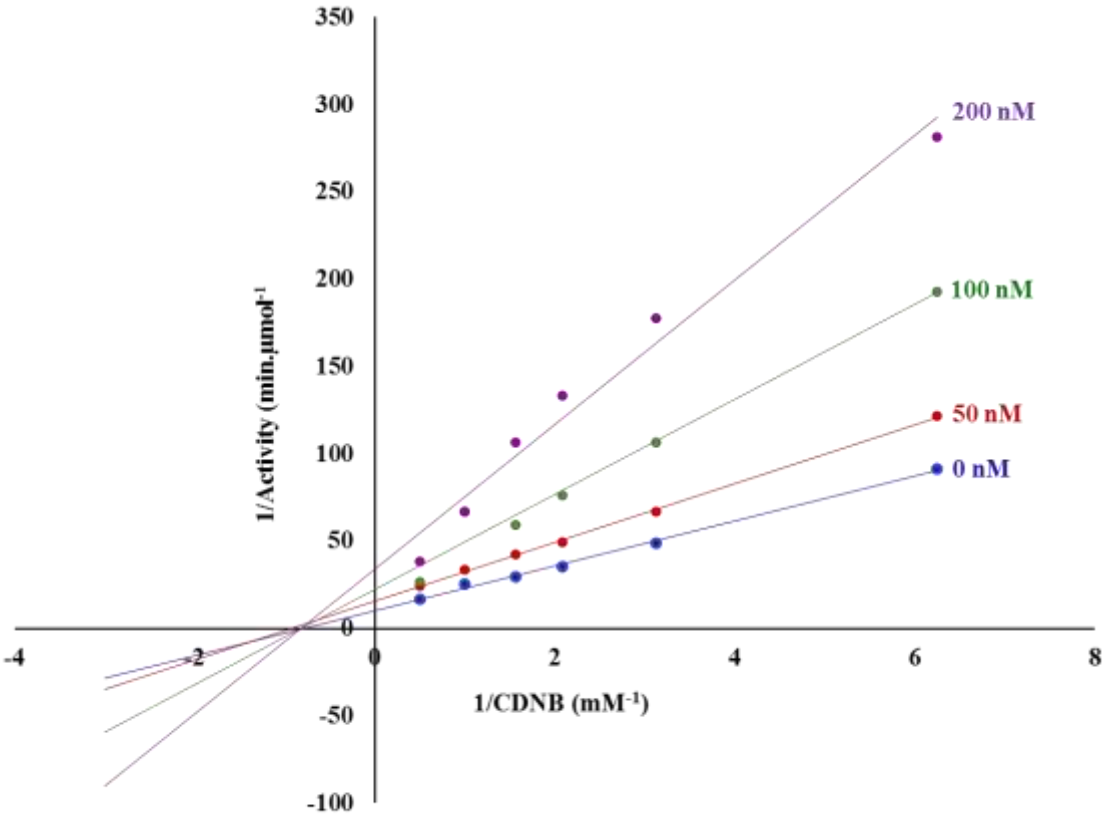


Figure 4.10: SjGST H-site inhibition kinetics. Lineweaver-Burk plots of 1/activity against 1/[CDNB] were derived from Michaelis-Menten plot (Figure 3.8B). Non-competitive inhibition as indicated by intersecting plots on the *x*-axis.

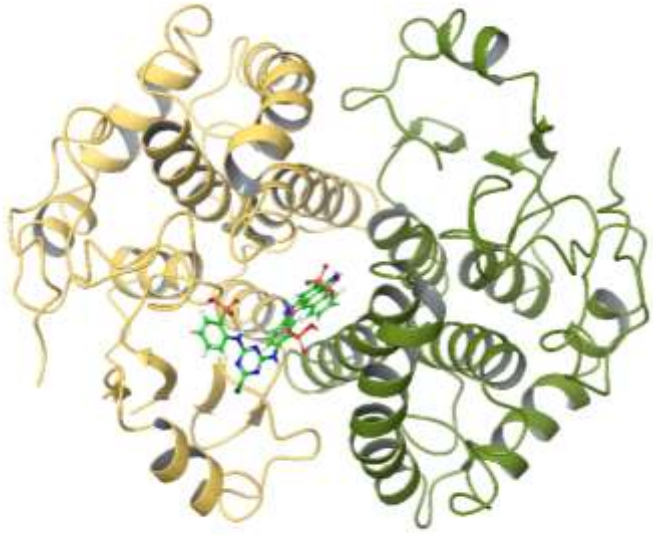
4.6 Molecular docking studies

Kinetic studies did not give conclusive results on the mode of inhibition of SjGST by CB3GA. CB3GA is not directly inhibiting SjGST active sites rather affects the structure remote to the active sites. IFD was used to theoretically prediction of CB3GA interaction with SjGST. Glide XP Emodel scoring function which provides the best pose for the ligand based on the force field and the molecular interactions of the ligand and the protein. SjGST was kept rigid while of CB3GA was flexible during the conformational search. Glide XP predicted that CB3GA binds to the dimer interface of dimeric SjGST with the highest pose based on Emodel scoring 742 kJ/mol (Figure 4.11A). Two-dimensional interaction of CB3GA and SjGST (Figure 4.11B) indicates that the binding is characterised by hydrogen bonding. Chain A (Tyr 6, Trp 7, Asn 53, Met 68, Arg 107, and Trp 110) and Chain B (Arg 100 and Asp 107), suggesting that CB3GA binds to the dimer interface of SjGST (Figure 4.11A). Validation of docking was done by running Apo human GST-Pi (PDB: 5DCG) with and CB3GA which showed binds adjacent to the H-site blocking part of the H site as shown in Figure 4.12A with a Emodel score of 528 kJ/mol. Two-dimensional interaction of SjGST and CB3GA (Figure 4.11B) is characterised by hydrogen bonding with Asp 98 and Lys 103. However, CB3GA seems to be interacting with GSH bound the G site of SjGST. This was comparable with crystal structure of human GST-Pi with CB3GA (PDB: 20GS). RMSD was used for validating the docking protocol with a value of 0.024 Å.

4.7 Binding affinity calculation

MM-GBSA was used to estimate SjGST affinity to CB3GA based on the Glide docking. MM-GBSA protocol puts into accounts for energy landscapes defining ligand binding which contribute to the final free energy of binding (Table 4). The predicted free energy of binding (ΔG_{pred}) is -310 kJ/mol. Two-dimensional presentation of SjGST-CB3GA complex (Figure 4.13), CB3GA forms hydrogen bonds with: Chain A (Arg 107, Tyr 110 and Asn 53) and Chain B (Arg 107), π-π* stacking with Trp 40. Experimental free energy of binding (ΔG_{exp}) was determined to be 46.93 kJ/mol.

A



B

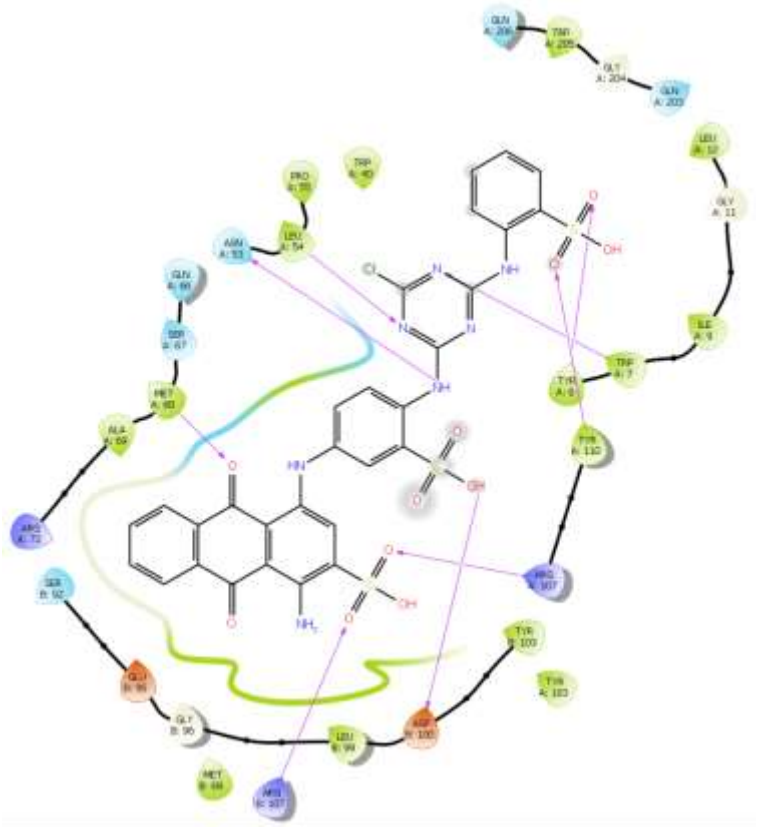
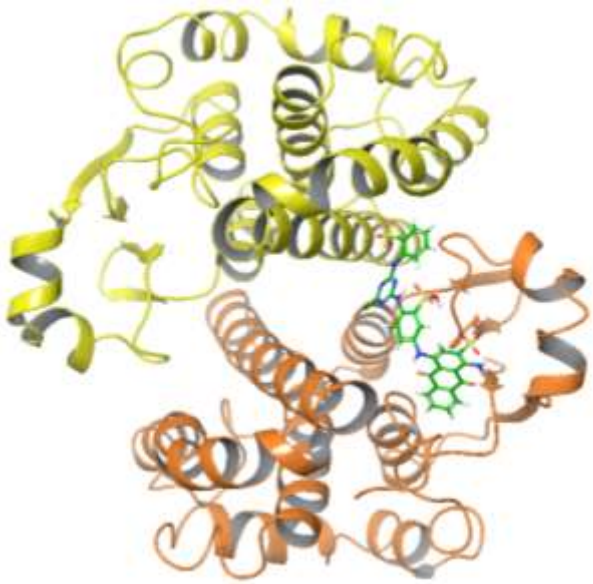


Figure 4.11: Induced fit molecular docking of CB3GA into SjGST. (A) Three-dimensional structure of SjGST (grey) PDB: 1Y6E showing the CB3GA (green and red) binds in the core dimer interface of SjGST. (B) Two-dimensional structure of SjGST and CB3GA interaction. Amino acids coloured blue are polar, dark blue are positively charged, green are hydrophobic and red negatively charged. The purple lines represent hydrogen bond. Grey spheres represent solvent exposed

A



B

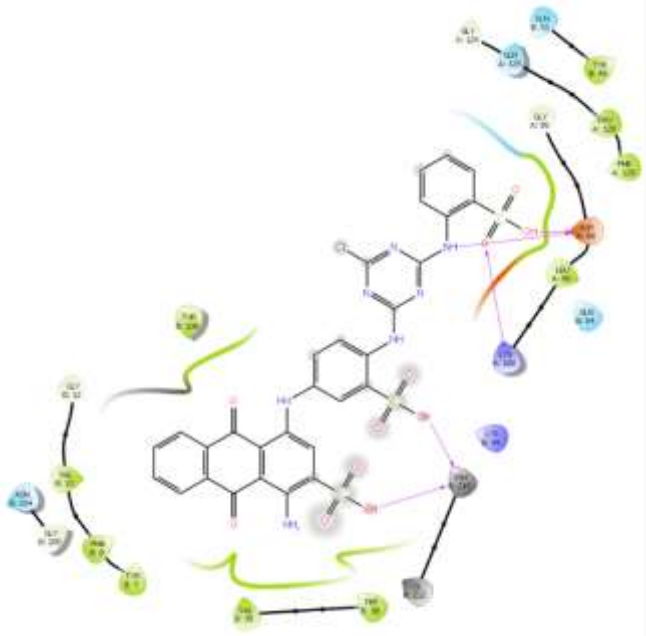


Figure 4.12: Induced fit molecular docking of CB3GA into human pi-GST. (A) Three-dimensional structure of hGSTPi (grey) PDB: 5DCG were CB3GA (green and red) binds on H-site region of hGSTPi. **(B)** Two-dimensional structure of hGSTPi and CB3GA interaction. Amino acids coloured blue are polar, dark blue are positively charged, green are hydrophobic and red negatively charged. The purple lines represent hydrogen bond.

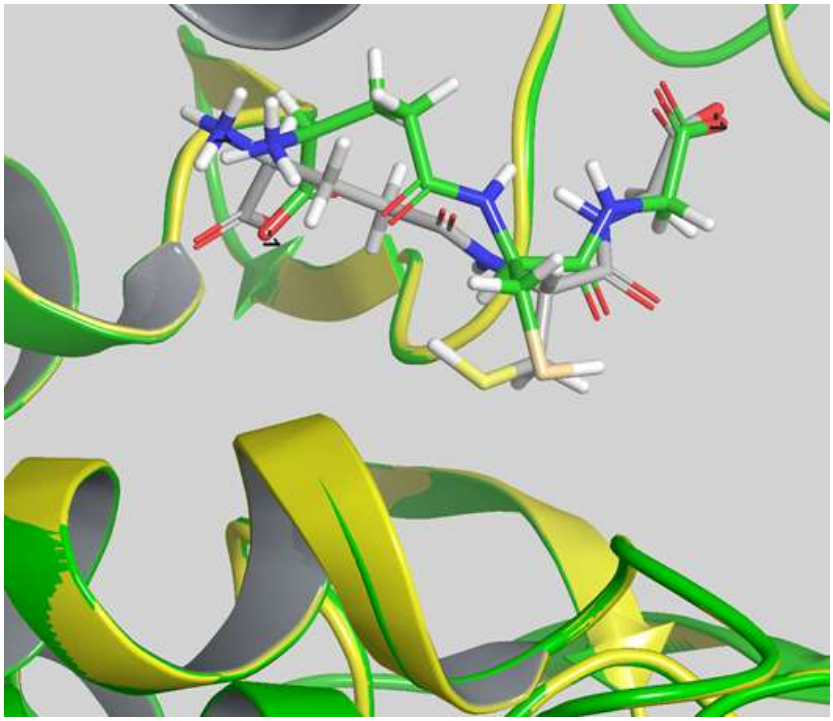


Figure 4.13: Docking protocol validation. Stereo-view of superposed structure of SjGST-GSH complex (re-docked) over SjGST-GSH complex (co-crystal). Co-crystal is shown by grey stick (GSH) and grey ribbon (SjGST), whereas re-docked complex has green stick (GSH) and green ribbon (SjGST). RMSD = 0.0240 Å.

Table 4: Binding free energy estimation for SjGST-CB3GA complex.

Parameter	Energy (kJ/mol)
$\Delta G_{Coulomb}$	134.27
$\Delta G_{Covalent}$	0
ΔG_{Hbond}	-18.67
ΔG_{Lipo}	-75
$\Delta G_{Packing}$	-21.35
$\Delta G_{SelfCont}$	0
$\Delta G_{Solv\ GB}$	222.67
ΔG_{vdW}	-284.03
ΔG_{Pred}	-310.12
ΔG_{Exp}	-49.93
IC_{50} (nM)	100

All the ΔG units are in kJ/mol. All free energy ΔG contributions are based on Glide docking pre-processing, $\Delta G_{Coulomb}$ (Coulomb energy), $\Delta G_{Covalent}$ (Covalent binding energy), ΔG_{Hbond} (Hydrogen-bonding energy), ΔG_{Lipo} (Lipophilic energy), $\Delta G_{Packing}$ (π-π* packing energy), $\Delta G_{SelfCont}$ (Self-contact correction), $\Delta G_{Solv\ GB}$ Generalized Born electrostatic solvation energy and ΔG_{vdW} (van der Waals). ΔG_{Pred} is theoretical (MM-GBSA) free energy of binding. ΔG_{Exp} is experimental binding free energy calculated from experimental IC_{50} values according to $\Delta G \approx RT \ln IC_{50}$

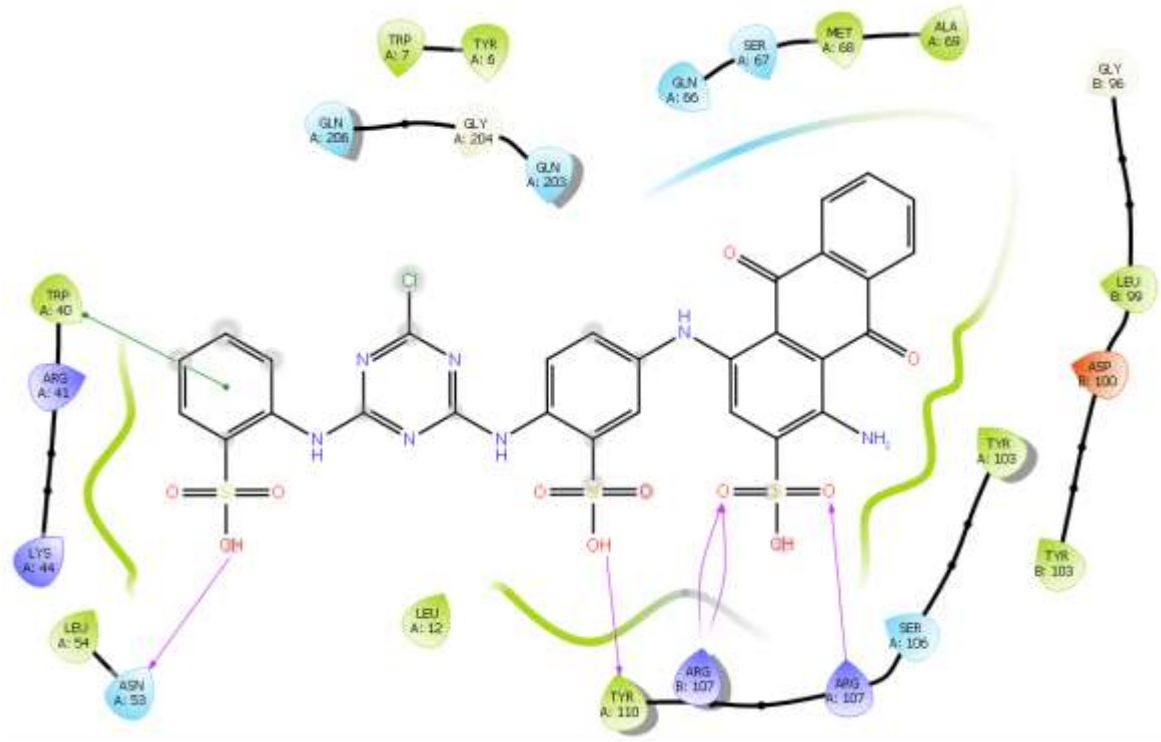


Figure 4.13: MM-GBSA docking of CB3GA into SjGST. Two-dimensional structure of SjGST -CB3GA complex conformation. Amino acids coloured blue are polar, dark blue are positively charged, green are hydrophobic and red negatively charged. The purple lines represent hydrogen bonds and green line represents π-π*staking.

CHAPTER V

DISCUSSION

Schistosomiasis is a major neglected tropical disease with unacknowledged chronic impact affecting schistosomiasis-endemic areas due to repeated cycles of infection. Praziquantel is the only drug available for the treatment of schistosomiasis and resistance against praziquantel has been observed in some schistosomiasis-endemic areas which is a huge concern for the public health sector. Hence, new strategies and chemotherapeutic treatments have to be devolved to combat schistosomiasis.

In this study, the effect of CB3GA (GST inhibitor) on the structure and function of SjGST was analysed using low resolution spectroscopic techniques. SjGST is a key enzyme involved in the detoxification, ligand transportation, and modulation of cellular activities in *Schistosoma*. Hence, SjGST maybe a possible therapeutic target due to its multiple cellular activities in the parasite. CB3GA is a known inhibitor of GSTs (Mahajan and Atkins, 2005). The aim of the study was to obtain an insight of the mode of inhibition of CB3GA on SjGST using biophysical, functional and molecular modelling studies.

Heterologous protein expression and purification of target protein is often a challenge in most structural biology studies. SjGST was over-expressed using the pGEX4T-1 expression vector which encodes SjGST as a fusion tag for heterologous protein expression. The structure and biochemical properties of native SjGST and recombinant SjGST have comparable structural and functional properties (McTigue *et al*., 1995; Parker *et al*., 1990). All of the over-expressed protein was in the soluble fraction with high expression yield (Figure 4.1B). Proteins are studied in the soluble form to mimic cytosolic conditions.

Purification of SjGST was done using GSH-Agarose column. SjGST binds efficiently to the column, only a small fraction was obtained in the flow-through (Figure 4.1B). In this study protein purification was done using non-reducing conditions (no DTT) because SjGST was in a soluble aggregated (oxidative) form (Figure 4.6B) with no priotein fraction in the native conformation. The active site of SjGST was still available to bind to immobilised GSH. SjGST has four cysteine residues (Cys 84, Cys 138, Cys 169 and Cys 178), only Cys 169 is buried in the core of SjGST. The exposed cysteine residues lead to the formation higher order oligomers through the formation of intermolar disulfide bonds. None of the cysteine residues are directly involved or in close proximity with the active site of SjGST. Also, these cysteine residues are not involved in intra- or inter- disulfide linkages which facilitate functional conformation in the active dimeric enzyme

(McTigue *et al*., 1995b). In the presence of DTT, oxidative aggregation of SjGST is reversed (Figure 4.6B) because SjGST exists as a dimer. Glycine-NaOH at pH 10 was used to elute SjGST compared with using GSH, this is to avoid bias in functional investigations of SjGST since GSH was to be used as a substrate in downstream experiments. Glycine-NaOH (pH 10) alters specific non-covalent interactions between SjGST and immobilised GSH, leading to SjGST elution. A single step elution was done and a pure (98%) protein sample was obtained; no other protein band was predominant in the SDS-PAGE electrophoretogram (Figure 4.1B). SjGST is a highly soluble protein and stable because the protein can be concentrated to 10 mg/ml without aggregation. The initial enzyme activity can be maintained after 2 weeks when kept at -4°C. The standard curve (Figure 4.1A) is not a reliable method for the estimation of molecular weight because the porosity of the gel can become irregular; Hence, altering the size of a protein resolved using SDS-PAGE (Chrambach and Rodbard, 1971).

Protein quality assessment is a critical step in biophysical and structural characterisation because level of protein purity has impact on the accuracy and reproducibility of results. The absorbance spectrum (Figure 4.2A) was used to assess quality of the purified protein sample, the spectrum showed a characteristic of pure protein. The highest peak is at 280 nm and no signal detected at 340 nm indicates absence of aggregation and nucleic acid contamination. SE-HPLC showed that SjGST is pure, homogenous and that SjGST exist as a dimer (Figure 3.6B). Protein quantification was done to determine working sample concentrations, the value of $A_{340\,nm}$ was not accounted for since it was close to zero or negative. The highest point on the absorbance spectrum and concentration determination curve was below 1. Absorbance readings above 1 can be misleading since the Beer-Lambert law might deviate giving inaccurate results (Kaplan *et al*., 1997). Linearity of the standard curve was not determined at higher absorbance values to determine if they correlate with lower values. Beer-Lambert law linearity is dependent on the machinery used.

Structural characterisation enables to elucidate the structure-function relationship of proteins and how alteration of protein structure affects the functional capacity of a protein (Otaki *et al*., 2010). In this study CB3GA was to be used as a probe to monitor structural changes. However, due to its complex multiple ring structure upon interaction with light anomalous behaviour was observed. The effect of CB3GA on the resultant spectra is in a concentration dependent manner. In a study

by Axarli *et al*. (2004), the formation of *Zea mays* GST-CB3GA complex was detected by an increase at 650 nm in absorbance spectra, this was not observed for SjGST-CB3GA complex.

For CB3GA to act as an efficient structural probe, intrinsic and extrinsic optical activity properties of anthraquinone ring (CB3GA chromophore) must to be determined. Optical activity of CB3GA highly dependent on solvent properties for its spectroscopic behaviour (Edwards and Woody, 1983). Secondary structural characterisation was done to analyse backbone conformation of SjGST. The results indicated that SjGST is predominantly α-helical (98%). The far-UV spectrum showed troughs at 210 and 222 nm. This was in line with the crystal structure PDB:1Y6E (Rufer *et al*., 2005). Far-UV CD spectra obtained for SjGST is comparable with studies by Brockwell *et al*. (2001).

Tertiary structure characterisation using Trp as a probe indicated that most of the Trp residues are partially accessible with maximum emission wavelength at ~340 nm. This partial exposure is in line with the crystal structure PDB:1DUG. The peak shows a shoulder (Figure 4.4) which is indicative of unresolved vibrational transitions of the excitation of the Trp residues (Albrecht, 2008). However, it is a challenge to separate the spectral contributions of each tryptophan in a multi-tryptophan protein. SjGST contains four Trp residues namely Trp 7, Trp 40, Trp 200, and Trp 205 in each subunit. When SjGST was denatured (8 M urea), there was complete loss of fluorescent properties, which was unexpected. This is not comparable with other studies where a red shift coupled with reduced quantum yield is observed. This may be due to quenching of the Trp fluorescence by the protein backbone (Eftink, 2006) in the presence of 8 M urea where SjGST is in an elongated form. In a study by Kaplan *et al*. (1997) shows that Trp residues in SjGST are located in the hydrophobic environment in the native state, due to the red shift from 335 nm to 355 nm upon unfolding coupled with quenching of Trp fluorescence which occurs during SjGST unfolding rather than complete loss of fluorescent properties.

Tertiary structure analysis with ANS probe shows presence of ANS accessible hydrophobic cavity due to the increase in quantum yield coupled with a blue shift in the maximum emission wavelength of ANS (Figure 4.5). The observations made in this study are consistent with Mu-GST class which SjGST is evolutionary related with (McTigue *et al*., 1995b). ANS also bind to rat GSTM1-1 a class Mu-GST enzyme (Kinsley *et al*., 2008) which was used for molecular replacement in the elucidation of SjGST crystal structure (Lim *et al*., 1994). Therefore, comparable

with closely related GST isoenzymes. The extent of the blue-shift emission maxima is determined by the ANS binding site polarity (Lakowicz, 1999). A less polar environment leads to high quantum yield as indicated by lipid binding proteins (Sayed *et al*., 2000). Evaluation of enhancement or quenching of the ANS is an indication of the degree of exposure of hydrophobic surfaces of the protein being studied to the surrounding environment. ANS is also able bind to polar regions of a protein using its negatively charged sulfonate group. The sulfonate group interacts with cationic amino acid residues in the protein forming ion pairs. These are followed by hydration changes which allow ANS binding to hydrophobic patches. Therefore, polar environments to a greater extent are the primary determinants of ANS binding to protein (Matulis and Lovrien, 1998). This is true for SjGST because hydrophobic van der Waals forces are not the only interacting forces participates in the binding of ANS to SjGST as determined by isothermal calorimetry (Yassin *et al*., 2004). The study was done under the assumption that ANS does not alter the structure of SjGST because it was shown that ANS can alter the structure of some proteins (Celej *et al*., 2005). In a study by Dirr *et al.*, (2005) showed that ANS binds to the non-polar active site (H-site) of human Alpha GST.

Quaternary structure characterisation was done using SE-HPLC to monitor the hydrodynamic volume and apparent molecular weight of SjGST in the presence and absence of CB3GA. We postulated that CB3GA could alter the quaternary structure of the native dimeric structure SjGST. In the presence of 1 mM CB3GA, SjGST maintained its dimer conformation and no aggregates were observed (Figure 4.6B). This was useful for functional characterisation as SjGST maintained its native conformation in the presence of CB3GA. Hence, any inhibition due CB3GA interaction will not be as a result of changes in the quaternary structure of SjGST. An apparent molecular weight of 55 kDa was obtained, in the presence and absence of CB3GA, which is greater than the theoretical molecular weight because it accounts for gaps within the protein structure. Hence, it is a true representative of the globular size of SjGST. The apparent molecular weight does not deviate much from the dimeric theoretical molecular weight 52 kDa, this is within reasonable limits. Structural changes, would be difficult to monitor using low resolution techniques such as Far-UV CD and Trp fluorescence (considering SjGST is a multitryptophan protein) since SjGST remains a dimer in the presence of CB3GA. To date there are no ligands known to alter the quaternary structure of GSTs. GST normally exist in an active dimeric form. The presence of a functionally stable monomeric form remains unclear, Abdalla *et al*. (2002) showed that monomeric human Pi-

GST is dysfunctional. SjGST has similar structural characteristics when compared to other GSTs (Salinas and Wong, 1999; Wilce and Parker, 1994), predominantly α-helical in structure with comparable tertiary structure. This conservation of secondary, tertiary and quaternary structure ensures conservation of functional properties in GSTs.

The functional characterisation SjGST was done using the universal CDNB-GSH conjugation assay. Mode of SjGST inhibition by CB3GA has not yet been identified. Reversible enzyme inhibition is generally classified in mainly three classes namely: competitive, non-competitive, mixed and uncompetitive inhibition. This gives an idea on how an inhibitor interacts with an enzyme. In this study GSH (G-site) and CDNB (H-site) were used as substrates to determine mode of inhibition, SjGST activity in this study is based on this assay. Beyond the G and H site there could be other binding sites that can alter the conformation of the active site, resulting in the inhibition of SjGST. IC_{50} value determination was the starting point for analysing SjGST inhibition by CB3GA under assumption that CB3GA does inhibit SjGST as observed in other GSTs (Mahajan and Atkins, 2005). An IC_{50} value will also be indicative of the optimal CB3GA concentration to be used in subsequent inhibition studies. IC_{50} of CB3GA was determined to be 100 nM (Figure 4.7A). The IC_{50} value of CB3GA in GSTs varies greatly from 15 nM to 250 nM (Ilio *et al*., 1988). However, that of GST is comparable with a helminth GST *Fasciola gigantica* of 135 nM (Kalita *et al*., 2017). IC_{50} value of CB3GA on SjGST falls within the range of Mu-GST isoenzyme with a range of 50 nM to 700 nM. However, it is not useful since the range is extensive hence not comparable. The Mu-GST class has the highest sensitivity to CB3GA in cytosolic GSTs (Mannervik *et al*., 1985). There is no defined range for CB3GA inhibition on GSTs. The nanomolar range inhibition makes CB3GA a worth candidate to effective GST inhibition because at low CB3GA concentration there is substantial inhibition of SjGST. However, due to CB3GA promiscuous nature of binding, it has to be modified for GST specificity. Efficient inhibition of SjGST is essential for effective *Schistosoma* elimination.

Specific activity of SjGST in the presence of CB3GA was 8.3 µmol. $min^{-1}.mg^{-1}$ compared with 19.8 µmol. $min^{-1}.mg^{-1}$ in the absence of CB3GA (Figure 4.7B). Specific activity of SjGST was reduced by ~50%. Specific activity obtained in this study for free SjGST is comparable with studies by Walker *et al*. (1993) and Smith *et al*. (1988). Inhibition steady state kinetics of SjGST were analysed to determine the mode of inhibition of CB3GA on SjGST using GSH as a probe for

G site and CDNB for the H site. The concentrations used for the inhibition studies were set based on the IC_{50} value. The GSH-CDNB conjugation assay in the presence of CB3GA was used in the to study inhibition kinetics of SjGST.

Lineweaver-Burke plots were derived from Michaelis-Menten data in order to determine the CB3GA mode of inhibition. The goodness of fit of regression coefficients was greater than 0.95 for all fits except for CDNB plots for 100 nM and 200 nM. This deviation can be attributed to superimposition of either product inhibition or enzyme memory loss of SjGST (Mannervik *et al*., 1988). SjGST is bi-substrate enzyme, the G-site and the H-site do not display cooperativity active sites, since GSH and CDNB plots show a hyperbolic plot for Michelis-Manten kinetics (Figure 4.8) (Berg *et al*., 2002). Change in $K_M^{GSH/CDNB}$ and $V_{max}^{GSH/CDNB}$ in the presence of CB3GA is shown in Table 2. Control $K_M^{GSH/CDNB}$ were consistent with what was obtained by Walker *et al*. (1993) and Stefanidis *et al*. (2018). With respect to G-site CB3GA showed uncompetitive inhibition as described by the Dixon plot (Figure 3.9B) on the other hand the H-site CB3GA showed non-competitive inhibition (Figure 3.10). The results indicate that SjGST has higher affinity to GSH (K_M = 0.33 mM) compare with CDNB (K_M = 1.10 mM), this is consistent with observations in most GSTs (Armstrong, 1991). SjGST requires no specific order for substrate/ligand association its catalytic mechanism (random sequential single displacement) which has been observed in most parasitic GSTs (Torres and Landa, 2008). GSH has been suggested to be the first to bind to SjGST due high cytosolic GSH concentration (up to 10 mM) considering that the K_M of GSH is in most cases is below 1 mM (Clark, 1989). Lineweaver-Burke plots are prone to error at low substrate concentrations due to 1/[S] derivation inflating the influence of low substrate concentrations on the overall shape of the graph and mathematical flaws as described by Ochs (2010). However, they give an idea on the mode of enzyme inhibition not actual numeric kinetic parameters. It is better to use more accurate techniques such as isothermal titration calorimetry to determine the kinetic parameters for CB3GA binding to SjGST. CB3GA seems to be remotely affecting both active sites suggesting another binding site on SjGST. The assumption of the presence of an alternative binding site prompted the use of molecular docking to theoretically determine the location of this site.

Schrödinger IFD protocol was used to predict the conformation of SjGST-CBG3A complex. It is generally accepted that induced fit docking is a more reliable method of docking when compared

with rigid docking. Induced fit docking used in this study allows for ligand flexibility hence exploring a wide range of possible binding conformations in the rigid protein structure. Induced fit docking is a valid method to predict ligand binding conformation as demonstrated by Sherman *et al*. (2006) where IFD provided a better fit (RMSD) comparable with crystal structures. Co-crystallised protein-ligand complexes were compared to IFD results of protein and respective ligand. The study demonstrated that structures obtained induced fit docking are of sufficient quality assisting in lead molecule optimization effort.

Glide Emodel scoring function was used for analysis of CB3GA binding to SjGST. Emodel scoring uses more significant force field components (electrostatic and van der Waal energies) for the conformation of the ligand. These are suited for comparing ligand conformations ultimately selecting the optimal ligand pose in the lowest energy state in the protein binding site. The lower the Emodel value the better the binding affinity between protein and ligand. IFD determined that within 4 Å of CB3GA makes hydrogen bond contacts with: from Chain A Tyr 6, Trp 7, Leu 54, Asn 53, Met 68, Arg 107, Tyr 110 and on Chain B Arg 107 and Asp 100 (Figure 4.11B). One molecule of CB3GA binds per dimeric GST in the long groove of the dimer interface in proximity to the catalytic active sites (Figure 4.11A) protruding into the H-site (Figure 4.11B). CB3GA forms a direct hydrogen bond with Trp 7 a residue critical for GST catalysis. Trp 7 has been postulated to be responsible for stabilising GSH thiolate anion and enhancing nucleophilicity of protonated thiol (Andújar-Sánchez *et al*., 2003). Try 111 is important for the water molecule coordination in SjGST active site (Lim *et al*., 1994). CB3GA interacts with Tyr 110 which can affect atomic arrangement that allow for suitable water molecule coordination. These factors could be the cause of efficient CB3GA inhibition because it interacts with Trp 7 and Tyr 110 residues which have key roles in SjGST catalytic mechanism (Cardoso *et al*., 2003). SjGST W7F mutation displays high affinity for GSH than wild type SjGST and complete loss of activity towards CDNB (Andújar-Sánchez *et al*., 2003). Suggesting that Trp 7 plays a key role in SjGST catalysis. CB3GA seems to be protruding into the H-site of SjGST (Figure 4.11B) this is consistent with non-competitive inhibition observed experimentally (Figure 4.10) and a stoichiometry of 1 CB3GA molecule binging to the dimer interface, which is associated with ligandin type inhibitors of GST (Mahajan and Atkins, 2005). The promiscuity of the L-site suggests that the inhibition observed is dependent on the nature of the binding ligand due to different residues being involved L-site binding. An important consideration when IFD is done is that: the observed protein-complex

conformation may not be the same as the one observed in the cell. The energy minimised state *in-silico* may not be the most populated protein conformation which will bind to the ligand. Therefore, other high energy states need to be considered. This could be done by considering other protein-ligand conformations with a higher Emodel score (Carlson, 2002b; Teague, 2003).

CB3GA binds on the dimer interface of SjGST, this site is referred to as the non-substrate binding site (L-Site) which is poorly defined in most GSTs. CB3GA seems to be binding in a similar site as praziquantel. However, praziquantel does not inhibit the SjGST activity (Milhon *et al*., 1997). It might be because praziquantel does not interact with SjGST residues involved in catalysis particularly Trp 7. The non-competitive steady state kinetic nature of CB3GA inhibition of SjGST with respect to CDNB, is a feature observed for "ligandin" inhibitors (bind to L-site) of GSTs. In some cases partially occupying the H-site within the cleft (Mahajan and Atkins, 2005). This further validates the L-site binding of CB3GA to SjGST based on the IFD results. The ability of CB3GA and praziquantel to bind on a similar site indicates the versatility of the L-site. Hence, wide range of L-site inhibitors can be formulated. Validation of the induced fit docking method was done by using human Pi-GST. Docking results observed were comparable with the crystal structure of human Pi-GST-CB3GA complex (Oakley *et al*., 1999). The CB3GA occupies a part of the H-site in Pi-GST, this lead to the suggestion that the L-site of Pi-GST is not on the dimer interface (Oakley *et al*., 1999). Pi-GST-CB3GA complex shows that the L-site is different in GST isoforms, therefore more studies have to be done to characterise the L-site in GSTs. The RMSD value of 0.024 Å shows that the IFD protocol was valid, since the SjGST-GSH complex re-docked structure was similar to a solved crystal SjGST-GSH complex. Therefore, RMSD validation provides a strategy to explore multi-objective optimisation for the development of docking procedures (Poli *et al*., 2016).

Binding affinity prediction was done using a SjGST-CB3GA complex structure obtained Glide docking rather than Quantum Mechanics/Molecular Mechanics (QM/MM) docking because CB3GA is a highly charged molecule. Highly charged molecules have shown to alter MM-GBSA predictions (Sun *et al*., 2014), QM/MM increases formal partial charge to ligands in this case CB3GA is a highly charged hence MM-GBSA may fail to perform free energy predictions for the protein-ligand complex with high ligand charges. The advantage of using MM-GBSA is that it breaks down ΔG_{Pred} to individual components, giving a better understanding of the binding process

involved in complex formation. Table 4 shows that $\Delta G_{Covalent}$ and $\Delta G_{Solv\ GB}$ unfavourable contributions for binding. This can be attributed to the unfavourable displacement of implicit solvent model in the dimer interface of SjGST which has a large surface area of 40 Å (McTigue *et al*., 1995b). Favourable $\Delta G_{Coulomb}$ and ΔG_{vdW} drive binding, this may be due to the configuration of SjGST and the net charge of CB3GA that favour binding. However, it should be noted that MM-GBSA only accounts for the residues proximal to the binding site. It does not include ensembles and alternative conformers on the protein or ligand that remotely affect binding affinity (Du *et al*., 2016). SjGST-CB3GA complex assumes a different conformation in MM-GBSA when compared with IFD conformation. However, CB3GA still binds in the dimer interface of SjGST. π-π*-staking between SjGST (Trp 40) and CB3GA is observed in MM-GBSA complex and not in the IFD complex. π-π*-staking is directional form of interaction hence it can be the primary force driving CB3GA binding. However, standard force field methods have insufficient treatment of π-π*-staking interaction (Li *et al*., 2011). Free energy of binding from MM-GBSA ΔG_{Pred} (- 265.15 kJ/mol) compared with experimental ΔG_{Exp} (-49.93 kJ/mol) differ substantially. This was expected since MM-GBSA does not account for all molecular forces affecting free energy of binding. However, both show that binding is favourable at different magnitudes. Molecular dynamics (MD) may be a better starting method for MM-GBSA to give a better depiction when compared with experimental binding affinity. MD uses multiple conformations for MM-GBSA at different time points during the simulation while IFD uses one conformation. Also, MD can dictate other conformations that are have not been considered in Glide docking due to limited computational power.

Conclusion and future work.

CB3GA is an efficient inhibitor of SjGST that binds to the dimer interface of SjGST altering catalytic activity of both the G-site and H-site. The forces that govern the efficient inhibition of SjGST should be analysed close so that they can be applied to drug design for efficient inhibition. Ligandin function of SjGST can be exploited for rational drug design since ligands such as CB3GA can affect the activity of both catalytic active sites paying special attention to the L-site which is overlaps onto the H-site (distinct xenobiotic binding) providing expansive binding surface of ligands. However, the binding process to the L-site is dependent on size, structure and nature of the ligand. The unique characteristic of the L-site provides an opportunity for highly specific

rational drug design. Theoretical and experimental binding affinities favour SjGST-complex formation. Further work will involve crystallisation of SjGST with CB3GA, without crystallography data the exact binding mode of CB3GA remains elusive. Isothermal titration calorimetry to analyse thermodynamics involved in SjGST binding to CB3GA.

REFERENCES

.

1. **Abdalla, A.-M., Bruns, C.M., Tainer, J.A., Mannervik, B., Stenberg, G.**, (2002). Design of a monomeric human glutathione transferase GSTP1, a structurally stable but catalytically inactive protein. *Protein Engineering* 15, 827-834.
2. **Adenowo, A.F., Oyinloye, B.E., Ogunyinka, B.I., Kappo, A.P.**, (2015). Impact of human schistosomiasis in sub-Saharan Africa. *Brazilian Journal of Infectious Diseases* 19**,** 196-205.
3. **Albrecht, C.,** (2008). Joseph R. Lakowicz: Principles of fluorescence spectroscopy. *Analytical and Bioanalytical Chemistry* 390, 1223-1224.
4. **Alfarano, P.** (2010). Structure-based Methods for Virtual Screening, Protein Design, and Protein Function Studies (Doctoral dissertation).
5. **Alger, H.M., Williams, D.L., (2002)**. The disulfide redox system of Schistosoma mansoni and the importance of a multifunctional enzyme, thioredoxin glutathione reductase. *Molecular and Biochemical Parasitology* 121, 129-139.
6. **Andújar-Sánchez, M., Clemente-Jiménez, J.M.a., Las Heras-Vázquez, F.J., Rodríguez-Vico, F., Cámara-Artigas, A., Jara-Pérez, V.**, (2003). Thermodynamics of glutathione binding to the tyrosine 7 to phenylalanine mutant of glutathione S-transferase from *Schistosoma japonicum*. *International Journal of Biological Macromolecules* 32, 77-82.
7. **Armstrong, R. N.,** (1991). Glutathione S-transferases: reaction mechanism, structure, and function. *Chemical research in toxicology*, *4*(2), 131-140.
8. Arthur, J., (2001). The glutathione peroxidases. *Cellular and Molecular Life Sciences* 57, 1825-1835.
9. **Axarli, I.A., Rigden, D.J., Labrou, N.E.**, (2004). Characterization of the ligandin site of maize glutathione S-transferase I. *Biochemical Journal* 382, 885-893.
10. **Baan, M., Galappaththi-Arachchige, H.N., Gagai, S., Aurlund, C.G., Vennervald, B.J., Taylor, M., van Lieshout, L., Kjetland, E.F.**, (2016). The Accuracy of Praziquantel Dose Poles for Mass Treatment of Schistosomiasis in School Girls in KwaZulu-Natal, South Africa. *PLoS Neglected Tropical Diseases* 10, e0004623.
11. **Berg, J., Tymoczko, J., Stryer, L.**, (2002). The Michaelis-Menten model accounts for the kinetic properties of many enzymes. *Biochemistry*, 5.
12. **Bhargava, M. M., Listowsky, I., & Arias, I. M.** (1978). Ligandin. Bilirubin binding and glutathione-S-transferase activity are independent processes. *Journal of Biological Chemistry* 253(12), 4112-4115.
13. **Braschi, S., Curwen, R.S., Ashton, P.D., Verjovski-Almeida, S., Wilson, A.**, (2006). The tegument surface membranes of the human blood parasite *Schistosoma mansoni*: a proteomic analysis after differential extraction. *Proteomics* 6**,** 1471-1482.
14. **Brockwell, D., Yu, L., Cooper, S., Mccleland, S., Cooper, A., Attwood, D., Gaskell, S.J., Barber, J.**, (2001). Physicochemical consequences of the perdeuteriation of glutathione S-transferase from *S. japonicum*. *Protein Science* 10, 572-580.

15. **Brophy, P.**, (1988). The role of glutathione S-transferase in cestodes. Institute of Biological Sciences. University of Wales, Aberystwyth.
16. **Brophy, P., Barrett, J.**, (1990). Glutathione transferase in helminths. *Parasitology* 100, 345-349.
17. **Brophy, P.M., Pritchard, D.I.**, (1994). Parasitic helminth glutathione S-transferases: an update on their potential as targets for immuno-and chemotherapy. *Experimental Parasitology* 79, 89-96.
18. **Brown, D.S.**, (2002). Freshwater snails of Africa and their medical importance. CRC press.
19. **Cardoso, R. M., Daniels, D. S., Bruns, C. M., & Tainer, J. A.B,** (2003). Characterization of the electrophile binding site and substrate binding mode of the 26-kDa glutathione S-transferase from Schistosoma japonicum. *Proteins: Structure, Function, and Bioinformatics*, *51*(1), 137-146.
20. **Carlson, H.A.**, (2002a). Protein flexibility and drug design: how to hit a moving target. *Current Opinion in Chemical Biology* 6, 447-452.
21. **Carlson, H.A.**, (2002b). Protein flexibility is an important component of structure-based drug discovery. *Current Pharmaceutical Design* 8, 1571-1578.
22. **Celej, M.S., Dassie, S.A., Freire, E., Bianconi, M.L., Fidelio, G.D.**, (2005). Ligand-induced thermostability in proteins: Thermodynamic analysis of ANS–albumin interaction. *Biochimica et Biophysica Acta (BBA)-Proteins and Proteomics* 1750, 122-133.
23. **Chaudhary, K.K., Mishra, N.**, (2016). A Review on Molecular Docking: Novel Tool for Drug Discovery. *Databases* 3, 4.
24. **Chitsulo, L., Engels, D., Montresor, A., Savioli, L.**, (2000). The global status of schistosomiasis and its control. *Acta Tropica* **77**, 41-51.
25. **Chrambach, A., Rodbard, D.**, (1971). Polyacrylamide gel electrophoresis. *Science* 172, 440-451.
26. **Cioli, D., Pica-Mattoccia, L., Basso, A., Guidi, A.**, (2014). Schistosomiasis control: praziquantel forever ?. *Molecular and Biochemical Parasitology* 195, 23-29.
27. **Clark, A.G.**, (1989). The comparative enzymology of the glutathione S-transferases from non-vertebrate organisms. *Comparative Biochemistry and Physiology Part B: Comparative Biochemistry* 92, 419-446.
28. **Colley, D., Secor, W.**, (2014). Immunology of human schistosomiasis. *Parasite Immunology* 36, 347-357.
29. **da Paixão Siqueira, L., Fontes, D.A.F., Aguilera, C.S.B., Timóteo, T.R.R., Ângelos, M.A., Silva, L.C.P.B.B., de Melo, C.G., Rolim, L.A., da Silva, R.M.F., Neto, P.J.R.**, (2017). Schistosomiasis: drugs used and treatment strategies. *Acta Tropica* **176**, 179-187.
30. **De Boer, H.A., Comstock, L.J., Vasser, M.**, (1983). The tac promoter: a functional hybrid derived from the trp and lac promoters. *Proceedings of the National Academy of Sciences* 80, 21-25.
31. **De Sousa, C. A. P., Brigham, T., Chasekwa, B., Mbuya, M. N., Tielsch, J. M., Humphrey, J. H., & Prendergast, A. J**., (2014). Dosing of praziquantel by height in sub-

Saharan African adults. *The American Journal of Tropical Medicine and Hygiene* 90(4), 634-637.

32. **Dirr, H.W., Little, T., Kuhnert, D.C., Sayed, Y.**, (2005). A conserved N-capping motif contributes significantly to the stabilization and dynamics of the C-terminal region of class Alpha Glutathione S-transferases. *Journal of Biological Chemistry* 280, 19480-19487.
33. **Doenhoff, M., Hagan, P., Cioli, D., Southgate, V., Pica-Mattoccia, L., Botros, S., Coles, G., Tchuenté, L.T., Mbaye, A., Engels, D.**, (2009). Praziquantel: its use in control of schistosomiasis in sub-Saharan Africa and current research needs. *Parasitology* 136, 1825-1835.
34. **Doenhoff, M.J., Cioli, D., Utzinger, J.**, (2008). Praziquantel: mechanisms of action, resistance and new derivatives for schistosomiasis. *Current Opinion in Infectious Diseases* 21, 659-667.
35. **Du, X., Li, Y., Xia, Y.-L., Ai, S.-M., Liang, J., Sang, P., Ji, X.-L., Liu, S.-Q.**, (2016). Insights into protein–ligand interactions: mechanisms, models, and methods. *International Journal of Molecular Sciences* 17, 144.
36. **Edwards, R.A., Woody, R.W.**, (1983). Molecular orbital calculations of the optical properties of Congo Red and Cibacron Blue and their complexes with proteins. The *Journal of Physical Chemistry* 87, 1329-1337.
37. **Eftink, M.R.**, (2006). Fluorescence techniques for studying protein structure. Methods of Biochemical Analysis: *Protein Structure Determination* 35, 127-205.
38. **Fallon, P.G., Doenhoff, M.J.**, (1994). Drug-resistant schistosomiasis: resistance to praziquantel and oxamniquine induced in *Schistosoma mansoni* in mice is drug specific. *The American Journal of Tropical Medicine and Hygiene* 51, 83-88.
39. **Feldmeier, H., Chitsulo, L.**, (1999). Therapeutic and operational profiles of metrifonate and praziquantel in *Schistosoma haematobium* infection. *Arzneimittelforschung* 49, 557-565.
40. **Ferrari, M., Coelho, P., Antunes, C., Tavares, C., Da Cunha, A.**, (2003). Efficacy of oxamniquine and praziquantel in the treatment of *Schistosoma mansoni* infection: a controlled trial. *Bulletin of the World Health Organization* 81, 190-196.
41. **Fong, I.W.**, (2012). Challenges in infectious diseases. Springer Science & Business Media.
42. **Friesner, R.A., Banks, J.L., Murphy, R.B., Halgren, T.A., Klicic, J.J., Mainz, D.T., Repasky, M.P., Knoll, E.H., Shelley, M., Perry, J.K.**, (2004). Glide: a new approach for rapid, accurate docking and scoring. Method and assessment of docking accuracy. *Journal of Medicinal Chemistry* 47, 1739-1749.
43. **Gadhe, C.G., Balupuri, A., Kothandan, G., Cho, S.J.**, (2014). Theoretical characterization of binding mode of organosilicon inhibitor with p38: Docking, MD simulation and MM/GBSA free energy approach. *Bulletin of the Korean Chemical Society* 35, 2494-2504.
44. **Gasteiger, E., Hoogland, C., Gattiker, A., Wilkins, M.R., Appel, R.D., Bairoch, A.**, (2005). Protein identification and analysis tools on the ExPASy server. Springer.

45. **Graminski, G. F., Kubo, Y., & Armstrong, R. N.**, (1989). Spectroscopic and kinetic evidence for the thiolate anion of glutathione at the active site of glutathione S-transferase. *Biochemistry* 28(8), 3562-3568.
46. **Habig, W.H., Jakoby, W.B.**, (1981). Assays for differentiation of glutathione S-Transferases, *Methods in enzymology*. 398-405.
47. **Habig, W.H., Pabst, M.J., Jakoby, W.B.**, (1974). Glutathione S-transferases the first enzymatic step in mercapturic acid formation. *Journal of Biological Chemistry* 249, 7130-7139.
48. **Harnett, W., Kusel, J.**, (1986). Increased exposure of parasite antigens at the surface of adult male Schistosoma mansoni exposed to praziquantel in vitro. *Parasitology* 93, 401-405.
49. **Hawe, A., Sutter, M., Jiskoot, W.**, (2008). Extrinsic fluorescent dyes as tools for protein characterization. *Pharmaceutical Research* 25, 1487-1499.
50. **Hou, T., Wang, J., Li, Y., Wang, W.**, (2010). Assessing the performance of the MM/PBSA and MM/GBSA methods. The accuracy of binding free energy calculations based on molecular dynamics simulations. *Journal of Chemical Information and Modeling* 51, 69-82.
51. **Huang, Y., Manderson, L.**, (1992). Schistosomiasis and the social patterning of infection. *Acta Tropica* 51, 175-194.
52. **Ilio, C., Aceto, A., Boccio, G., Casalone, E., Pennelli, A., Federici, G.**, (1988). Purification and characterization of five forms of glutathione transferase from human uterus. *The FEBS Journal* 171, 491-496.
53. **Ismail, M., Metwally, A., Farghaly, A., Bruce, J., Tao, L.-F., Bennett, J.L.**, (1996). Characterization of isolates of *Schistosoma mansoni* from Egyptian villagers that tolerate high doses of praziquantel. *The American Journal of Tropical Medicine and Hygiene* 55, 214-218.
54. **Ismail, M.M., Taha, S.A., Farghaly, A.M., El-Azony, A.**, (1994). Laboratory induced resistance to praziquantel in experimental schistosomiasis. *Journal of the Egyptian Society of Parasitology* 24, 685-695.
55. **Jiang, Q.Q.**, (2013). Discovery of potent inhibitors of human β-tryptase by protein surface recognition. (PhD Dissertation).
56. **Jolly, E.R., Chin, C.-S., Miller, S., Bahgat, M.M., Lim, K., DeRisi, J., McKerrow, J.H**., (2007). Gene expression patterns during adaptation of a helminth parasite to different environmental niches. *Genome Biology* 8, R65.
57. **Jordan, P.**, Webbe, G., Sturrock, R.F., (1993). Human schistosomiasis. *CAB International*.
58. **Kalita, J., Shukla, R., Shukla, H., Gadhave, K., Giri, R., Tripathi, T.**, (2017). Comprehensive analysis of the catalytic and structural properties of a mu-class glutathione s-transferase from Fasciola gigantica. *Scientific Reports* 7, 17547.

59. **Kallestrup, P., Zinyama, R., Gomo, E., Butterworth, A.E., van Dam, G.J., Gerstoft, J., Erikstrup, C., Ullum, H.**, (2006). Schistosomiasis and HIV in rural Zimbabwe: efficacy of treatment of schistosomiasis in individuals with HIV coinfection. *Clinical Infectious Diseases* 42, 1781-1789.
60. **Kaplan, W., Erhardt, J., Sluis-Cremer, N., Dirr, H., Hüsler, P., Klump, H.**, (1997). Conformational stability of pGEX-expressed *Schistosoma japonicum* glutathione S-transferase: a detoxification enzyme and fusion-protein affinity tag. *Protein Science* **6**, 399-406.
61. **Kelly, S.M., Jess, T.J., Price, N.C.**, (2005). How to study proteins by circular dichroism. *Biochimica et Biophysica Acta (BBA)-Proteins and Proteomics* **1751**, 119-139.
62. **Kelly, S.M., Price, N.C.**, (2000). The use of circular dichroism in the investigation of protein structure and function. *Current Protein and Peptide Science* **1**, 349-384.
63. **Kinsley, N., Sayed, Y., Mosebi, S., Armstrong, R.N., Dirr, H.W.**, (2008). Characterization of the binding of 8-anilinonaphthalene sulfonate to rat class Mu GST M1-1. *Biophysical Chemistry* **137**, 100-104.
64. **Kraut, D. A., Carroll, K. S., & Herschlag, D**., (2003). Challenges in enzyme mechanism and energetics. *Annual Review of Biochemistry* **72(1)**, 517-571.
65. **Kursula, I., Heape, A. M., & Kursula, P.** (2005). Crystal Structure of Non-Fused Glutathione S-Transferase from Schistosoma 709 japonicum in Complex with Glutathione. *Protein and peptide letters*, **12(7)**, 709-712.
66. **Laemmli, U.K.**, (1970). Cleavage of structural proteins during the assembly of the head of bacteriophage T4. *Nature* **227**, 680-685.
67. **Lakowicz, J. R.**, (1999) Principles of Fluorescence Spectroscopy. *Plenum Press, New York.*
68. **Li, J., Abel, R., Zhu, K., Cao, Y., Zhao, S., Friesner, R.A.**, (2011). The VSGB 2.0 model: a next generation energy model for high resolution protein structure modeling. *Proteins: Structure, Function, and Bioinformatics* **79**, 2794-2812.
69. **LigPrep**, (2009). 2.3, Schrodinger. LLC, New York, NY.
70. **Lim, K., Ho, J.X., Keeling, K., Gilliland, G.L., Ji, X., Rüker, F., Carter, D.C.**, (1994). Three-dimensional structure of Schistosoma japonicum glutathione S-transferase fused with a six-amino acid conserved neutralizing epitope of gp41 from HIV. *Protein Science* 3, 2233-2244.
71. **Liu, J., Wang, R.**, (2015). Classification of current scoring functions. *Journal of Chemical Information and Modelling* 55, 475-482.
72. **Lyne, P.D., Lamb, M.L., Saeh, J.C.**, (2006). Accurate prediction of the relative potencies of members of a series of kinase inhibitors using molecular docking and MM-GBSA scoring. *Journal of Medicinal Chemistry* 49, 4805-4808.
73. **Mahajan, S., Atkins, W.**, (2005). The chemistry and biology of inhibitors and pro-drugs targeted to glutathione S-transferases. *Cellular and Molecular Life Sciences* 62, 1221-1233.

74. **Mannervik, B., Alin, P., Guthenberg, C., Jensson, H., Tahir, M.K., Warholm, M., Jörnvall, H.**, (1985). Identification of three classes of cytosolic glutathione transferase common to several mammalian species: correlation between structural data and enzymatic properties. *Proceedings of the National Academy of Sciences* 82, 7202-7206.
75. **Mannervik, B., Helena Danielson, U., Ketterer, B.**, (1988). Glutathione transferases—structure and catalytic activit. *Critical Reviews in Biochemistry* 23, 283-337.
76. **Martin, J.L.**, (1995). Thioredoxin-a fold for all reasons. *Structure* 3, 245-250.
77. **Matulis, D., Lovrien, R.**, (1998). 1-Anilino-8-naphthalene sulfonate anion-protein binding depends primarily on ion pair formation. *Biophysical Journal* 74, 422-429.
78. **Mazigo, H.D., Dunne, D.W.**, Wilson, S., Kinung'hi, S.M., de Moira, A.P., Jones, F.M., Morona, D., Nuwaha, F., (2014). Co-infection with Schistosoma mansoni and Human Immunodeficiency Virus-1 (HIV-1) among residents of fishing villages of north-western Tanzania. *Parasites & Vectors* 7, 587.
79. **McTigue, M.A., Bernstein, S.L., Williams, D.R., Tainer, J.A**., (1995a). Purification and crystallization of a schistosomal glutathione S-Transferase. *Proteins: Structure, Function, and Bioinformatics* 22, 55-57.
80. **McTigue, M.A., Williams, D.R., Tainer, J.A.**, (1995b). Crystal Structures of a Schistosomal Drug and Vaccine Target: Glutathione S-Transferase from *Schistosoma japonica* and its Complex with the Leading Antischistomal Drug Praziquantel. *Journal of Molecular Biology* 246, 21-27.
81. **Michaelis, L., Menten, M.**, (1913). *Die kinetik der invertinwirkung Biochem Z* 49: 333–369.
82. **Mkoji, G., Smith, J., Prichard, R.**, (1988). Antioxidant systems in *Schistosoma mansoni*: evidence for their role in protection of the adult worms against oxidant killing. *International Journal for Parasitology* 18, 667-673.
83. **Mobley, D.L., Dill, K.A.**, (2009). Binding of small-molecule ligands to proteins:"what you see" is not always "what you get". *Structure* 17, 489-498.
84. **Muhumuza, S., Kitimbo, G., Oryema-Lalobo, M., Nuwaha, F.**, (2009). Association between socio economic status and schistosomiasis infection in Jinja District, Uganda. *Tropical Medicine & International Health* 14, 612-619.
85. **Oakley, A.J., Bello, M.L., Nuccetelli, M., Mazzetti, A.P., Parker, M.W.**, (1999). The ligandin (non-substrate) binding site of human pi class glutathione transferase is located in the electrophile binding site (H-site). *Journal of Molecular Biology* 291, 913-926.
86. **Ochs, R.**, (2010). The Problem with double reciprocal plots. *Current Enzyme Inhibition* 6, 164-169.
87. **Otaki, J.M., Tsutsumi, M., Gotoh, T., Yamamoto, H.**, (2010). Secondary structure characterization based on amino acid composition and availability in proteins. *Journal of Chemical Information and Modeling* 50, 690-700.
88. **Pearce, E.J., MacDonald, A.S.**, (2002). The immunobiology of schistosomiasis. *Nature Reviews Immunology* 2, 499.

89. **Peterson, W.P., von Lichtenberg, F**., (1965). Studies on granuloma formation. IV: In vivo antigenicity of schistosome egg antigen in lung tissue. *The Journal of Immunology* 95, 959-965.
90. **Poli, G., Martinelli, A., Tuccinardi, T.**, (2016). Reliability analysis and optimization of the consensus docking approach for the development of virtual screening studies. *Journal of Enzyme Inhibition and Medicinal Chemistry* 31, 167-173.
91. **Reich, M.R., Govindaraj, R., Dumbaugh, K., Yang, B.-m., Brinkmann, A., El-Saharty, S., Organization, W.H.**, (1998). International Strategies for Tropical Disease Treatments: Experiences with Praziquantel.
92. **Ressurreição, M., Elbeyioglu, F., Kirk, R.S., Rollinson, D., Emery, A.M., Page, N.M., Walker, A.J.**, (2016). Molecular characterization of host-parasite cell signalling in Schistosoma mansoni during early development. Scientific Reports 6, 35614.
93. **Ricciardi, A., Ndao, M.**, (2015). Still hope for schistosomiasis vaccine. *Human Vaccines & Immunotherapeutics* 11, 2504-2508.
94. **Rollinson, D.**, (2009). A wake-up call for urinary schistosomiasis: reconciling research effort with public health importance. *Parasitology* 136, 1593-1610.
95. **Rufer, A.C., Thiebach, L., Baer, K., Klein, H.W., Hennig, M.**, (2005). X-ray structure of glutathione S-transferase from *Schistosoma japonicum* in a new crystal form reveals flexibility of the substrate-binding site. *Acta Crystallographica Section F: Structural Biology and Crystallization Communications* 61, 263-265.
96. **Saboury, A.**, (2009). Enzyme inhibition and activation: a general theory. *Journal of the Iranian Chemical Society* 6, 219-229.
97. **Sady, H., Al-Mekhlafi, H.M., Mahdy, M.A., Lim, Y.A., Mahmud, R., Surin, J.**, (2013). Prevalence and associated factors of schistosomiasis among children in Yemen: implications for an effective control programme. *PLoS Neglected Tropical Diseases* 7, 2377.
98. **Salinas, A.E., Wong, M.G.**, (1999). Glutathione S-transferases-a review. *Current Medicinal Chemistry* 6, 279-310.
99. **Sayed, Y., Wallace, L.A., Dirr, H.W.**, (2000). The hydrophobic lock-and-key intersubunit motif of glutathione transferase A1-1: implications for catalysis, ligandin function and stability. *FEBS letters* 465, 169-172.
100. **Schägger, H.,** (2006). Tricine–SDS-PAGE. *Nature Protocols* **1**, 16-22.
101. **Secor, W.E.**, (2012). The effects of schistosomiasis on HIV/AIDS infection, progression and transmission. *Current Opinion in HIV and AIDS* **7**, 254-259.
102. **Segel, I.H.**, (1975). Enzyme kinetics: behaviour and analysis of rapid equilibrium and steady state enzyme systems. Biochemistry and Molecular Biology Education 4, 16
103. **Sheehan, D., Meade, G., Foley, V.M., Dowd, C.A.**, (2001). Structure, function and evolution of glutathione transferases: implications for classification of non-mammalian members of an ancient enzyme superfamily. *Biochemical Journal* 360, 1.

104. **Sherman, W., Day, T., Jacobson, M.P., Friesner, R.A., Farid, R.**, (2006). Novel procedure for modeling ligand/receptor induced fit effects. *Journal of Medicinal Chemistry* 49, 534-553.
105. **Smith, D.B., Rubira, M.R., Simpson, R.J., Davern, K.M., Tiu, W.U., Board, P.G., Mitchell, G.F.**, (1988). Expression of an enzymatically active parasite molecule in Escherichia coli: *Schistosoma japonicum* glutathione S-transferase. *Molecular and Biochemical Parasitology* 27, 249-256.
106. **Sousa, S.F., Fernandes, P.A., Ramos, M.J.**, (2006). Protein–ligand docking: current status and future challenges. *Proteins: Structure, Function, and Bioinformatics* **65**, 15-26.
107. **Southgate, V.**, (1997). Schistosomiasis in the Senegal River Basin: before and after the construction of the dams at Diama, Senegal and Manantali, Mali and future prospects. *Journal of Helminthology* 71, 125-132.
108. **Srivani, P., Srinivas, E., Raghu, R., Sastry, G.N.**, (2007). Molecular modeling studies of pyridopurinone derivatives—potential phosphodiesterase 5 inhibitors. Journal of *Molecular Graphics and Modelling* 26, 378-390.
109. **Srivastava, H.K., Sastry, G.N.**, (2012). Molecular dynamics investigation on a series of HIV protease inhibitors: assessing the performance of MM-PBSA and MM-GBSA approaches. *Journal of Chemical Information and Modeling* 52, 3088-3098.
110. **Stefanidis, L., Scinto, K.V., Strada, M.I., Alper, B.J.**, (2018). Bisubstrate Kinetics of Glutathione S-Transferase: A Colorimetric Experiment for the Introductory Biochemistry Laboratory. *Journal of Chemical Education*.
111. **Sun, H., Li, Y., Tian, S., Xu, L., Hou, T.**, (2014). Assessing the performance of MM/PBSA and MM/GBSA methods. 4. Accuracies of MM/PBSA and MM/GBSA methodologies evaluated by various simulation protocols using PDBbind data set. *Physical Chemistry Chemical Physics* 16, 16719-16729.
112. **Tame, J.R.**, (2005). Scoring functions–the first 100 years. *Journal of Computer-Aided Molecular Design* 19, 445-451.
113. **Teague, S.J.**, (2003). Implications of protein flexibility for drug discovery. *Nature Reviews Drug Discovery* 2, 527.
114. **Torres, A., Landa, A.,** (2008). Glutathione transferases from parasites: a biochemical view. *Acta Tropica* 105, 99-112.
115. **van Bladeren, P.J., van Ommen, B.**, (1991). The inhibition of glutathione S-transferases: mechanisms, toxic consequences and therapeutic benefits. *Pharmacology & Therapeutics* 51, 35-46.
116. **van der Werf, M.J., de Vlas, S.J., Brooker, S., Looman, C.W., Nagelkerke, N.J., Habbema, J.D.F., Engels, D**., (2003). Quantification of clinical morbidity associated with schistosome infection in sub-Saharan Africa. *Acta Tropica* 86, 125-139.
117. **Walker, J., Crowley, P., Moreman, A.D., Barrett, J.**, (1993). Biochemical properties of cloned glutathione S-transferases from *Schistosoma mansoni* and *Schistosoma japonicum*. *Molecular and Biochemical Parasitology* 61, 255-264.

118. **Wami, W.M.**, (2015). Paediatric Schistosomiasis: diagnosis, morbidity and treatment.(PhD Dissertation)
119. **Wang, W., Wang, L., Liang, Y.S.**, (2012). Susceptibility or resistance of praziquantel in human schistosomiasis: a review. *Parasitology Research* 111, 1871-1877.
120. **Ware, S., Donahue, J. P., Hawiger, J., Anderson, W. F.**, (1999). Structure of the fibrinogen γ-chain integrin binding and factor XIIIa cross-linking sites obtained through carrier protein driven crystallization. *Protein Science*, 8(12)**,** 2663-2671.
121. **Whitmore, L., Wallace, B.**, (2004). DICHROWEB, an online server for protein secondary structure analyses from circular dichroism spectroscopic data. *Nucleic Acids Research* 32, 668-673.
122. **WHO**, (2013). Schistosomiasis: progress report 2001-2011, strategic plan 2012-2020.
123. **WHO**, (2017). Crossing the billion: lymphatic filariasis, onchocerciasis, schistosomiasis, soil-transmitted helminthiases and trachoma: preventive chemotherapy for neglected tropical diseases.
124. **Wilce, M.C., Parker, M.W.**, (1994). Structure and function of glutathione S-transferases. *Biochimica et Biophysica Acta (BBA)-Protein Structure and Molecular Enzymology* 1205, 1-18.
125. **Wong, S.E., Lightstone, F.C.**, (2011). Accounting for water molecules in drug design. *Expert Opinion on Drug Discovery* 6, 65-74.
126. **Yalçin, S., Jensson, H., Mannervik, B.**, (1983). A set of inhibitors for discrimination between the basic isozymes of glutathione transferase in rat liver. *Biochemical and Biophysical Research Communications* 114, 829-834.
127. **Yassin, Z., Ortiz-Salmerón, E., García-Maroto, F., Barón, C., García-Fuentes, L.**, (2004). Implications of the ligandin binding site on the binding of non-substrate ligands to Schistosoma japonicum-glutathione transferase. *Biochimica et Biophysica Acta (BBA)-Proteins and Proteomics* 1698, 227-237.
128. **Zelck, U., Von Janowsky, B.**, (2004). Antioxidant enzymes in intramolluscan Schistosoma mansoni and ROS-induced changes in expression. *Parasitology* 128, 493-501.
129. **Zhou, X.-N., Wang, L.-Y., Chen, M.-G., Wu, X.-H., Jiang, Q.-W., Chen, X.-Y., Zheng, J., Jürg, U.**, (2005). The public health significance and control of schistosomiasis in China—then and now. *Acta Tropica* 96, 97-105.

APPENDIX

Table A1: Volumes used for SjGST specific activity determination.

Protein concentration (nM)	Protein volume (µL)	Volume buffer (µL)	GSH (µL)	CDNB (µL)	Total Volume (mL)
0	0	2733	167	100	3000
5	15	2718	167	100	3000
10	30	2703	167	100	3000
15	45	2688	167	100	3000
20	60	2673	167	100	3000
25	75	2658	167	100	3000
30	90	2643	167	100	3000
35	105	2628	167	100	3000
40	120	2613	167	100	3000
50	150	2583	167	100	3000

Protein stock- 1 µM, GSH stock concentration-18 mM, CDNB stock concentration-30 mM. GSH and CDNB have a final concentration of 1 mM.

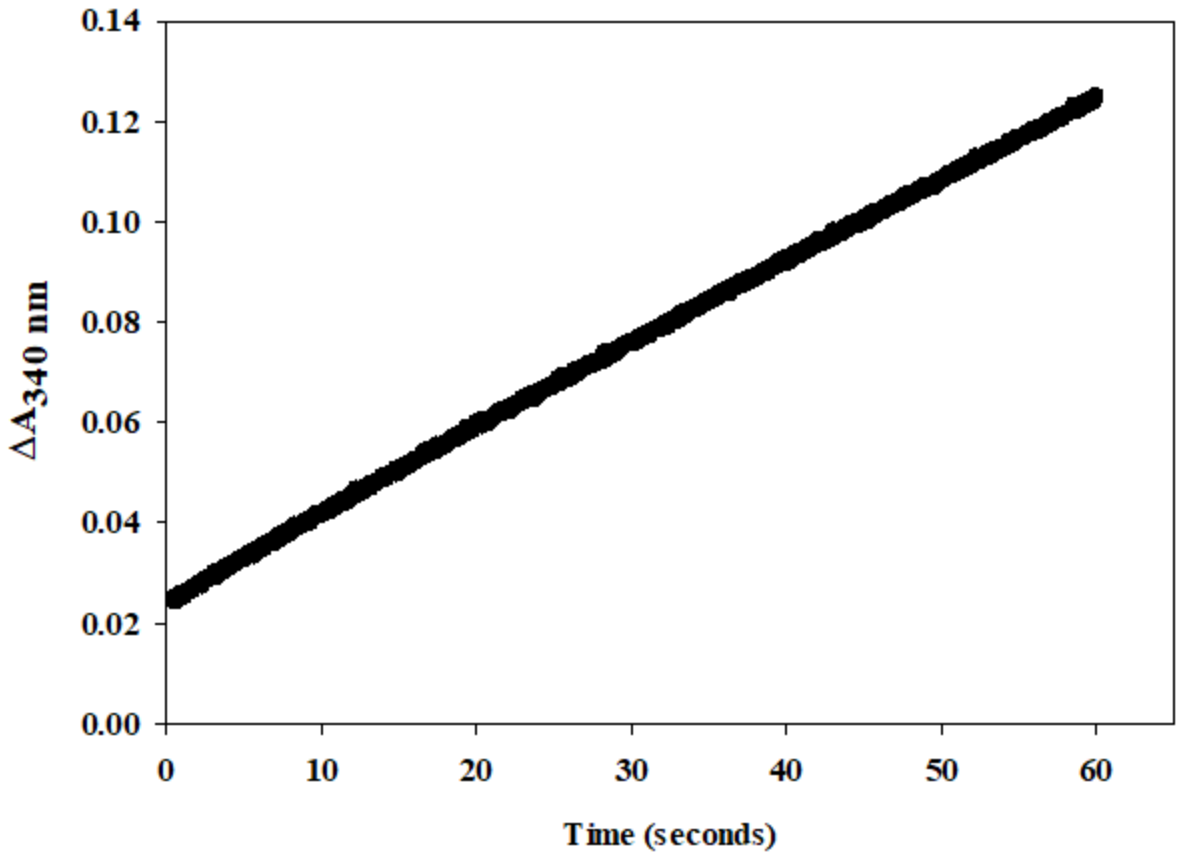


Figure A1: Representative plot for GST activity by measuring the conjugation of CDNB with reduced GSH. Conjugation is coupled with an increase in the amount 1-(*S*-glutathionyl)-2,4-dinitrobenzene which absorbs at 340 nm. Rate of increase is directly proportional to the GST activity in the sample. In this experiment 15 nM of SjGST was used, with slope = 0.0017 and R^2 = 0.9995. The final concentration of GSH and CDNB was 1 mM.

Table A2: Rate of 1-(*S*-glutathionyl)-2,4-dinitrobenzene production at different SjGST concentrations. These values are used to determine specific activity of SjGST.

[SjGST] (nM)	Slope ($\Delta A_{340\ nm}$)	R^2
0	0.00004	0.9849
5	0.0003	0.9951
10	0.0010	0.9995
15	0.0017	0.9995
20	0.0025	0.9994
25	0.0031	0.9992
30	0.0037	0.9991
40	0.0050	0.9985
50	0.0062	0.9998

Calculation:

$$Activity\ (\mu mol.mol^{-1}) = \frac{(\Delta A_{340}/\min Sample - \Delta A_{340}/\min Blank).0.003\ L.10^6}{(9600\ M^{-1}.cm^{-1}).\ 1\ cm}$$

were 0.003L is total sample volume, extinction coefficient of 1-(S-dinitrophenyl)-2,4-dinitrobenzene formed, 10^6 is the conversion of moles to µmoles.

To obtain mg of SjGST used:

$$SjGST(mg) = [SjGST\ used](nM).Vol\ of\ SjGST(L).26000.\ [SjGST\ stock](M).10^2$$

were 26000 is the molecular weight of monomeric GST. 10^2 is the conversion from grams to milligrams.